

Design-Conditional Prior Elicitation for Dirichlet Process Mixtures: A Unified Framework for Cluster Counts and Weight Control

JoonHo Lee

ABSTRACT. Dirichlet process mixture (DPM) models are widely used for semiparametric Bayesian analysis in educational and behavioral research, yet specifying the concentration parameter remains a critical barrier. Default hyperpriors often impose strong, unintended assumptions about clustering, while existing calibration methods based on cluster counts suffer from computational inefficiency and fail to control the distribution of mixture weights. This article introduces Design-Conditional Elicitation (DCE), a unified framework that translates practitioner beliefs about cluster structure into coherent Gamma hyperpriors for a fixed design size J . DCE makes three contributions. First, it solves the computational bottleneck using Two-Stage Moment Matching (TSMM), which couples a closed-form approximation with an exact Newton refinement to calibrate hyperparameters without grid search. Second, addressing the “unintended prior” phenomenon, DCE incorporates a Dual-Anchor protocol to diagnose and optionally constrain the risk of weight dominance while transparently reporting the resulting trade-off against cluster-count fidelity. Third, the complete workflow is implemented in the open-source **DPprior** R package with reproducible diagnostics and a reporting checklist. Simulation studies demonstrate that common defaults such as $\text{Gamma}(1, 1)$ induce posterior collapse rates exceeding 60% regardless of the true cluster structure, while DCE-calibrated priors substantially reduce bias and improve recovery across varying levels of data informativeness.

Keywords: Dirichlet process mixture; concentration parameter; prior elicitation; Bayesian nonparametrics; design-conditional inference; multisite trials; hyperprior calibration

Date: February 9, 2026.

Lee: The University of Alabama, jlee296@ua.edu.

This research was supported by the Institute of Education Sciences, U.S. Department of Education, through Grant R305D240078 to University of Alabama. The opinions expressed are those of the author and do not represent views of the Institute or the U.S. Department of Education.

1. Introduction

Dirichlet process mixture (DPM) models have become indispensable tools for semi-parametric Bayesian analysis in the educational and behavioral sciences. By replacing the restrictive parametric assumptions of traditional hierarchical models—such as the normality of random effects—DPMs allow data to reveal latent structures, skewness, and multimodality that standard approaches might obscure (Antonelli et al., 2016; Jackson & White, 2018). Whether estimating treatment effect heterogeneity in multisite trials and clinical settings (Cardoso et al., 2024; Daniels et al., 2023; Lee et al., 2025), synthesizing evidence across heterogeneous studies in meta-analyses (Burr & Doss, 2005; Cao et al., 2024; Dunson et al., 2008; Muthukumarana & Tiwari, 2016), or capturing latent variability in psychometric and developmental research (Bonafos et al., 2024; Finch & Edwards, 2016; Mignemi & Manolopoulou, 2025; Navarro et al., 2006; Paganin et al., 2023; Qiu et al., 2025), the DPM serves as a robust default that protects inference against model misspecification.

However, the methodological flexibility of the DPM comes with a specific cost: the difficulty of specifying the concentration parameter α . This parameter governs the model’s clustering behavior—controlling both how many distinct clusters tend to emerge among J exchangeable units and how probability mass is distributed across those clusters. When data are strongly informative, the posterior for α is largely determined by the likelihood, and prior specification may seem like a secondary concern. But in many applied settings—particularly those with moderate sample sizes and noisy observations—the prior on α can substantially influence posterior inference (Dorazio, 2009; Giordano et al., 2023; Matza & Bistritz, 2021; Murugiah & Sweeting, 2012). In such contexts, seemingly innocuous “default” or “vague” hyperpriors can encode strong implicit assumptions about clustering that may be entirely at odds with substantive domain knowledge (Gill & Casella, 2009; Greve et al., 2022; Iwashige & Hashimoto, 2025; Kyung et al., 2010).

The fundamental difficulty is one of translation. Practitioners rarely possess direct intuition about the concentration parameter α itself—asking a researcher “What is your prior belief about α ?” is unlikely to yield a meaningful answer. In contrast, practitioners *can* often articulate beliefs about design-relevant quantities: “Among the 100 sites in our study, how many substantively distinct treatment effect patterns do we expect?” or “Is it plausible that most sites share essentially the same effect, or do we anticipate considerable heterogeneity?” These questions concern the expected

number of occupied clusters K_J and the degree of concentration across clusters—quantities that are directly interpretable in terms of substantive hypotheses about the phenomenon under study (McCullagh & Yang, 2008).

The disconnect between practitioner-accessible quantities and the technical hyperparameters required by statistical software creates what we term the *translation gap*. To implement a DPM model with a Gamma hyperprior $\alpha \sim \text{Gamma}(a, b)$ —the most common choice in practice (Neal, 2000)—researchers must specify shape and rate parameters (a, b) . Yet the mapping from beliefs about cluster structure to (a, b) is neither direct nor intuitive. As a result, researchers often resort to one of two unsatisfying approaches: either they adopt common defaults such as $\text{Gamma}(1, 1)$ (e.g., Cao et al., 2024; Ma & Chen, 2020; Mignemi & Manolopoulou, 2025) without interrogating their implications, or they conduct ad hoc sensitivity analyses without a principled framework for interpreting the results (e.g., see Kottas, 2006; Leslie et al., 2007).

This translation gap is consequential. Lee et al. (2025) demonstrate that in multi-site trial settings with moderate informativeness—measured by the ratio of between-site variance to total variance—the prior on α can meaningfully shift posterior estimates of site-specific effects and their distribution. When researchers adopt vague hyperpriors under the assumption that “the data will speak for themselves,” they may inadvertently impose strong assumptions about pooling behavior—for instance, a $\text{Gamma}(1, 1)$ prior places substantial mass near $\alpha = 0$, implying a strong *a priori* expectation of few clusters and considerable pooling.

The literature has recognized the need to calibrate α based on the induced distribution of K_J , the number of occupied clusters (Greve et al., 2022; Paganin et al., 2023). Dorazio (2009) proposed a principled approach that calibrates the Gamma hyperprior by minimizing the Kullback–Leibler divergence between the induced marginal distribution $p(K_J | a, b)$ and a target distribution such as a discrete uniform over a plausible range of cluster counts. Murugiah and Sweeting (2012) proposed a scalable specification strategy (SCAL) that fixes interpretable tail probabilities for the occupied-cluster count and solves for (a, b) as a function of the design size. These K_J -based methods align well with practitioner intuition because cluster counts are interpretable: a researcher can reason about whether expecting “roughly 5 distinct subgroups” versus “roughly 15” reflects their domain knowledge (Bonafos et al., 2024).

However, existing K_J -based calibration methods face three significant limitations. First, there is a *translation gap*: even when practitioners can articulate beliefs about

K_J , there is no standard closed-form map from those beliefs to (a, b) , making elicitation feel opaque. Second, there is a *computational gap*: as Dorazio (2009) explicitly notes, “a closed-form solution does not exist” for the optimal hyperparameters, requiring grid search over a two-dimensional parameter space—and alternative empirical Bayes strategies fare no better, often demanding repeated MCMC runs (Antonelli et al., 2016; Dorazio et al., 2008)—a burden that becomes prohibitive for systematic sensitivity analyses (Giordano et al., 2023). Third, and perhaps most importantly, there is a *coherence gap*: calibrating a prior solely to match beliefs about cluster counts does not guarantee that the implied behavior of the mixture weights aligns with substantive expectations. A hyperprior calibrated to yield an expected cluster count of about 10 for $J = 100$ units might imply a substantial prior probability that one cluster dominates the mixture—a strong pooling assumption that contradicts the intended “ten moderately sized groups” interpretation. Vicentini and Jermyn (2025) term this mismatch an *unintended prior* phenomenon.

Vicentini and Jermyn (2025) sharpen this coherence concern with a conceptual critique. They observe that K_J -based approaches are *sample-size dependent* (SSD): the calibrated hyperprior depends on J , creating what they term a “prior sequence” that changes as the sample size changes. This may be undesirable in settings where multiple analyses with different sample sizes should share a coherent common prior, or in streaming contexts where J grows over time. More fundamentally, Vicentini and Jermyn (2025) demonstrate that a prior that appears “diffuse” with respect to cluster counts can nonetheless encode strong assumptions about weight concentration. They advocate for *sample-size independent* (SSI) approaches that anchor priors on weight functionals rather than cluster counts.

We take a different but complementary view. In many educational and behavioral applications—including multisite trials with a fixed set of sites, meta-analyses of a defined collection of studies, and psychometric assessments with specified samples—the sample size J is not arbitrary but is determined by the research design. In such fixed- J contexts, elicitation through K_J is not a conceptual defect; it is an explicit encoding of a substantively meaningful question: “Among *these* J units, how many distinct patterns do we anticipate?” The relevant criterion is not whether the prior would remain coherent under hypothetical changes to J , but whether the implied prior-predictive behavior at the actual design size is substantively plausible. At the same time, we take seriously the critique that cluster-count matching alone may hide unintuitive weight implications. Our resolution is to treat K_J -based elicitation as

the primary anchor for fixed- J applications while *requiring* that weight diagnostics be reported alongside partition summaries. When the implied weight behavior is substantively unacceptable, we provide an explicit mechanism to incorporate a second constraint on weight concentration while transparently reporting the resulting trade-off.

This paper develops *Design-Conditional Elicitation* (DCE), a unified framework for translating practitioner beliefs about cluster structure into Gamma hyperpriors for the DP concentration parameter. The framework addresses the translation, computational, and coherence gaps through three contributions. First, we introduce *Two-Stage Moment Matching* (TSMM), which provides a closed-form initialization that maps elicited beliefs about the expected value and variance of K_J directly to Gamma hyperparameters, followed by an exact Newton refinement that enforces the targeted moments under the finite- J DP-induced distribution. This two-stage approach eliminates the grid search required by existing methods: calibration completes in approximately 50 milliseconds with machine precision, representing roughly a 900-fold speedup relative to discrepancy-optimization approaches. Second, we introduce a *Dual-Anchor* diagnostic and refinement protocol that quantifies the dominance risk implied by any K_J -calibrated prior. When diagnostics indicate unacceptable weight concentration, an optional refinement step constrains dominance while explicitly reporting the trade-off against the cluster-count target—incorporating the substantive concerns motivating the SSI critique without abandoning the interpretability of design-conditional elicitation. Third, the complete workflow—elicitation, calibration, diagnostics, and reporting—is implemented in the `DPprior` R package with reproducible vignettes and a reporting checklist.

The remainder of this paper proceeds as follows. [Section 2](#) provides minimal DPM background, emphasizing partition and weight perspectives on α . [Section 3](#) presents the DCE methodology. [Section 4](#) reports simulation results comparing DCE to existing approaches. [Section 5](#) discusses implications and future directions. Technical details are provided in the Online Supplemental Materials (OSM).

2. Theoretical Framework

This section introduces minimal background for prior specification on the Dirichlet process (DP) concentration parameter α in DP mixture models. Our goal is not to review DP mixtures broadly, but to clarify *what a prior on α means in applied terms* and why a single interpretive target can be misleading.

A prior on α governs clustering in two distinct but complementary ways. First, it shapes the induced *partition* of J exchangeable units, summarized by the occupied-cluster count K_J . Second, it shapes the induced *mixture weights* (w_1, w_2, \dots) , which determine how concentrated the mixture is and how likely it is that one cluster dominates. These perspectives are linked through α , but they are not interchangeable: calibrating a prior to yield a plausible distribution for K_J does not automatically yield plausible weight behavior. [Figure 1](#) illustrates this “unintended prior” phenomenon and motivates the diagnostics (and optional dual-anchor refinement) in [Section 3](#).

Throughout, we use the shape–rate parameterization $\alpha \sim \text{Gamma}(a, b)$, so that $\mathbb{E}(\alpha) = a/b$ and $\text{Var}(\alpha) = a/b^2$.

2.1. A Minimal DP Mixture Setup and Notation. We work with J exchangeable units indexed by $j = 1, \dots, J$. In multisite trials, meta-analyses, and related “many-units” applications, each unit has a latent parameter τ_j (e.g., a site-specific treatment effect) observed with estimation noise (e.g., [Cao et al., 2024](#)):

$$\hat{\tau}_j \mid \tau_j \sim \mathbf{N}(\tau_j, \hat{s}e_j^2), \quad \tau_j \mid G \stackrel{\text{i.i.d.}}{\sim} G, \quad G \sim \text{DP}(\alpha, G_0). \quad (2.1)$$

Here G_0 is a centering distribution and $\alpha > 0$ controls the *a priori* tendency to create new clusters ([Escobar & West, 1995](#); [Ferguson, 1973](#)). Because draws from a DP are almost surely discrete, the latent values τ_1, \dots, τ_J exhibit ties, inducing a random partition of $\{1, \dots, J\}$ ([Hanson et al., 2005](#); [Sethuraman, 1994](#)). Let z_j denote the cluster label for unit j ; the key design-conditional summary is the number of *occupied clusters* among J units, $K_J = \#\{z_1, \dots, z_J\}$.

A constructive representation that makes the role of α transparent is the stick-breaking representation ([Ishwaran & Zarepour, 2000](#); [Sethuraman, 1994](#)). Under $G \sim \text{DP}(\alpha, G_0)$,

$$G = \sum_{h=1}^{\infty} w_h \delta_{\theta_h}, \quad \theta_h \stackrel{\text{i.i.d.}}{\sim} G_0, \quad (2.2)$$

where

$$v_h \stackrel{\text{i.i.d.}}{\sim} \text{Beta}(1, \alpha), \quad w_1 = v_1, \quad w_h = v_h \prod_{\ell < h} (1 - v_{\ell}), \quad h \geq 2. \quad (2.3)$$

The weight sequence follows $\text{GEM}(\alpha)$ and is in *size-biased order* (not ranked from largest to smallest). We use K_J and (w_h) to articulate two interpretive lenses on α .

2.2. Two Interpretive Lenses on α : Partitions and Weights. Partition Lens: Granularity Through K_J . From a practitioner’s perspective, K_J answers a concrete design-conditional question: *Among these J units, how many substantively distinct patterns do we anticipate?* Larger α increases the chance that a new unit initiates a new cluster and therefore increases K_J on average (Congdon, 2019; Escobar & West, 1995). Conditionally on α , K_J follows the Antoniak distribution (Antoniak, 1974):

$$\Pr(K_J = k \mid \alpha) = |s(J, k)| \alpha^k \frac{\Gamma(\alpha)}{\Gamma(\alpha + J)}, \quad k = 1, \dots, J, \quad (2.4)$$

where $|s(J, k)|$ are unsigned Stirling numbers of the first kind. In Section 3, this partition lens underlies our design-conditional elicitation target: practitioners specify J and beliefs about $\mathbb{E}(K_J)$ and $\text{Var}(K_J)$, and we calibrate a Gamma hyperprior on α to match those targets.

Weight Lens: Concentration and Dominance Through (w_h) . The weights answer a different question: *Even if multiple clusters exist, how is mass distributed across them—roughly even, or with substantial prior probability of a dominant cluster?* A convenient diagnostic is the first stick-breaking weight (Navarro et al., 2006):

$$w_1 \mid \alpha \sim \text{Beta}(1, \alpha), \quad (2.5)$$

so $\Pr(w_1 > t \mid \alpha) = (1 - t)^\alpha$. Tail probabilities such as $\Pr(w_1 > 0.5)$ and $\Pr(w_1 > 0.9)$ provide interpretable summaries of moderate and extreme dominance risk (Miller & Harrison, 2018). Under $\alpha \sim \text{Gamma}(a, b)$, these tail probabilities admit a simple closed form; see Section 3.4.

Interpretability caveat. Because $\text{GEM}(\alpha)$ is in size-biased order, w_1 is not necessarily the largest weight (Sethuraman, 1994; Vicentini & Jermyn, 2025). A faithful interpretation is: w_1 is the asymptotic mass of the cluster containing a randomly selected unit. Accordingly, $\Pr(w_1 > t)$ is the probability that a random unit belongs to a cluster with mass exceeding t , not the probability that the largest cluster exceeds t .

As an additional summary, we consider the co-clustering (Simpson) index

$$\rho = \sum_{h \geq 1} w_h^2, \quad (2.6)$$

which equals the probability that two randomly selected units belong to the same cluster. Together, K_J , w_1 , and ρ provide a small set of *interpretive functionals* that can

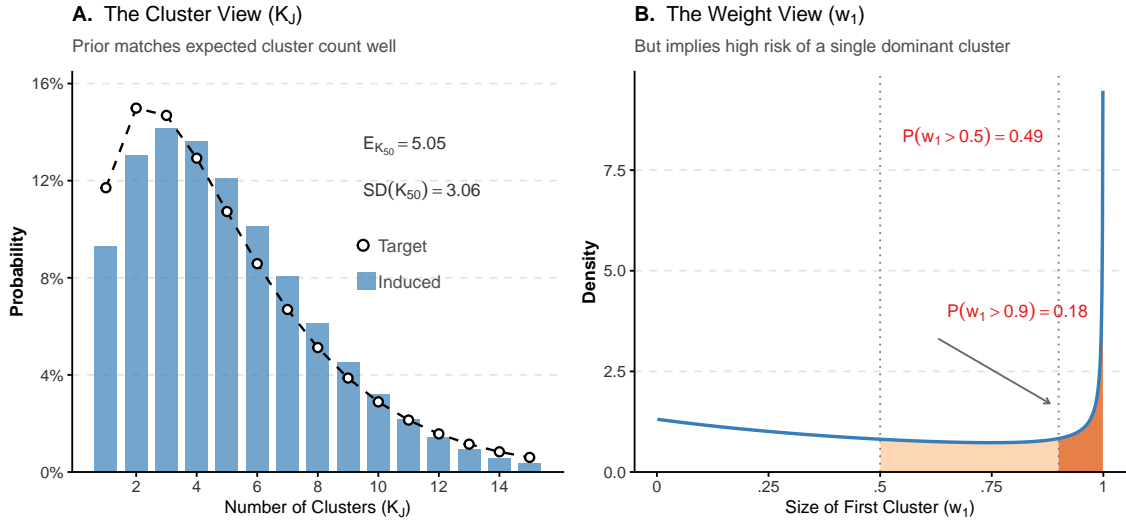
TABLE 1. Interpretive Functionals for Practitioner Communication

Quantity	Statistical Meaning	Practitioner Question	How to Report
$\mathbb{E}[K_J]$	Expected number of occupied clusters among J units	“How many distinct subgroups do I expect?”	“We expect approximately X clusters.”
$\text{Var}(K_J)$	Uncertainty in the occupied cluster count	“How confident am I about that number?”	“Central interval (e.g., 80% or 95%): $[L, U]$.”
$\Pr(K_J = k)$	Marginal probability that exactly k clusters occur	“What is the chance of exactly k groups?”	“Mode at k^* ; most mass in $[a, b]$.”
$\Pr(w_1 > 0.5)$	Probability a random unit belongs to a cluster exceeding 50% mass	“Could one group dominate the sample?”	“ $X\%$ chance of majority-cluster dominance.”
$\Pr(w_1 > 0.9)$	Probability of extreme concentration ($> 90\%$ mass)	“Could almost all units be in one group?”	“ $X\%$ extreme dominance risk.”
$\rho = \sum_{h \geq 1} w_h^2$	Co-clustering (Simpson) index; probability two random units share a cluster	“If I pick two units at random, will they be in the same cluster?”	“ $X\%$ chance of same-cluster membership.”

Note. For $\alpha \sim \text{Gamma}(a, b)$, all quantities admit closed-form expressions or efficient numerical evaluation (see Appendix A in the OSM for exact moment derivations and Appendix E for weight distribution theory).

be communicated to practitioners and reported transparently. [Table 1](#) summarizes these quantities.

2.3. Fixed-Design Elicitation and the Unintended-Prior Phenomenon. In many educational and behavioral applications—multisite trials, meta-analyses, and psychometric studies—the number of exchangeable units J is fixed by design, and investigators often target finite-population estimands (e.g., “the J sites in our study”). In such settings, it is natural to elicit beliefs in design-conditional terms (“among these J units, how many distinct patterns?”), making K_J a coherent primary anchor. At the same time, recent work has emphasized that K_J -anchored priors may hide



Note: $J = 50$. Prior $\alpha \sim \text{Gamma}(1.60, 1.22)$. w_1 is the size-biased (GEM-order) first cluster proportion.

FIGURE 1. The unintended-prior phenomenon: A K_J -calibrated prior can imply substantial dominance risk under the weight view. Panel A: target (circles) vs. induced (bars) distribution of K_{50} . Panel B: marginal density of w_1 with dominance-tail probabilities. $J = 50$; $\alpha \sim \text{Gamma}(1.60, 1.22)$.

unintuitive implications for weight concentration (Vicentini & Jermyn, 2025). Our approach retains the interpretability of K_J while requiring that weight behavior be reported (and, if needed, controlled) alongside partition summaries.

Figure 1 provides a representative illustration. A Gamma hyperprior calibrated to match a plausible target distribution for K_{50} closely reproduces the intended cluster-count behavior (Panel A), yet it implies substantial dominance risk under the weight view (Panel B). Concretely, with $J = 50$ and $\alpha \sim \text{Gamma}(1.60, 1.22)$, the prior matches the cluster-count target well ($\mathbb{E}[K_{50}] = 5.05$, $\text{SD}(K_{50}) = 3.06$) but implies $\Pr(w_1 > 0.5) = 0.49$ and $\Pr(w_1 > 0.9) = 0.18$. Because w_1 is size-biased, the latter statements mean that a randomly selected unit has nearly a 50% prior probability of belonging to a majority cluster and an 18% probability of belonging to an almost-universal ($> 90\%$) cluster.

This contrast is often surprising: “expecting about five groups” is frequently (implicitly) interpreted as “five moderately sized groups,” but that intuition is not guaranteed by K_J calibration alone when α is uncertain under a hyperprior. The key implication for practice is not that K_J -based elicitation should be abandoned, but

that it should be paired with transparent weight diagnostics and (when warranted) an explicit trade-off.

3. Methodology: Design-Conditional Elicitation (DCE)

This section presents *Design-Conditional Elicitation (DCE)*, a workflow that translates practitioner beliefs about cluster structure into a Gamma hyperprior for the DP concentration parameter. DCE is “design-conditional” because practitioners typically reason about heterogeneity among a *fixed* set of J units (e.g., sites, schools, teachers, studies, respondents), and the same prior on α can imply substantively different partition behavior at different J .

The central elicitation target is the occupied-cluster count K_J , defined as the number of distinct clusters represented among J exchangeable units under the DP prior. DCE complements this partition-based anchor with diagnostics (and, if desired, additional calibration) for the implied mixture-weight behavior. In particular, we use summaries based on the first stick-breaking weight w_1 in the GEM(α) representation, and optionally the co-clustering probability $\rho = \sum_{h \geq 1} w_h^2$.

3.1. Overview and Workflow. DCE begins from a practical observation: while practitioners rarely have direct intuition about α , many can articulate (i) how many substantively distinct clusters they expect to observe among the J units in their design, and (ii) how uncertain they are about that expectation. Concretely, the required inputs are the design size J , a target mean $\mu_K = \mathbb{E}(K_J)$, and an uncertainty summary such as $\sigma_K^2 = \text{Var}(K_J)$ (or a qualitative confidence label mapped to a variance; see Appendix G.4 in the OSM for default confidence-to-variance mappings). As an optional fourth input, practitioners may state a dominance tolerance, for example a requirement of the form $\Pr(w_1 > 0.9) \leq \delta$.

Given these inputs, DCE returns calibrated hyperparameters (a, b) for $\alpha \sim \Gamma(a, b)$ and a compact diagnostic report summarizing the induced prior-predictive distribution $p(K_J)$ and the implied weight concentration behavior, including tail probabilities $\Pr(w_1 > t)$ at default thresholds $t \in \{0.5, 0.9\}$ and (optionally) ρ . The workflow is shown in [Figure 2](#) and consists of two components: *Two-Stage Moment Matching (TSMM)* for calibrating (a, b) to match (μ_K, σ_K^2) , and a *Dual-Anchor protocol* that diagnoses (and, if desired, constrains) weight dominance.

The design-conditional framing incorporates the key caution motivating the sample-size-independent critique: calibrating a prior only through K_J does not automatically control the induced weights (Vicentini & Jermyn, [2025](#)). For that reason, DCE makes

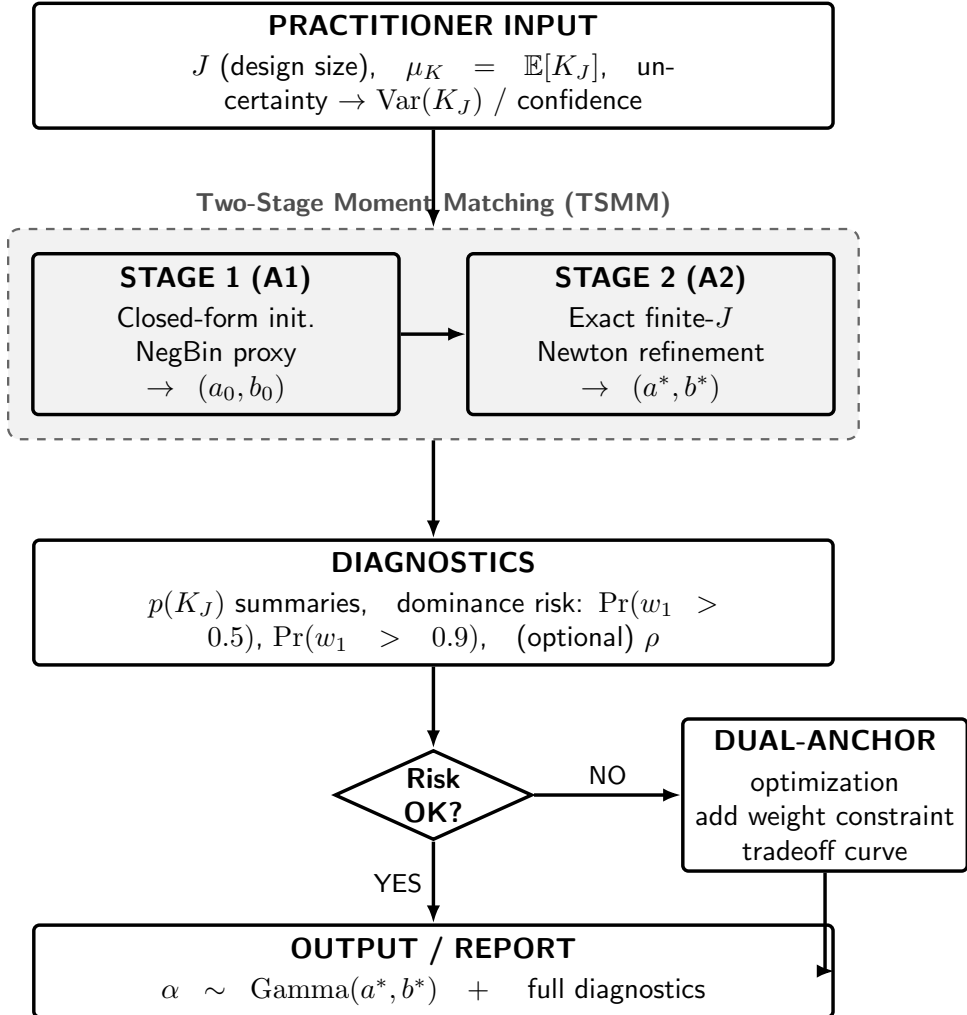


FIGURE 2. Design-conditional elicitation (DCE) workflow. Practitioners specify J , target $\mu_K = \mathbb{E}(K_J)$, and uncertainty σ_K^2 . TSMM calibrates (a, b) ; diagnostics report $p(K_J)$ and $\Pr(w_1 > t)$. Optional Dual-Anchor refines when dominance risk exceeds tolerance.

weight implications explicit through diagnostics and provides an optional dual-anchor refinement when dominance risk is unacceptable.

3.2. TSMM Stage 1: Closed-Form Initialization. The distribution of K_J under a DP prior has a well-known exact form (Equation (2.4); Antoniak, 1974), but it does not yield a simple closed-form inversion from (μ_K, σ_K^2) to (a, b) ; existing calibrations often rely on numerical search (e.g., Dorazio, 2009). TSMM therefore starts from a large- J proxy that is accurate enough to provide an effective initializer.

Algorithm 1 Two-Stage Moment Matching (TSMM) with Diagnostic Reporting

Inputs: J ; target moments (μ_K, σ_K^2) for K_J ; optional dominance tolerance (t, δ) .
Output: (a^*, b^*) defining $\alpha \sim \Gamma(a^*, b^*)$ and a diagnostic report.

- 1: *Stage 1 (closed-form initialization)*. Set $\mu_0 = \mu_K - 1$ and $c_J = \log J$. Compute $a_0 = \mu_0^2 / (\sigma_K^2 - \mu_0)$ and $b_0 = \mu_0 c_J / (\sigma_K^2 - \mu_0)$.
- 2: *Stage 2 (exact finite- J refinement)*. Starting from (a_0, b_0) , apply a Newton update in $(\log a, \log b)$ until the exact mixed moments satisfy $\mathbb{E}_{a,b}(K_J) = \mu_K$ and $\text{Var}_{a,b}(K_J) = \sigma_K^2$ (see [Section C](#) for moment evaluation via Gauss–Laguerre quadrature and analytic Jacobian derivation).
- 3: *Diagnostics*. Report summaries of $p(K_J)$ (e.g., median and central interval), $\Pr(w_1 > 0.5)$, $\Pr(w_1 > 0.9)$, and optionally $\mathbb{E}(\rho)$.
- 4: *Escalation (optional)*. If a dominance tolerance is provided and $\Pr(w_1 > t) > \delta$, apply [Algorithm 2](#).

We adopt a shifted approximation that respects the support constraint $K_J \geq 1$ ([Arratia et al., 2000](#); [Miller & Harrison, 2018](#); [Murugiah & Sweeting, 2012](#); [Vicentini & Jermyn, 2025](#)):

$$K_J - 1 \mid \alpha \approx \text{Poisson}(\alpha c_J), \quad c_J = \log J. \quad (3.1)$$

Under $\alpha \sim \Gamma(a, b)$, the Poisson–Gamma mixture implies a negative-binomial proxy for $K_J - 1$, and the inversion follows by matching the proxy mean $\mu_0 = \mu_K - 1$ and variance σ_K^2 :

$$a_0 = \frac{\mu_0^2}{\sigma_K^2 - \mu_0}, \quad b_0 = \frac{\mu_0 c_J}{\sigma_K^2 - \mu_0}. \quad (3.2)$$

[Section B](#) provides the full derivation of this closed-form mapping from the Gamma–Poisson conjugacy and documents the approximation quality at finite J .

The Stage 1 map is well-defined when $\mu_0 > 0$ and $\sigma_K^2 > \mu_0$, which is the natural regime when practitioners express non-degenerate uncertainty. When inputs fall close to the boundary (e.g., near-deterministic beliefs about K_J), numerical safeguards are applied (see [Appendix B.3.3](#) in the OSM for feasibility projection policy). Stage 1 is used as an initializer; Stage 2 removes finite- J bias.

3.3. TSMM Stage 2: Exact-Moment Refinement. Stage 1 is intentionally simple, but it can be biased for moderate J because the conditional distribution $K_J \mid \alpha$ is not Poisson: it is a sum of Bernoulli indicators and is typically underdispersed relative to the Poisson proxy ([Arratia et al., 2000](#)). Stage 2 therefore refines (a, b) so that the prior-predictive (mixed) moments of K_J under $\alpha \sim \Gamma(a, b)$ match the elicited targets exactly.

Let $\kappa_J(\alpha) = \mathbb{E}(K_J \mid \alpha)$ and $v_J(\alpha) = \text{Var}(K_J \mid \alpha)$. These conditional moments admit closed forms in terms of the digamma function $\psi(\cdot)$ and trigamma function $\psi_1(\cdot)$ (Antoniak, 1974):

$$\kappa_J(\alpha) = \alpha \{ \psi(\alpha + J) - \psi(\alpha) \}, \quad (3.3)$$

$$v_J(\alpha) = \kappa_J(\alpha) - \alpha^2 \{ \psi_1(\alpha) - \psi_1(\alpha + J) \}. \quad (3.4)$$

The derivation of these conditional moments from the Poisson–binomial representation and their derivatives with respect to α are provided in [Section A.2.3](#).

Stage 2 computes the exact mixed moments $\mathbb{E}_{a,b}(K_J) = \mathbb{E}_{a,b}\{\kappa_J(\alpha)\}$ and $\text{Var}_{a,b}(K_J) = \mathbb{E}_{a,b}\{v_J(\alpha)\} + \text{Var}_{a,b}\{\kappa_J(\alpha)\}$ by numerical integration with respect to the Gamma density, and then applies a Newton update to solve the two moment-matching equations. We implement the update in $(\log a, \log b)$ to maintain positivity and use analytic derivatives for stability. In typical applications, convergence occurs in a small number of iterations from the Stage 1 initializer. All derivations, Jacobian expressions via score-function identities, and convergence safeguards are provided in [Section C](#).

3.4. Dual-Anchor Protocol: Diagnose and Optionally Refine. Moment-matching on K_J anchors a prior on the partition structure, but it does not uniquely determine weight concentration. DCE therefore reports explicit weight diagnostics and offers an optional refinement when dominance risk is unacceptable.

3.4.1. Weight and Co-Clustering Diagnostics. Under the stick-breaking representation, the first weight satisfies $w_1 \mid \alpha \sim \text{Beta}(1, \alpha)$, so $\Pr(w_1 > t \mid \alpha) = (1 - t)^\alpha$. If $\alpha \sim \Gamma(a, b)$, then the tail probability integrates in closed form (Vicentini & Jermyn, 2025):

$$\Pr(w_1 > t \mid a, b) = \left(\frac{b}{b - \log(1 - t)} \right)^a, \quad 0 < t < 1. \quad (3.5)$$

We recommend reporting $\Pr(w_1 > 0.5)$ and $\Pr(w_1 > 0.9)$ as default summaries of moderate and extreme dominance risk. The derivation of this closed-form tail probability via Laplace transform integration, along with its gradients for optimization, is provided in Appendix E.3 of the OSM.

As an additional, unit-level summary, we optionally report the co-clustering probability $\rho = \sum_{h \geq 1} w_h^2$, which equals the probability that two randomly selected units belong to the same cluster. Under the DP, $\mathbb{E}(\rho \mid \alpha) = 1/(1 + \alpha)$, so $\mathbb{E}(\rho)$ under $\alpha \sim \Gamma(a, b)$ can be computed by one-dimensional integration (see Appendix E.4 in the OSM for closed-form expressions and variance computation).

Algorithm 2 Dual-Anchor Refinement (Optional)

Inputs: TSMM solution (a_K, b_K) ; dominance tolerance $\Pr(w_1 > t) \leq \delta$ (optional); trade-off weight $\lambda \in (0, 1]$ (optional).

Output: Refined (a^*, b^*) and a trade-off report.

- 1: Compute dominance diagnostics at (a_K, b_K) using [Equation \(3.5\)](#). If $\Pr(w_1 > t) \leq \delta$, stop and retain (a_K, b_K) .
- 2: Otherwise, define a trade-off criterion that penalizes (i) deviation from the target K_J moments and (ii) violation of the dominance tolerance; λ controls the relative emphasis.
- 3: Optimize the criterion over (a, b) using (a_K, b_K) as an initializer.
- 4: Report the refined (a^*, b^*) and the resulting changes in $\mathbb{E}(K_J)$, $\text{Var}(K_J)$, and $\Pr(w_1 > t)$, making the trade-off transparent.

3.4.2. Optional Refinement via Dual Anchors. When a practitioner provides a dominance tolerance (e.g., $\Pr(w_1 > 0.9) \leq \delta$) and the TSMM-calibrated prior violates it, we offer a dual-anchor refinement that makes the implied trade-off explicit. The refinement solves a constrained (or penalized) optimization problem over (a, b) that balances fidelity to the K_J targets against the desired dominance control. Varying the trade-off weight yields a Pareto frontier between cluster-count fit and dominance risk. Because this step is optional and application-dependent, the objective function, constraint handling, and numerical optimization details are provided in [Appendix E.5](#) of the OSM, including the Pareto frontier visualization for trade-off analysis.

3.5. Worked Example and Reporting Guidance. To illustrate the workflow, consider a design with $J = 50$ units where a practitioner expects about five substantively distinct clusters, with moderate uncertainty. Suppose the elicited targets are $\mu_K = \mathbb{E}(K_{50}) = 5$ and $\sigma_K^2 = \text{Var}(K_{50}) = 10$.

Stage 1 yields $\mu_0 = 4$ and $c_{50} = \log(50)$, producing the closed-form initializer $(a_0, b_0) \approx (2.667, 2.608)$. Stage 2 refines this to the exact-moment solution $(a^*, b^*) \approx (1.407, 1.076)$, which matches $\mathbb{E}(K_{50}) = 5$ and $\text{Var}(K_{50}) = 10$ by construction. Under this calibrated prior, the induced prior-predictive distribution $p(K_{50})$ has median approximately 4 with a central 90% interval approximately [1, 11]. Weight diagnostics give $\Pr(w_1 > 0.5) \approx 0.50$ and $\Pr(w_1 > 0.9) \approx 0.20$, and the optional co-clustering summary is $\mathbb{E}(\rho) \approx 0.52$.

If a practitioner were uncomfortable with a 20% probability that a randomly selected unit lies in a cluster exceeding 90% mass (i.e., if they required $\Pr(w_1 > 0.9) \leq 0.10$), DCE would retain the TSMM solution as the K -anchored baseline and then

invoke the optional dual-anchor refinement to explicitly trade off moment fidelity against dominance control.

Reporting Guidance. To promote transparency and reproducibility, we recommend that researchers using DCE-calibrated priors report the following core elements:

- (1) *Design specification:* J and why it is treated as fixed.
- (2) *Elicitation targets:* $\mathbb{E}(K_J)$ and $\text{Var}(K_J)$, with brief substantive justification.
- (3) *Calibrated hyperprior:* (a, b) for $\alpha \sim \Gamma(a, b)$ (shape–rate).
- (4) *Weight diagnostics:* $\Pr(w_1 > 0.5)$ and $\Pr(w_1 > 0.9)$ —these are *required*, not optional.
- (5) *Dual-Anchor summary (if applied):* the trade-off parameter λ and resulting changes in moments and dominance probability.

Weight diagnostics should be treated as routine: even without applying Dual-Anchor, reporting $\Pr(w_1 > 0.5)$ and $\Pr(w_1 > 0.9)$ makes the implied pooling geometry transparent and directly addresses the central concern of the SSI critique. A detailed reporting checklist, example reporting statement, and extended guidance are provided in Appendix E.6 of the OSM.

4. Simulation Study

Sections 2 and 3 established the theoretical framework for design-conditional prior elicitation and introduced the Two-Stage Moment Matching (TSMM) algorithm with optional Dual-Anchor refinement. This section evaluates whether these methods deliver on their promise: improving posterior inference for the number of occupied clusters K_J relative to conventional defaults and existing calibration approaches.

The simulation study addresses three substantive questions. First, how sensitive is posterior clustering to prior specification, and under what conditions does this sensitivity matter most? Second, does TSMM calibration meaningfully improve posterior recovery of the true cluster structure compared to vague defaults and the discrepancy-optimization approach of Dorazio (2009)? Third, when does the Dual-Anchor extension—which incorporates a weight concentration constraint—provide additional benefit beyond K -only calibration?

4.1. Simulation Design. Data-Generating Process. We adopt a hierarchical model that mirrors the multisite trial and meta-analysis settings described in [Section 1](#). Following Lee et al. (2025), let J exchangeable units have latent parameters

τ_j observed with estimation noise:

$$\hat{\tau}_j \mid \tau_j \sim N(\tau_j, \hat{s}e_j^2), \quad j = 1, \dots, J. \quad (4.1)$$

The true effects τ_j are drawn from a discrete K^* -component mixture with equal weights $\pi_k = 1/K^*$ and evenly-spaced component means on a symmetric grid $\mu_k \in [-2.5, 2.5]$. Within-cluster variation of $\sigma_{\text{within}} = 0.15$ creates distinguishable but overlapping clusters. Each simulated dataset guarantees that all K^* clusters are represented, ensuring that the “true” cluster count is meaningful as a reference. We fix $J = 100$ units, a sample size typical of educational multisite trials (Weiss et al., 2017), and set $\sigma_\tau = 0.25$.

Interpretation Caveat. In finite samples with overlapping mixture components, exact recovery of K^* is neither expected nor required. We use K^* as a reference line for comparing methods, not as a gold standard for exact recovery. The metrics reported below diagnose prior-induced shrinkage and collapse in a controlled setting; they are not claims about frequentist coverage for a structural truth.

Factorial Design and Informativeness Calibration. The simulation employs a 3×3 factorial design crossing two factors:

True cluster count ($K^* \in \{5, 10, 30\}$). These values span the range from “few substantive subgroups” to “many distinct patterns,” covering typical applied scenarios.

Data informativeness ($I \in \{0.2, 0.5, 0.8\}$). Following Lee et al. (2025), informativeness is defined as

$$I = \frac{\sigma_\tau^2}{\sigma_\tau^2 + \exp\left(\frac{1}{J} \sum_{j=1}^J \log \hat{s}e_j^2\right)}, \quad (4.2)$$

where the denominator adds a typical within-unit variance (geometric mean of $\hat{s}e_j^2$) to the between-unit variance σ_τ^2 . Low informativeness ($I = 0.2$) represents noisy settings where priors are critical; high informativeness ($I = 0.8$) represents data-rich settings where practitioners might assume “the data will speak for themselves.”

We generated standard errors via $\hat{s}e_j^2 = \kappa/n_j$ with $\kappa = 4$ and site sizes n_j drawn from a truncated lognormal distribution (coefficient of variation 0.5, minimum 5). Across the $R = 200$ replications per scenario, realized informativeness values were 0.194 (SD = 0.008), 0.500 (SD = 0.014), and 0.793 (SD = 0.009) for targets 0.2, 0.5, and 0.8, respectively.

Methods Compared. We compare four hyperprior specifications for $\alpha \sim \text{Gamma}(a, b)$:

- (1) **Vague**: $\text{Gamma}(1, 1)$, a common default that implies $\mathbb{E}(\alpha) = 1$ and substantial prior mass on small α values (e.g., Cao et al., 2024; Dunson et al., 2007; Ma & Chen, 2020; Mignemi & Manolopoulou, 2025).
- (2) **DORO-Unif**: The KL-divergence minimization approach of Dorazio (2009), calibrated to produce an approximately uniform prior on $K_J \in \{1, \dots, m\}$ where $m = \min\{2\mu_K - 1, J\}$.
- (3) **TSMM**: Two-Stage Moment Matching (Section 3.3), calibrated to match elicited targets $\mathbb{E}(K_J) = K^*$ and $\text{Var}(K_J) = \text{VIF} \cdot (\mu_K - 1)$ with $\text{VIF} = 2.5$ (medium confidence).
- (4) **Dual-Anchor**: TSMM with optional weight constraint (Section 3.4), triggered when $\Pr(w_1 > 0.5) > 0.40$ under the TSMM solution, targeting $\Pr(w_1 > 0.5) \leq 0.25$ with trade-off weight $\lambda = 0.70$.

For each replication, we fit a DP mixture model via MCMC (two chains of 1,000 iterations with 500 burn-in) and record the posterior mean cluster count $\mathbb{E}[K_J \mid \text{data}]$, collapse probability $\Pr(K_J = 1 \mid \text{data})$, 95% credible interval for K_J , and posterior mean of α . Full MCMC diagnostics, additional baselines (including χ^2 -DORO), and the complete hyperprior parameter table are reported in Section F of the OSM.

4.2. The Hazard of Default Priors: Cluster Collapse. A central premise of Bayesian analysis is that the influence of the prior diminishes as data accumulate. However, our results demonstrate that in finite-sample mixture models ($J = 100$), the choice of hyperprior on α remains consequential even when data appear informative (Matza & Bistritz, 2021).

Systematic Failure of Vague Defaults. Figure 3 displays the central finding: regardless of the true cluster count or data informativeness, the Vague prior produces posterior estimates $\mathbb{E}[K_J \mid \text{data}] \approx 2$. This systematic collapse occurs because $\text{Gamma}(1, 1)$ places substantial prior mass near $\alpha = 0$, inducing a strong penalty on complexity that the likelihood cannot easily overwhelm. Even when $K^* = 30$ and $I = 0.8$ —a setting with 30 true clusters and relatively precise measurements—the Vague prior yields $\mathbb{E}[K_J \mid \text{data}] = 1.83$ ($\text{SD} = 0.65$).

We term this phenomenon *cluster collapse*: the posterior assigns substantial probability to $K_J = 1$, implying that all units belong to a single cluster. The Vague prior exhibits a collapse rate of approximately 60–67% across all scenarios—that is, in more than half of all analyses, the posterior concentrates on single-cluster solutions regardless of whether the true structure involves 5, 10, or 30 clusters (Table 2).

Posterior Expected Cluster Count by Method and Data Informativeness

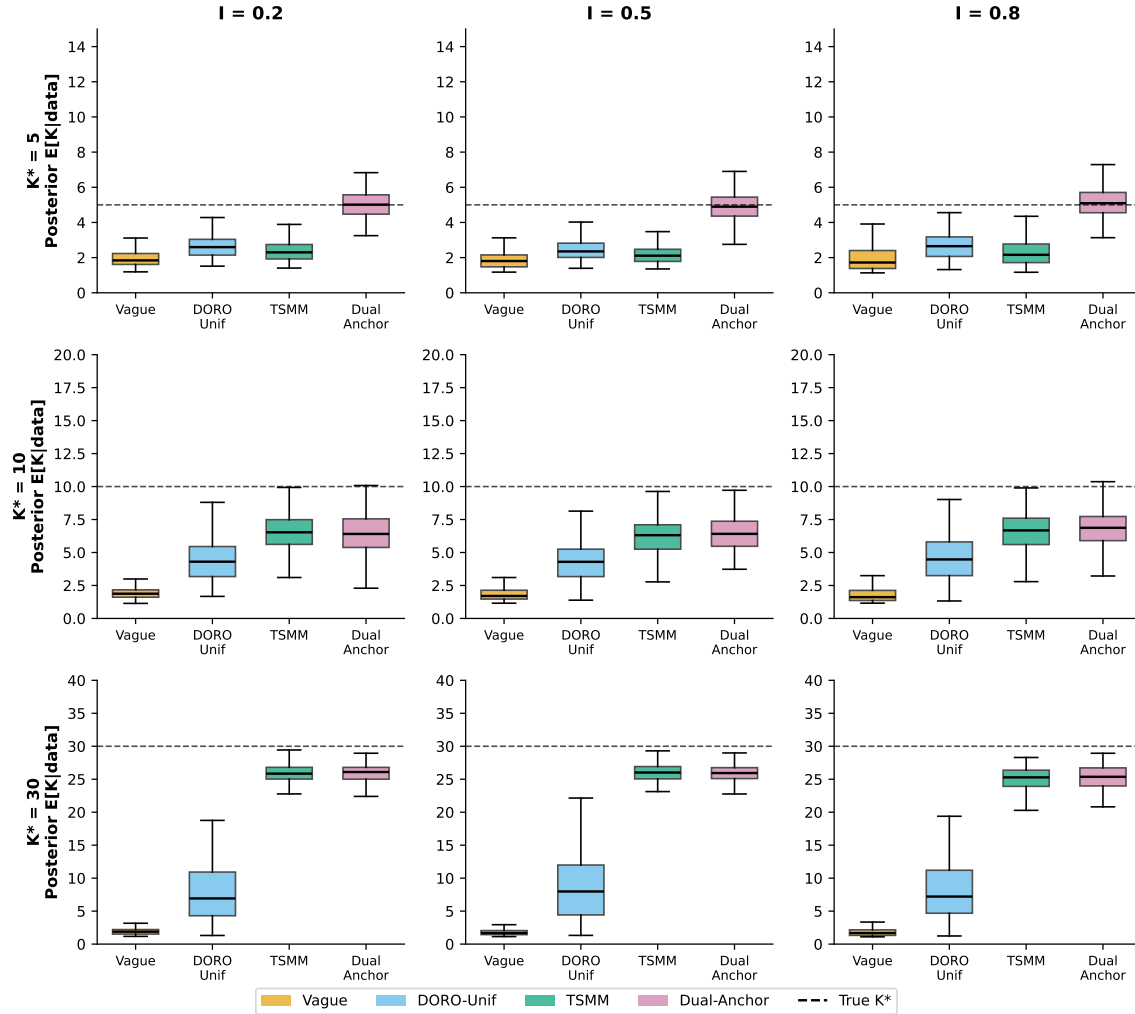


FIGURE 3. Posterior expected cluster count $\mathbb{E}[K_J \mid \text{data}]$ by method and scenario. Rows: $K^* \in \{5, 10, 30\}$; columns: $I \in \{0.2, 0.5, 0.8\}$. Boxplots across 200 replications; dashed lines indicate true K^* .

TSMM Substantially Improves Recovery. The TSMM-calibrated prior achieves a qualitative improvement by explicitly encoding a design-conditional expectation. For $K^* = 30$ with $I = 0.2$, TSMM yields $\mathbb{E}[K_J \mid \text{data}] = 25.89$ (SD = 1.30), compared to 1.96 under the Vague prior—a shift from recovering 7% to 86% of the true cluster structure. The 95% credible intervals achieve 100% coverage for $K^* = 30$, and collapse probability drops to 0%.

The improvement is most pronounced when the gap between the elicited target and the Vague-induced posterior is largest. For $K^* = 30$, where $\text{Gamma}(1, 1)$ implies

$\mathbb{E}(K_J) \approx 5$ a priori, the mismatch is severe and TSMM’s correction is dramatic. For $K^* = 5$, where the Vague prior is closer to the target, TSMM provides more modest improvement—and, as we show next, encounters a limitation that motivates the Dual-Anchor extension.

DORO-Unif: Partial but Insufficient. The Dorazio (2009) approach improves upon the Vague prior but falls substantially short of TSMM. For $K^* = 30$ with $I = 0.2$, DORO-Unif yields $\mathbb{E}[K_J | \text{data}] = 8.04$ ($\text{SD} = 4.96$), recovering only about 25% of the true cluster count. By targeting a uniform distribution over the entire range $\{1, \dots, J\}$, it spreads probability mass too thinly, failing to provide the regularization needed to support complex partition structures.

4.3. Weight Control and the Dual-Anchor Advantage. TSMM’s Vulnerability for Small K^* . A critical pattern emerges for $K^* = 5$: TSMM reduces collapse probability relative to the Vague prior, but the reduction is modest (from $\sim 60\%$ to $\sim 48\text{--}54\%$). This phenomenon aligns with the “unintended prior” critique of Vicentini and Jermyn (2025): a prior calibrated solely to match the moments of K_J can inadvertently imply a high probability of a dominant cluster weight.

Recall from [Section 3.4](#) that the TSMM solution for $K^* = 5$ with medium confidence yields $\Pr(w_1 > 0.5) \approx 0.56$ —a 56% prior probability that a randomly selected unit belongs to a cluster exceeding half the total mass. This weight concentration translates into posterior vulnerability: when the data are noisy and the likelihood mildly favors parsimony, the prior’s tolerance for dominance permits the posterior to concentrate on single-cluster solutions.

Dual-Anchor Provides Targeted Protection. The Dual-Anchor extension addresses this vulnerability by incorporating a constraint on weight dominance. When TSMM’s solution exceeds the dominance tolerance ($\Pr(w_1 > 0.5) > 0.40$), the algorithm adjusts the hyperparameters to constrain weight concentration while preserving K -matching as closely as possible.

For $K^* = 5$, Dual-Anchor reduces the collapse probability from TSMM’s $\sim 48\%$ to approximately 10–14%—a five-fold reduction. This protection yields dramatically improved estimation: $\mathbb{E}[K_J | \text{data}] = 5.04$ (essentially unbiased) with RMSE of only 0.76, compared to TSMM’s RMSE of 2.70. The 95% credible intervals achieve 100% coverage ([Table 2](#)).

Crucially, for $K^* \geq 10$, the Dual-Anchor mechanism does not activate because TSMM’s solution already satisfies the dominance tolerance. The results are virtually identical to TSMM, confirming that the constraint is adaptive—it only intervenes

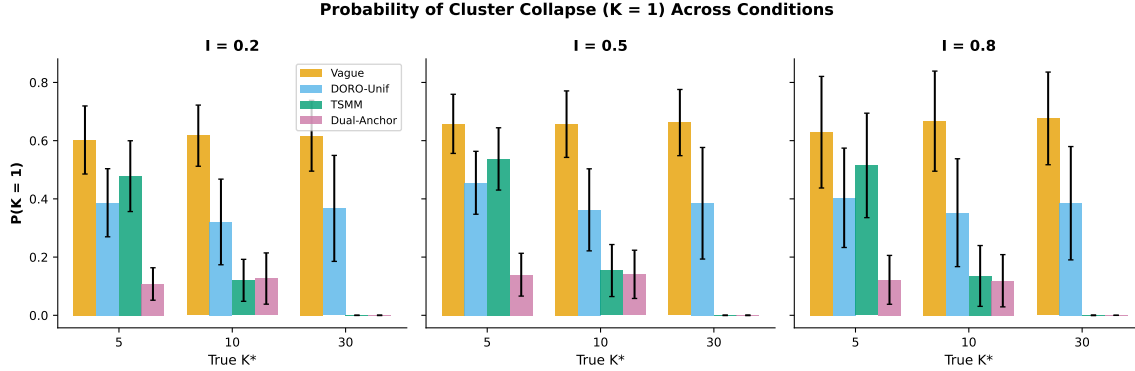


FIGURE 4. Probability of cluster collapse $\Pr(K_J = 1 | \text{data})$ across conditions. Bars: mean collapse probability; error bars: SD across 200 replications.

when the K -calibrated prior conflicts with the weight stability required for robust clustering.

4.4. Informativeness Does Not Rescue Poor Priors. A perhaps surprising finding is that increasing data informativeness from $I = 0.2$ to $I = 0.8$ produces only modest improvements for poorly specified priors. Figure 3 shows that the method rankings are essentially unchanged across informativeness levels: Vague priors collapse regardless of I , and the relative advantages of TSMM and Dual-Anchor persist even when the data are “informative.”

This pattern challenges the intuition that “the data will overwhelm the prior” when information is abundant. With $J = 100$ units and the DGP’s overlapping cluster structure, even $I = 0.8$ does not provide sufficient likelihood information to overcome a prior that concentrates mass near $\alpha \approx 0$. The posterior for K_J remains dominated by the prior’s structural assumptions.

The practical implication is that principled prior specification matters even in settings that might appear data-rich. Researchers cannot rely on large sample sizes or precise measurements to compensate for default priors that encode inappropriate clustering assumptions.

4.5. Summary and Practical Implications. Table 2 consolidates the main findings for the low-information setting ($I = 0.2$), which represents the most challenging—and arguably most policy-relevant—scenario for multisite trials and meta-analyses.

TABLE 2. Summary of Method Performance in Low-Information Setting ($I = 0.2$)

K^*	Method	$\mathbb{E}[K \mid \text{data}]$	Bias	RMSE	$\Pr(K=1)$	Coverage	CI Width
5	Vague	1.99 (0.55)	-3.01	3.06	0.602	0.775	5.84
5	DORO-Unif	2.64 (0.63)	-2.36	2.44	0.387	0.955	6.73
5	TSMM	2.37 (0.61)	-2.63	2.70	0.478	0.900	6.58
5	Dual-Anchor	5.04 (0.76)	+0.04	0.76	0.108	1.000	10.83
10	Vague	1.95 (0.49)	-8.05	8.07	0.617	0.175	5.97
10	DORO-Unif	4.51 (1.75)	-5.49	5.76	0.321	0.880	14.37
10	TSMM	6.54 (1.27)	-3.46	3.69	0.120	1.000	16.01
10	Dual-Anchor	6.37 (1.47)	-3.63	3.91	0.126	0.990	15.49
30	Vague	1.96 (0.55)	-28.04	28.04	0.617	0.000	5.82
30	DORO-Unif	8.04 (4.96)	-21.96	22.51	0.367	0.570	30.08
30	TSMM	25.89 (1.30)	-4.11	4.31	0.000	1.000	31.18
30	Dual-Anchor	25.97 (1.39)	-4.03	4.27	0.000	1.000	31.47

Note. Values are Mean (SD) across 200 replications. Coverage refers to whether K^* lies within the 95% posterior interval for K_J . Full results for all informativeness levels, confidence-level sensitivity analysis, and computational benchmarks are provided in [Section F](#) of the OSM (Tables F.4–F.8).

Taken together, these simulations support three practical conclusions. First, defaults can be systematically misleading in finite samples. Even when data are moderately informative, vague hyperpriors may induce posterior collapse toward one or two clusters. The failure of $\text{Gamma}(1, 1)$ is not a matter of conservative inference but of systematic bias that cannot be overcome by additional data. Second, moment-based elicitation (TSMM) is an effective first-line remedy when analysts can articulate a plausible range for the number of occupied clusters in their design. TSMM reduces MSE by 76–98% relative to the Vague prior across scenarios. Third, weight diagnostics are not optional when small- μ_K elicitation is used. In precisely those settings where practitioners most naturally think in terms of a small number of subtypes (e.g., “a few effect patterns”), the implied size-biased weights can still concentrate strongly, and Dual-Anchor refinement can materially change posterior behavior.

In line with the reporting checklist in [Section 3.5](#), we recommend that applied analyses disclose the elicited targets (μ_K, σ_K^2) , the resulting hyperparameters (a, b) , and at least one dominance-risk diagnostic (e.g., $\Pr(w_1 > 0.5)$). Based on these findings, we recommend Dual-Anchor as the default approach for design-conditional elicitation

in applications where the design size J is fixed and protection against cluster collapse is important.

5. Discussion

This paper introduced Design-Conditional Elicitation (DCE), a framework for translating practitioner beliefs about cluster structure into Gamma hyperpriors for the DP concentration parameter. DCE addresses three gaps in existing practice: the *translation gap* between substantive intuition and formal hyperparameters, the *computational gap* that makes principled calibration burdensome, and the *coherence gap* whereby K_J -calibrated priors can produce unintended weight behavior. By shifting elicitation focus from the abstract parameter α to the tangible, design-specific question—*among these J units, how many distinct patterns do we anticipate?*—while ensuring weight implications are diagnosed and controlled, DCE provides a complete workflow for principled prior specification.

5.1. Summary of Contributions. Three features distinguish DCE from existing approaches. First, Two-Stage Moment Matching (TSMM) achieves machine-precision calibration with minimal overhead. The closed-form initialization followed by Newton refinement converges rapidly, yielding approximately $900\times$ speedup relative to grid-based calibration. This efficiency makes principled prior design a practical component of applied analysis rather than an aspirational add-on.

Second, the framework makes explicit what is often implicit: matching a target distribution for K_J does not automatically produce a “neutral” prior on weight concentration. [Figure 1](#) illustrated that a hyperprior calibrated for $\mathbb{E}[K_{50}] \approx 5$ can imply nearly 50% probability that a random unit belongs to a majority cluster. By requiring diagnostics—specifically $\Pr(w_1 > 0.5)$ and $\Pr(w_1 > 0.9)$ —and providing Dual-Anchor refinement when needed, DCE ensures weight implications are transparent.

Third, the simulation study demonstrated that default hyperpriors can produce systematically misleading inferences. Under $\text{Gamma}(1, 1)$, collapse probabilities exceeded 60% regardless of true cluster count or informativeness—increasing informativeness from $I = 0.2$ to $I = 0.8$ did not rescue poorly specified priors. TSMM reduced RMSE dramatically (e.g., from 28.04 to 4.31 for $K^* = 30$), while Dual-Anchor provided additional protection for small- K^* scenarios where dominance risk is elevated (reducing collapse from 48% to 10–14% for $K^* = 5$). These results support a practical takeaway: in moderate- J problems, vague defaults can behave as strong pooling

priors, and increasing data informativeness does not automatically neutralize that effect.

5.2. Design-Conditional Elicitation and the SSD/SSI Debate. A recent critique by Vicentini and Jermyn (2025) identifies a tension between two approaches to prior specification on α : *sample-size-dependent (SSD)* methods that calibrate the prior to achieve a target behavior at a particular J and *sample-size-independent (SSI)* methods that anchor the prior on quantities invariant to J , such as stick-breaking weights.

The critique has merit. When the sample size varies (as in streaming settings) or when multiple datasets share a common prior on α (as in hierarchical BNP models), an SSD prior produces a “sequence of priors” that depends on design context. Vicentini and Jermyn (2025) argue that SSI perspectives—anchoring on weight summaries rather than cluster counts—provide a more principled foundation in such contexts.

However, the applications motivating this paper—multisite trials, meta-analyses, and fixed-design studies—share a common structural feature: J is fixed by design rather than accumulating over time. In such settings, the analyst typically targets a finite-population estimand, and “what happens as $J \rightarrow \infty$ ” is less directly relevant. As Vicentini and Jermyn (2025) themselves acknowledge, “in applications where J is always fixed and prior belief can be naturally expressed in terms of K_J , SSD priors may still have a place.” In this regime, design-conditional elicitation via K_J is not a pathological dependence; it is an explicit encoding of a substantively meaningful question: *among these J units, how many distinct patterns do we anticipate?*

DCE operationalizes this fixed- J perspective while absorbing the core insight of the SSI critique: calibrating on K_J alone can produce unintended weight behavior. Our resolution treats K_J as the primary anchor because it is cognitively accessible, then uses weight diagnostics as a mandatory check. The Dual-Anchor protocol represents a synthesis: it preserves K_J -based interpretability while making explicit the trade-off between partition and weight perspectives. This synthesis is supported by three safeguards: weight diagnostics are required (not optional) for any K -calibrated prior; Dual-Anchor produces explicit trade-off reports when dominance tolerance is violated; and practitioners can reverse the emphasis, using weight beliefs as the primary anchor with K_J implications as diagnostics.

In summary, SSD and SSI are best understood as addressing *different inferential targets*—SSD for finite- J design-conditional questions, SSI for asymptotic or cross- J coherence. For the fixed- J settings motivating this paper, K_J -based elicitation with

weight transparency offers a practical and defensible workflow. The trade-off between partition and weight perspectives is not a defect to be hidden; it is a substantive choice that should be reported.

5.3. Limitations and Future Directions. Several limitations warrant acknowledgment. First, the methods assume α follows a Gamma distribution; alternative structures such as partition-level Stirling–gamma priors (Zito et al., 2024) may offer advantages in certain contexts. Extending DCE to non-Gamma families is a natural direction for future work. Second, the framework is designed for fixed- J settings; streaming data, sequential updates, or hierarchical models with shared α require approaches where SSI perspectives become more directly relevant (Vicentini & Jermyn, 2025). Third, the quality of calibrated priors depends on the elicited inputs (μ_K, σ_K^2) . When practitioners have limited intuition for cluster granularity, sensitivity analysis over plausible inputs is advisable—and TSMM’s computational efficiency makes such analysis feasible (Giordano et al., 2023). Finally, while the simulation study focused on $J = 100$ with specific data-generating conditions, performance may vary in more extreme settings; extended simulations addressing confidence-level sensitivity and alternative baselines are provided in [Section F](#) of the OSM, but practitioners should exercise judgment when extrapolating.

Several extensions merit investigation. Extending DCE to other Bayesian nonparametric priors—particularly the Pitman–Yor process (Pitman & Yor, 1997) and hierarchical DP models—would broaden applicability. Preliminary results suggest analogous moment-matching calibrations are available for the two-parameter Poisson–Dirichlet process (Ishwaran & Zarepour, 2000); extending to HDPs where α governs top-level atoms and γ governs group-level clustering would serve the multilevel modeling community. Additionally, integrating DCE with Bayesian workflow toolkits such as `bayesplot` and `loo` (Gelman et al., 2020; Roos et al., 2015) would lower barriers to principled prior specification and facilitate end-to-end reproducibility.

5.4. Conclusion. As Bayesian nonparametrics matures from a niche statistical tool to a standard engine for flexible inference in the social sciences, the “black box” of prior specification must be opened. The question is not *whether* to use informative priors—since all priors are informative in low-to-moderate information regimes—but *how* to make those priors transparent, interpretable, and aligned with the study design (Richardson & Green, 1997). The Design-Conditional Elicitation framework provides the necessary tools: practitioners can articulate beliefs in the language of cluster

granularity, translate those beliefs into calibrated hyperparameters with machine-precision accuracy, diagnose unintended weight implications, and report complete prior specifications that enable scrutiny and replication. The accompanying **DPprior** R package operationalizes this workflow with reproducible diagnostics and reporting templates (see Appendix G in the OSM for installation, API reference, and worked examples). By harnessing the flexibility of the Dirichlet process without surrendering control of the underlying assumptions, researchers can move toward a more principled and reproducible practice of Bayesian nonparametric modeling in educational and behavioral research.

References

Abramowitz, M., & Stegun, I. A. (1964). *Handbook of mathematical functions with formulas, graphs, and mathematical tables*. National Bureau of Standards. [36, 60, 69].

Antonelli, J., Trippa, L., & Haneuse, S. (2016). Mitigating bias in generalized linear mixed models: The case for Bayesian nonparametrics. *Statistical Science*, 31(1), 80–95. <https://doi.org/10.1214/15-STS533> [2, 4].

Antoniak, C. E. (1974). Mixtures of Dirichlet processes with applications to Bayesian nonparametric problems. *The Annals of Statistics*, 2(6), 1152–1174. <https://doi.org/10.1214/aos/1176342871> [7, 11, 13, 32, 35, 42].

Arratia, R., Barbour, A. D., & Tavaré, S. (2000). The number of components in a logarithmic combinatorial structure. *The Annals of Applied Probability*, 10(2), 331–361. <https://doi.org/10.1214/aoap/1019487347> [12, 34, 38, 41, 42].

Arratia, R., Barbour, A. D., & Tavaré, S. (2003). *Logarithmic combinatorial structures: A probabilistic approach*. European Mathematical Society. <https://doi.org/10.4171/000> [38, 47, 59].

Barbour, A. D., & Hall, P. (1984). On the rate of Poisson convergence. *Mathematical Proceedings of the Cambridge Philosophical Society*, 95(3), 473–480. <https://doi.org/10.1017/S0305004100061806> [59].

Barbour, A. D., Holst, L., & Janson, S. (1992). *Poisson approximation*. Oxford University Press. <https://doi.org/10.1093/oso/9780198522355.001.0001> [59].

Barbour, A. D., & Xia, A. (1999). Poisson perturbations. *ESAIM: Probability and Statistics*, 3, 131–150. <https://doi.org/10.1051/ps:1999106> [42].

Blackwell, D., & MacQueen, J. B. (1973). Ferguson distributions via Pólya urn schemes. *The Annals of Statistics*, 1(2), 353–355. <https://doi.org/10.1214/aos/1176342372> [32, 33].

Bonafos, G., Bourot, C., Pudlo, P., Freyermuth, J.-M., Reboul, L., Tronçon, S., & Rey, A. (2024). Dirichlet process mixture model based on topologically augmented signal representation for clustering infant vocalizations. [2, 3].

Burr, D., & Doss, H. (2005). A Bayesian semiparametric model for random-effects meta-analysis. *Journal of the American Statistical Association*, 100(469), 242–251. <https://doi.org/10.1198/016214504000001024> [2].

Cao, W., Chu, H., Hanson, T., & Siegel, L. (2024). A Bayesian nonparametric meta-analysis model for estimating the reference interval. *Statistics in Medicine*, 43(10), 1905–1919. <https://doi.org/10.1002/sim.10001> [2, 3, 6].

Cardoso, P., Dennis, J. M., Bowden, J., Shields, B. M., McKinley, T. J., & MASTERMIND Consortium. (2024). Dirichlet process mixture models to impute missing predictor data in counterfactual prediction models: An application to predict optimal type 2 diabetes therapy. *BMC Medical Informatics and Decision Making*, 24(1), 12. <https://doi.org/10.1186/s12911-023-02400-3> [2].

Casella, G., & Berger, R. L. (2002). *Statistical inference* (2nd). Duxbury. [49].

Congdon, P. D. (2019). *Bayesian hierarchical models: With applications using R* (2nd). Chapman; Hall/CRC. [7].

Daniels, M. J., Linero, A., & Roy, J. (2023). *Bayesian nonparametrics for causal inference and missing data*. Chapman; Hall/CRC. [2].

Dennis, J. E., Jr., & Schnabel, R. B. (1996). *Numerical methods for unconstrained optimization and nonlinear equations* [Originally published by Prentice-Hall, 1983]. SIAM. <https://doi.org/10.1137/1.9781611971200> [49, 53].

Dorazio, R. M. (2009). On selecting a prior for the precision parameter of Dirichlet process mixture models. *Journal of Statistical Planning and Inference*, 139(9), 3384–3390. <https://doi.org/10.1016/j.jspi.2009.03.009> [2–4, 11, 35, 37, 56, 79, 84].

Dorazio, R. M., Mukherjee, B., Zhang, L., Ghosh, M., Jelks, H. L., & Jordan, F. (2008). Modeling unobserved sources of heterogeneity in animal abundance using a Dirichlet process prior. *Biometrics*, 64(2), 635–644. <https://doi.org/10.1111/j.1541-0420.2007.00873.x> [4].

Dunson, D. B., Xue, Y., & Carin, L. (2008). The matrix stick-breaking process: Flexible Bayes meta-analysis. *Journal of the American Statistical Association*, 103(481), 317–327. <https://doi.org/10.1198/01621450700001364> [2].

Escobar, M. D., & West, M. (1995). Bayesian density estimation and inference using mixtures. *Journal of the American Statistical Association*, 90(430), 577–588. <https://doi.org/10.1080/01621459.1995.10476550> [6, 7].

Ferguson, T. S. (1973). A Bayesian analysis of some nonparametric problems. *The Annals of Statistics*, 1(2), 209–230. <https://doi.org/10.1214/aos/1176342360> [6, 33].

Finch, H., & Edwards, J. M. (2016). Rasch model parameter estimation in the presence of a nonnormal latent trait using a nonparametric Bayesian approach. *Educational and Psychological Measurement*, 76(4), 662–684. <https://doi.org/10.1177/0013164415608418> [2].

Gelman, A., Vehtari, A., Simpson, D., Margossian, C. C., Carpenter, B., Yao, Y., Kennedy, L., Gabry, J., Bürkner, P.-C., & Modrák, M. (2020). Bayesian workflow. *arXiv preprint arXiv:2011.01808*. <https://doi.org/10.48550/arXiv.2011.01808> [24].

Gill, J., & Casella, G. (2009). Nonparametric priors for ordinal Bayesian social science models: Specification and estimation. *Journal of the American Statistical Association*, 104(486), 453–464. <https://doi.org/10.1198/jasa.2009.0039> [2].

Giordano, R., Liu, R., Jordan, M. I., & Broderick, T. (2023). Evaluating sensitivity to the stick-breaking prior in Bayesian nonparametrics (with discussion). *Bayesian Analysis*, 18(1), 287–366. <https://doi.org/10.1214/22-BA1309> [2, 4, 24].

Greve, J., Grün, B., Malsiner-Walli, G., & Frühwirth-Schnatter, S. (2022). Spying on the prior of the number of data clusters and the partition distribution in Bayesian cluster analysis. *Australian & New Zealand Journal of Statistics*, 64(2), 205–229. <https://doi.org/10.1111/anzs.12350> [2, 3].

Hanson, T. E., Branscum, A. J., & Johnson, W. O. (2005). Bayesian nonparametric modeling and data analysis: An introduction. In *Handbook of statistics* (pp. 245–278, Vol. 25). Elsevier. [6].

Ishwaran, H., & Zarepour, M. (2000). Markov chain Monte Carlo in approximate Dirichlet and beta two-parameter process hierarchical models. *Biometrika*, 87(2), 371–390. <https://doi.org/10.1093/biomet/87.2.371> [6, 24].

Iwashige, F., & Hashimoto, S. (2025). Bayesian mixture modeling using a mixture of finite mixtures with normalized inverse Gaussian weights. *arXiv preprint arXiv:2501.18854* [2].

Jackson, D., & White, I. R. (2018). When should meta-analysis avoid making hidden normality assumptions? *Biometrical Journal*, 60(6), 1040–1058. <https://doi.org/10.1002/bimj.201800071> [2].

Johnson, N. L., Kotz, S., & Kemp, A. W. (2005). *Univariate discrete distributions* (3rd). Wiley. <https://doi.org/10.1002/0471715816> [44].

Kingman, J. F. C. (1975). Random discrete distributions. *Journal of the Royal Statistical Society: Series B (Methodological)*, 37(1), 1–22. <https://doi.org/10.1111/j.2517-6161.1975.tb01024.x> [68].

Kottas, A. (2006). Dirichlet process mixtures of beta distributions, with applications to density and intensity estimation. *Workshop on Learning with Nonparametric Bayesian Methods, 23rd International Conference on Machine Learning (ICML)* [3].

Kyung, M., Gill, J., & Casella, G. (2010). Estimation in Dirichlet random effects models. *The Annals of Statistics*, 38(2), 979–1009. <https://doi.org/10.1214/09-AOS731> [2].

Le Cam, L. (1960). An approximation theorem for the Poisson binomial distribution. *Pacific Journal of Mathematics*, 10(4), 1181–1197. <https://doi.org/10.2140/pjm.1960.10.1181> [38, 41, 42, 47, 59].

Lee, J., Che, J., Rabe-Hesketh, S., Feller, A., & Miratrix, L. (2025). Improving the estimation of site-specific effects and their distribution in multisite trials. *Journal of Educational and Behavioral Statistics*, 50(5), 731–764. <https://doi.org/10.3102/10769986241254286> [2, 3, 76, 78, 79, 82, 84].

Leslie, D. S., Kohn, R., & Nott, D. J. (2007). A general approach to heteroscedastic linear regression. *Statistics and Computing*, 17(2), 131–146 [3].

Ma, Z., & Chen, G. (2020). Bayesian semiparametric latent variable model with DP prior for joint analysis: Implementation with nimble. *Statistical Modelling*, 20(1), 71–95 [3].

Matza, A., & Bistrizt, Y. (2021). Infinite Gaussian mixture modeling with an improved estimation of the number of clusters. *Proceedings of the AAAI Conference on Artificial Intelligence*, 35(10), 8921–8929 [2].

McCullagh, P., & Yang, J. (2008). How many clusters? *Bayesian Analysis*, 3(1), 101–120. <https://doi.org/10.1214/08-BA304> [3].

Mignemi, G., & Manolopoulou, I. (2025). Bayesian nonparametric models for multiple raters: A general statistical framework [Advance online publication]. *Psychometrika*. <https://doi.org/10.1017/psy.2025.10035> [2, 3].

Miller, J. W., & Harrison, M. T. (2018). Mixture models with a prior on the number of components. *Journal of the American Statistical Association*, 113(521), 340–356. <https://doi.org/10.1080/01621459.2016.1255636> [7, 12].

Murugiah, S., & Sweeting, T. (2012). Selecting the precision parameter prior in Dirichlet process mixture models. *Journal of Statistical Planning and Inference*, 142(7), 1947–1959. <https://doi.org/10.1016/j.jspi.2012.02.013> [2, 3, 12, 35, 37].

Muthukumarana, S., & Tiwari, R. C. (2016). Meta-analysis using Dirichlet process. *Statistical Methods in Medical Research*, 25(1), 352–365. <https://doi.org/10.1177/0962280212453891> [2].

Navarro, D. J., Griffiths, T. L., Steyvers, M., & Lee, M. D. (2006). Modeling individual differences using Dirichlet processes. *Journal of Mathematical Psychology*, 50(2), 101–122. <https://doi.org/10.1016/j.jmp.2005.11.006> [2, 7].

Neal, R. M. (2000). Markov chain sampling methods for Dirichlet process mixture models. *Journal of Computational and Graphical Statistics*, 9(2), 249–265. <https://doi.org/10.1080/10618600.2000.10474879> [3].

Nocedal, J., & Wright, S. J. (2006). *Numerical optimization* (2nd). Springer. <https://doi.org/10.1007/978-0-387-40065-5> [49, 73].

Ortega, J. M., & Rheinboldt, W. C. (1970). *Iterative solution of nonlinear equations in several variables* [Reprinted by SIAM, 2000]. Academic Press. <https://doi.org/10.1137/1.9780898719468> [49, 53].

Paganin, S., Paciorek, C. J., Wehrhahn, C., Rodríguez, A., Rabe-Hesketh, S., & de Valpine, P. (2023). Computational strategies and estimation performance with Bayesian semiparametric item response theory models. *Journal of Educational and Behavioral Statistics*, 48(2), 147–188. <https://doi.org/10.3102/10769986221136105> [2, 3].

Pitman, J. (1996). Random discrete distributions invariant under size-biased permutation. *Advances in Applied Probability*, 28(2), 525–539. <https://doi.org/10.2307/1428070> [32, 64, 68].

Pitman, J. (2006). *Combinatorial stochastic processes* (Vol. 1875). Springer. <https://doi.org/10.1007/b11601500> [33, 63, 64, 68].

Pitman, J., & Yor, M. (1997). The two-parameter Poisson-Dirichlet distribution derived from a stable subordinator. *The Annals of Probability*, 25(2), 855–900. <https://doi.org/10.1214/aop/1024404422> [24].

Qiu, M., Paganin, S., Ohn, I., & Lin, L. (2025). Bayesian nonparametric latent class analysis with different item types [Advance online publication]. *Psychological Methods*. <https://doi.org/10.1037/met0000728> [2].

Richardson, S., & Green, P. J. (1997). On Bayesian analysis of mixtures with an unknown number of components (with discussion). *Journal of the Royal Statistical Society Series B: Statistical Methodology*, 59(4), 731–792. <https://doi.org/10.1111/1467-9868.00095> [24].

Roos, M., Martins, T. G., Held, L., & Rue, H. (2015). Sensitivity analysis for Bayesian hierarchical models. *Bayesian Analysis*, 10(2), 321–349. <https://doi.org/10.1214/14-BA909> [24].

Rubin, D. B. (1981). Estimation in parallel randomized experiments. *Journal of Educational Statistics*, 6(4), 377–401. <https://doi.org/10.3102/10769986006004377> [77].

Sethuraman, J. (1994). A constructive definition of Dirichlet priors. *Statistica Sinica*, 4(2), 639–650 [6, 7, 34, 63, 64].

Vicentini, C., & Jermyn, I. H. (2025). Prior selection for the precision parameter of Dirichlet process mixtures. <https://arxiv.org/abs/2502.00864> [4, 7, 9, 10, 12, 13, 23, 24, 34, 39, 41, 44, 63, 66, 69, 70, 76].

Watterson, G. A. (1974). The sampling theory of selectively neutral alleles. *Advances in Applied Probability*, 6(3), 463–488. <https://doi.org/10.2307/1426228> [34].

Zito, A., Rigon, T., & Dunson, D. B. (2024). Bayesian nonparametric modeling of latent partitions via Stirling-gamma priors [Advance publication]. *Bayesian Analysis*, 1–28. <https://doi.org/10.1214/24-BA1463> [24, 39, 41, 44].

Online Supplemental Materials

Design-Conditional Prior Elicitation for Dirichlet Process Mixtures: A Unified Framework for Cluster Counts and Weight Control

JoonHo Lee

Contents

Online Supplemental Materials	32
Appendix A. DP/CRP Preliminaries and Exact K_J Distribution	32
A.1. Purpose and Scope	32
A.2. Distributional Theory	33
Appendix B. Stage 1 Closed-Form Derivation and Approximation Theory	41
B.1. Purpose and Scope	41
B.2. The Shifted Poisson–Gamma Proxy	41
B.3. The A1 Closed-Form Inversion	44
B.4. Confidence-to-Variance Mapping	46
B.5. Approximation Quality: When Is Stage 1 Sufficient?	47
Appendix C. Stage 2 Newton Refinement: Full Algorithm and Convergence	49
C.1. Purpose and Scope	49
C.2. Problem Statement and Target Equations	50
C.3. Jacobian Derivation via Score Identities	50
C.4. Algorithm C.1: A2-MN (Exact-Moment Newton Refinement)	52
C.5. Convergence: What Is Guaranteed (and What Is Not)	53
C.6. Worked Example and Typical Iteration Counts	54
C.7. Optional: A2-KL Refinement (Distributional Target on K_J)	55
Appendix D. Approximation Error Bounds and Finite- J Analysis	56
D.1. Purpose and Scope	56
D.2. Three-Way Error Decomposition	56
D.3. Conditional (Fixed- α) Bounds	58
D.4. Marginal (Gamma-Mixed) Bounds	61
D.5. When Is A2 Necessary? Practical Threshold Conditions	62
Appendix E. Weight Distribution Theory and Dual-Anchor Framework	63
E.1. Purpose and Scope	63

E.2.	Stick-Breaking Weights and Size-Biased Interpretation	63
E.3.	Closed-Form Marginal Distribution of w_1	65
E.4.	Co-Clustering Probability ρ	68
E.5.	Dual-Anchor Calibration Framework	70
E.6.	Interpretive Guidelines for Practitioners	74
Appendix F. Extended Simulation Study Results		76
F.1.	Purpose and Scope	76
F.2.	Full Factorial Design Specification	77
F.3.	Hyperprior Methods and Exact Parameters	79
F.4.	Inference Model and MCMC Configuration	80
F.5.	Outcome Metrics	81
F.6.	Complete Results Under Medium Confidence (Main Setting)	81
F.7.	Additional Baseline: χ^2 -DORO	82
F.8.	Sensitivity Analysis: Confidence Specification (TSMM / Dual-Anchor)	82
F.9.	Posterior Behavior of the Concentration Parameter α	83
F.10.	Mode-Based Recovery of K^*	83
F.11.	Bias–Variance Decomposition of MSE (Low-Information Setting)	83
F.12.	Computational Benchmarks (Calibration Cost)	84
Appendix G. Software Implementation		85
G.1.	Purpose and Scope	85
G.2.	Package Overview	86
G.3.	Mapping: Paper Components to DPprior Functions	87
G.4.	Core Workflow	88
G.5.	Worked Example: End-to-End Elicitation	90
G.6.	Reproducibility Checklist	97
G.7.	Repository and Resources	98

Appendix A. DP/CRP Preliminaries and Exact K_J Distribution

A.1. Purpose and Scope. This appendix establishes the reference-grade computational foundation for the Design-Conditional Elicitation (DCE) framework. The results presented here—while largely classical in the DP/CRP literature (e.g., Antoniak, 1974; Blackwell & MacQueen, 1973; Pitman, 1996)—are synthesized to provide (i) ground truth for approximation validation and (ii) a stable evaluation layer for the Two-Stage Moment Matching (TSMM) algorithm.

Throughout, we maintain notation consistent with Main Text §2.1:

- J : fixed design size (e.g., number of sites/studies/units in a multisite trial or meta-analysis).
- $\alpha > 0$: DP concentration parameter.
- K_J : number of occupied clusters (distinct values) among J DP draws.
- Hyperprior: $\alpha \sim \text{Gamma}(a, b)$ in shape–rate form:

$$p(\alpha | a, b) = \frac{b^a}{\Gamma(a)} \alpha^{a-1} e^{-b\alpha}, \quad a > 0, b > 0. \quad (\text{A.1})$$

Sections A.2.1–A.2.3 establish the exact conditional law of $K_J | \alpha$ and its moments. Sections A.2.4–A.2.6 describe the Gamma-mixed (marginal) distribution, asymptotic approximations motivating Stage 1, and numerically stable computation.

A.2. Distributional Theory.

A.2.1. *Chinese Restaurant Process and Partition Structure.* Let $G \sim \text{DP}(\alpha, G_0)$ with non-atomic base measure G_0 . Draw $\theta_1, \dots, \theta_J | G \stackrel{iid}{\sim} G$. Since a DP draw G is almost surely discrete (Ferguson, 1973), ties occur among (θ_j) and induce an exchangeable random partition of $\{1, \dots, J\}$. Define

$$K_J := \#\{\theta_1, \dots, \theta_J\}. \quad (\text{A.2})$$

A convenient constructive description is the *Chinese Restaurant Process* (CRP; Blackwell & MacQueen, 1973; Pitman, 2006). Interpreting draws θ_j as “customers” arriving sequentially:

- Customer 1 always starts a new table.
- Given the seating arrangement after $i - 1$ customers, customer i either sits at an existing table k with probability proportional to its current size $n_k^{(i-1)}$, or starts a new table with probability proportional to α :

$$\Pr(z_i = k | z_{1:i-1}, \alpha) = \begin{cases} \frac{n_k^{(i-1)}}{\alpha + i - 1}, & k = 1, \dots, K_{i-1}, \\ \frac{\alpha}{\alpha + i - 1}, & k = K_{i-1} + 1. \end{cases} \quad (\text{A.3})$$

Here z_i is the table label for customer i , K_{i-1} is the number of occupied tables after $i - 1$ customers, and $n_k^{(i-1)}$ is the number seated at table k .

The new-table probability $\alpha/(\alpha + i - 1)$ depends only on α and the step index i , which immediately yields a Bernoulli-sum representation for $K_J | \alpha$ (Theorem A.1).

This harmonic-like structure explains why digamma and trigamma functions appear in the exact conditional moments (Proposition A.1).

Connection to stick-breaking. The CRP partition law is equivalent to the stick-breaking representation (Sethuraman, 1994):

$$G = \sum_{h=1}^{\infty} w_h \delta_{\theta_h^*}, \quad w_h = v_h \prod_{\ell < h} (1 - v_{\ell}), \quad v_h \stackrel{iid}{\sim} \text{Beta}(1, \alpha). \quad (\text{A.4})$$

The weights $(w_1, w_2, \dots) \sim \text{GEM}(\alpha)$ represent asymptotic relative cluster sizes. The induced random partition among J draws from G has the CRP predictive rule (A.3) after marginalizing over (w_h) .

A.2.2. *Two Exact Representations of $K_J \mid \alpha$.* We give two equivalent descriptions: (i) a Poisson–binomial (independent Bernoulli-sum) representation useful for moments and concentration inequalities, and (ii) the Stirling-number PMF (Antoniak distribution) useful for exact probability evaluation.

Theorem A.1 (Poisson–Binomial Representation). *Conditionally on α ,*

$$K_J \stackrel{d}{=} \sum_{i=1}^J B_i, \quad B_i \text{ independent, } B_i \sim \text{Bernoulli}\left(\frac{\alpha}{\alpha + i - 1}\right). \quad (\text{A.5})$$

Equivalently, $K_J - 1$ is Poisson–binomial with success probabilities $\{\alpha/(\alpha + i - 1)\}_{i=2}^J$.

Attribution. This representation is classical in the Ewens/CRP literature; see Watterson (1974), Arratia et al. (2000), and Vicentini and Jermyn (2025) for its application to prior elicitation.

Proof. Define the new-table indicator

$$I_i := \mathbf{1}\{\text{customer } i \text{ starts a new table}\}, \quad i = 1, \dots, J, \quad (\text{A.6})$$

so that $K_J = \sum_{i=1}^J I_i$ and $I_1 \equiv 1$. Let \mathcal{F}_{i-1} be the σ -field generated by the seating arrangement up to step $i - 1$. From the CRP rule (A.3), for $i \geq 2$,

$$\Pr(I_i = 1 \mid \mathcal{F}_{i-1}, \alpha) = \frac{\alpha}{\alpha + i - 1} =: p_i(\alpha), \quad (\text{A.7})$$

which does not depend on \mathcal{F}_{i-1} . Hence I_i is conditionally independent of \mathcal{F}_{i-1} given α . By induction, I_1, \dots, I_J are mutually independent given α , with $I_i \sim \text{Bernoulli}(p_i(\alpha))$ for $i \geq 2$ and $I_1 \equiv 1$. \square

Boundary behavior. From the representation:

- As $\alpha \rightarrow 0$: $p_i(\alpha) \rightarrow 0$ for $i \geq 2$, so $K_J \mid \alpha \Rightarrow \delta_1$ (all J units in one cluster).

- As $\alpha \rightarrow \infty$: $p_i(\alpha) \rightarrow 1$, so $K_J \mid \alpha \Rightarrow \delta_J$ (each unit forms its own cluster).

Theorem A.2 (Antoniak Distribution). *For $k = 1, \dots, J$,*

$$\Pr(K_J = k \mid \alpha) = |s(J, k)| \cdot \alpha^k \cdot \frac{\Gamma(\alpha)}{\Gamma(\alpha + J)} = |s(J, k)| \cdot \frac{\alpha^k}{(\alpha)_J}, \quad (\text{A.8})$$

where $|s(J, k)|$ are *unsigned Stirling numbers of the first kind* and $(\alpha)_J := \alpha(\alpha + 1) \cdots (\alpha + J - 1)$ is the *rising factorial*.

Attribution. Equation (A.8) is the classical Antoniak distribution (Antoniak, 1974). It also appears as the computational bottleneck in prior-elicitation work for DP mixtures (Dorazio, 2009; Murugiah & Sweeting, 2012).

Unsigned Stirling numbers. The combinatorial quantities $|s(J, k)|$ count the number of permutations of J elements with exactly k cycles. They satisfy the recursion:

$$|s(J, k)| = |s(J - 1, k - 1)| + (J - 1) \cdot |s(J - 1, k)|, \quad (\text{A.9})$$

with boundary conditions $|s(0, 0)| = 1$, $|s(J, 0)| = 0$ for $J \geq 1$, and $|s(J, J)| = 1$.

Proof. Let $p_{n,k}(\alpha) := \Pr(K_n = k \mid \alpha)$. From the CRP, when adding the n -th customer, either a new table is created (probability $\alpha/(\alpha + n - 1)$) increasing the table count by 1, or an existing table is chosen (probability $(n - 1)/(\alpha + n - 1)$) leaving the table count unchanged. Therefore, for $n \geq 2$ and $1 \leq k \leq n$,

$$p_{n,k}(\alpha) = p_{n-1,k-1}(\alpha) \cdot \frac{\alpha}{\alpha + n - 1} + p_{n-1,k}(\alpha) \cdot \frac{n - 1}{\alpha + n - 1}. \quad (\text{A.10})$$

Define the candidate solution $\tilde{p}_{n,k}(\alpha) := |s(n, k)| \cdot \alpha^k \cdot \Gamma(\alpha)/\Gamma(\alpha + n)$. Using $\Gamma(\alpha + n) = (\alpha + n - 1)\Gamma(\alpha + n - 1)$ and the Stirling recurrence (A.9), one verifies directly that $\tilde{p}_{n,k}(\alpha)$ satisfies the same recursion (A.10). The base case holds because $K_1 \equiv 1$, hence $p_{1,1}(\alpha) = 1$, and also $\tilde{p}_{1,1}(\alpha) = |s(1, 1)| \cdot \alpha \cdot \Gamma(\alpha)/\Gamma(\alpha + 1) = 1$. By induction, $p_{n,k}(\alpha) = \tilde{p}_{n,k}(\alpha)$ for all n and k . \square

A.2.3. *Exact Conditional Moments.* Define

$$\kappa_J(\alpha) := \mathbb{E}[K_J \mid \alpha], \quad v_J(\alpha) := \text{Var}(K_J \mid \alpha). \quad (\text{A.11})$$

Proposition A.1 (Conditional Moments). *For $\alpha > 0$ and $J \geq 1$,*

$$\kappa_J(\alpha) = \alpha [\psi(\alpha + J) - \psi(\alpha)], \quad (\text{A.12})$$

$$v_J(\alpha) = \kappa_J(\alpha) - \alpha^2 [\psi_1(\alpha) - \psi_1(\alpha + J)], \quad (\text{A.13})$$

where $\psi(\cdot)$ is the digamma function and $\psi_1(\cdot)$ is the trigamma function.

Proof. (Step-by-step.) By [Theorem A.1](#), $K_J = \sum_{i=1}^J I_i$ with $\mathbb{E}[I_i \mid \alpha] = p_i(\alpha) = \alpha/(\alpha + i - 1)$. Hence

$$\kappa_J(\alpha) = \sum_{i=1}^J \frac{\alpha}{\alpha + i - 1} = \alpha \sum_{r=0}^{J-1} \frac{1}{\alpha + r}. \quad (\text{A.14})$$

Using the identity $\sum_{r=0}^{J-1} (\alpha + r)^{-1} = \psi(\alpha + J) - \psi(\alpha)$ (Abramowitz & Stegun, [1964](#), §6.3), we obtain [\(A.12\)](#).

For the variance, conditional independence gives

$$\text{Var}(K_J \mid \alpha) = \sum_{i=1}^J p_i(\alpha) \{1 - p_i(\alpha)\} = \sum_{r=0}^{J-1} \frac{\alpha}{\alpha + r} \left(1 - \frac{\alpha}{\alpha + r}\right) = \sum_{r=0}^{J-1} \frac{\alpha r}{(\alpha + r)^2}. \quad (\text{A.15})$$

Rewriting each summand as

$$\frac{\alpha r}{(\alpha + r)^2} = \frac{\alpha}{\alpha + r} - \frac{\alpha^2}{(\alpha + r)^2}, \quad (\text{A.16})$$

we obtain

$$v_J(\alpha) = \alpha \sum_{r=0}^{J-1} \frac{1}{\alpha + r} - \alpha^2 \sum_{r=0}^{J-1} \frac{1}{(\alpha + r)^2} = \kappa_J(\alpha) - \alpha^2 [\psi_1(\alpha) - \psi_1(\alpha + J)], \quad (\text{A.17})$$

using the trigamma identity $\sum_{r=0}^{J-1} (\alpha + r)^{-2} = \psi_1(\alpha) - \psi_1(\alpha + J)$. \square

Corollary A.1 (Conditional Underdispersion). *For $\alpha > 0$ and $J \geq 2$, $0 < v_J(\alpha) < \kappa_J(\alpha)$.*

Proof. For $i \geq 2$, $p_i(\alpha) \in (0, 1)$, so $p_i(1 - p_i) < p_i$. Also $p_1(1 - p_1) = 0$ since $p_1 = 1$. Therefore $v_J(\alpha) = \sum_{i=1}^J p_i(1 - p_i) < \sum_{i=1}^J p_i = \kappa_J(\alpha)$, and strict positivity holds because at least one $p_i \in (0, 1)$ when $J \geq 2$. \square

This underdispersion property—the conditional variance being strictly less than the conditional mean—distinguishes $K_J \mid \alpha$ from a Poisson distribution and constrains the admissible target moments in elicitation (see [Section B](#)).

Derivatives with respect to α . The Newton refinement in [Section C](#) uses derivatives of the conditional moments. Writing $r = i - 1 \in \{0, \dots, J - 1\}$:

Mean derivative:

$$\frac{\partial \kappa_J}{\partial \alpha} = \sum_{r=1}^{J-1} \frac{r}{(\alpha + r)^2} = [\psi(\alpha + J) - \psi(\alpha)] + \alpha [\psi_1(\alpha + J) - \psi_1(\alpha)]. \quad (\text{A.18})$$

Variance derivative (summation form):

$$\frac{\partial v_J}{\partial \alpha} = \sum_{r=1}^{J-1} \frac{r(r-\alpha)}{(\alpha+r)^3}. \quad (\text{A.19})$$

Variance derivative (special function form): Differentiating (A.13) directly yields an equivalent expression using the tetragamma function $\psi_2(\cdot)$:

$$\frac{\partial v_J}{\partial \alpha} = \frac{\partial \kappa_J}{\partial \alpha} - 2\alpha[\psi_1(\alpha) - \psi_1(\alpha+J)] - \alpha^2[\psi_2(\alpha) - \psi_2(\alpha+J)]. \quad (\text{A.20})$$

Computational note. Evaluating $\kappa_J(\alpha)$ and $v_J(\alpha)$ via special functions in (A.12)–(A.13) is $O(1)$ per α , whereas direct summation in (A.14)–(A.15) is $O(J)$. In the target regime $J \lesssim 300$, both are feasible; we prefer the special-function forms for speed and numerical smoothness.

A.2.4. Marginal Distribution Under Gamma Hyperprior. Suppose $\alpha \sim \text{Gamma}(a, b)$ with density (A.1). Mixing the Antoniak PMF (A.8) over α yields the prior-predictive distribution of K_J .

Theorem A.3 (Marginal PMF). *For $k = 1, \dots, J$,*

$$p(K_J = k \mid a, b) = \frac{b^a |s(J, k)|}{\Gamma(a)} \int_0^\infty \alpha^{k+a-1} e^{-b\alpha} \frac{\Gamma(\alpha)}{\Gamma(\alpha+J)} d\alpha. \quad (\text{A.21})$$

In general, the integral in (A.21) has no closed form and must be evaluated numerically.

Attribution. The “Stirling–Gamma” integral in (A.21) is the computational bottleneck highlighted by Dorazio (2009) for selecting α hyperpriors. This lack of closed form motivates both the asymptotic approximations (Section A.2.5) that provide initial values and the exact quadrature layer (Section A.2.6) that serves as the reference for validation. Murugiah and Sweeting (2012) present an equivalent Gamma-mixed marginal distribution for the cluster count that involves a one-dimensional integral.

Proof. By the law of total probability, $p(K_J = k \mid a, b) = \int p(K_J = k \mid \alpha) p(\alpha \mid a, b) d\alpha$. Substituting (A.8) and (A.1) and collecting terms gives (A.21). \square

Proposition A.2 (Marginal Moments via Total Expectation/Variance). *Under $\alpha \sim \text{Gamma}(a, b)$,*

$$\mathbb{E}[K_J \mid a, b] = \mathbb{E}_\alpha[\kappa_J(\alpha)], \quad (\text{A.22})$$

$$\text{Var}(K_J \mid a, b) = \mathbb{E}_\alpha[v_J(\alpha)] + \text{Var}_\alpha(\kappa_J(\alpha)). \quad (\text{A.23})$$

Proof. Equation (A.22) is the law of total expectation. For (A.23), apply the law of total variance: $\text{Var}(K_J) = \mathbb{E}\{\text{Var}(K_J | \alpha)\} + \text{Var}\{\mathbb{E}(K_J | \alpha)\}$. \square

The decomposition in Proposition A.2 is computationally advantageous: rather than computing marginal moments from the full PMF (which requires the Stirling–Gamma integral for each k), one can compute them by one-dimensional numerical integration of $\kappa_J(\alpha)$ and $v_J(\alpha)$. This is the approach used in the TSMM Stage 2 Newton iteration.

A.2.5. Asymptotic Approximations. This section records two approximations that motivate the Stage 1 closed-form initializer in Section B. They are not used as final answers—Stage 2 replaces them with exact finite- J moment matching.

Theorem A.4 (Poisson Approximation). *Let $\lambda_J(\alpha) := \kappa_J(\alpha) = \sum_{i=1}^J \alpha / (\alpha + i - 1)$. Then, as $J \rightarrow \infty$,*

$$d_{\text{TV}}(\mathcal{L}(K_J | \alpha), \text{Poisson}(\lambda_J(\alpha))) = O\left(\frac{1}{\log J}\right), \quad \text{for fixed } \alpha > 0. \quad (\text{A.24})$$

Attribution. Total-variation Poisson approximations for logarithmic combinatorial structures are developed in Arratia et al. (2000).

Proof. By Theorem A.1, $K_J | \alpha$ is a Poisson–binomial sum of independent Bernoulli variables with probabilities $p_i(\alpha) = \alpha / (\alpha + i - 1)$. A standard Poisson approximation bound (Le Cam, 1960) yields

$$d_{\text{TV}}(\mathcal{L}(K_J | \alpha), \text{Poisson}(\lambda_J(\alpha))) \leq \frac{\sum_{i=1}^J p_i(\alpha)^2}{\lambda_J(\alpha)}. \quad (\text{A.25})$$

For the numerator, note that $p_1(\alpha) = 1$ and for $i \geq 2$, with $r = i - 1 \geq 1$,

$$p_i(\alpha)^2 = \left(\frac{\alpha}{\alpha + r}\right)^2 \leq \frac{\alpha^2}{r^2}, \quad \Rightarrow \quad \sum_{i=1}^J p_i(\alpha)^2 \leq 1 + \alpha^2 \sum_{r=1}^{\infty} \frac{1}{r^2} < \infty. \quad (\text{A.26})$$

Meanwhile, $\lambda_J(\alpha) = \alpha \sum_{r=0}^{J-1} (\alpha + r)^{-1} \sim \alpha \log J$ by (A.12) and the asymptotic $\psi(\alpha + J) = \log J + O(1)$. Therefore $\lambda_J(\alpha)$ diverges like $\alpha \log J$ while $\sum_i p_i^2 = O(1)$, and the right-hand side of (A.25) is $O(1 / \log J)$, establishing (A.24). \square

Remark A.1. Arratia et al. (2003) emphasize that using the exact mean $\kappa_J(\alpha)$ rather than the asymptotic approximation $\alpha \log J$ improves accuracy for finite J , since $\kappa_J(\alpha) = \alpha \log J + O(1)$ with an α -dependent constant.

Theorem A.5 (Negative Binomial Approximation). *Suppose $\alpha \sim \text{Gamma}(a, b)$ and define $c_J := \log J$. For large J ,*

$$K_J \mid (a, b) \stackrel{d}{\approx} 1 + \text{NegBin}\left(a, \frac{b}{b + c_J}\right), \quad (\text{A.27})$$

where $\text{NegBin}(r, p)$ has mean $r(1 - p)/p$ and variance $r(1 - p)/p^2$.

Attribution. The large- J negative binomial limit under random α appears in Vincentini and Jermyn (2025) and Zito et al. (2024).

Proof. By Theorem A.4, for each fixed α , $K_J - 1 \mid \alpha$ is well-approximated in total variation by Poisson(αc_J) for large J . If $Y \mid \alpha \sim \text{Poisson}(\alpha c_J)$ and $\alpha \sim \text{Gamma}(a, b)$, then the Gamma–Poisson mixture is exactly negative binomial:

$$Y \sim \text{NegBin}\left(a, \frac{b}{b + c_J}\right). \quad (\text{A.28})$$

Indeed, integrating the Poisson PMF against the Gamma density yields $\Pr(Y = y) = \binom{a+y-1}{y} p^a (1-p)^y$ with $p = b/(b + c_J)$. Combining this with $K_J \approx 1 + Y$ gives (A.27). \square

Approximate marginal moments. Under (A.27):

$$\mathbb{E}[K_J \mid a, b] \approx 1 + \frac{a \log J}{b}, \quad \text{Var}(K_J \mid a, b) \approx \frac{a \log J}{b} + \frac{a(\log J)^2}{b^2}. \quad (\text{A.29})$$

Closed-form inversion for initial values. Given target marginal moments (μ_K, σ_K^2) with $\sigma_K^2 > \mu_K - 1$, the negative binomial approximation yields closed-form initial values. Setting $m := \mu_K - 1$:

$$a^{(0)} \approx \frac{m^2}{\sigma_K^2 - m}, \quad b^{(0)} \approx \frac{a^{(0)} \log J}{m}. \quad (\text{A.30})$$

These provide the starting point for Stage 1 of the TSMM algorithm, with subsequent refinement via exact moment matching in Stage 2.

A.2.6. *Numerically Stable Computation.* This section specifies stable computation of (i) the Antoniak PMF (A.8) and (ii) Gamma-mixed expectations in (A.22)–(A.23).

A.2.6.1 Log-Stirling Recursion. Unsigned Stirling numbers $|s(J, k)|$ grow rapidly; for example, $|s(50, 25)| \approx 1.4 \times 10^{54}$, exceeding double-precision range for moderate J . We therefore precompute $L_{n,k} := \log |s(n, k)|$ in log-space.

The recurrence (A.9) in log-space, with $\log 0 := -\infty$, becomes:

$$L_{n,k} = \text{logaddexp}(L_{n-1,k-1}, \log(n-1) + L_{n-1,k}), \quad (\text{A.31})$$

where $\text{logaddexp}(u, v) := \max(u, v) + \log\{1 + \exp(-|u - v|)\}$.

Algorithm A.1 (Log-Stirling Computation).

Input: Maximum sample size J_{\max} .

Output: Log-Stirling table $L[n, k]$ for $1 \leq n \leq J_{\max}$, $1 \leq k \leq n$.

1. **Initialize:** $L[1, 1] \leftarrow 0$ (since $\log|s(1, 1)| = \log 1 = 0$).
2. **For** $n = 2$ **to** J_{\max} :
 - (a) $L[n, 1] \leftarrow L[n - 1, 1] + \log(n - 1)$ (since $|s(n, 1)| = (n - 1)!$).
 - (b) **For** $k = 2$ **to** $n - 1$:

$$L[n, k] \leftarrow \text{logaddexp}(L[n - 1, k - 1], \log(n - 1) + L[n - 1, k]).$$

$$(c) L[n, n] \leftarrow 0 \quad (\text{since } |s(n, n)| = 1).$$

A.2.6.2 Log-PMF Evaluation. Given $\{L_{J,k}\}_{k=1}^J$, compute the Antoniak log-PMF for $k = 1, \dots, J$:

$$\log p_{J,k}(\alpha) = L_{J,k} + k \log \alpha + \log \Gamma(\alpha) - \log \Gamma(\alpha + J). \quad (\text{A.32})$$

To avoid underflow and enforce normalization, compute $\log Z = \text{logsumexp}\{\log p_{J,k}(\alpha) : k = 1, \dots, J\}$ and return $\log \pi_{J,k}(\alpha) = \log p_{J,k}(\alpha) - \log Z$.

Validation checks:

1. Row-sum identity: $\sum_{k=1}^J |s(J, k)| = J!$ (verify in log space).
2. Small- J sanity: Compare $|s(J, k)|$ against known tables for $J \leq 10$.
3. PMF checks: $\sum_{k=1}^J \Pr(K_J = k \mid \alpha) = 1$ and non-negativity.
4. Boundary checks: $\alpha \rightarrow 0 \Rightarrow \Pr(K_J = 1 \mid \alpha) \rightarrow 1$; $\alpha \rightarrow \infty \Rightarrow \Pr(K_J = J \mid \alpha) \rightarrow 1$.

A.2.6.3 Gauss–Laguerre Quadrature for Gamma-Mixed Expectations. For any measurable $g(\alpha)$ with $\mathbb{E}|g(\alpha)| < \infty$,

$$\mathbb{E}_{a,b}\{g(\alpha)\} = \int_0^\infty g(\alpha) p(\alpha \mid a, b) d\alpha = \frac{1}{\Gamma(a)} \int_0^\infty g(x/b) x^{a-1} e^{-x} dx, \quad (\text{A.33})$$

using the change of variables $x = b\alpha$. Generalized Gauss–Laguerre quadrature with parameter $a - 1$ provides nodes $\{x_m\}_{m=1}^M$ and weights $\{w_m\}_{m=1}^M$ such that

$$\frac{1}{\Gamma(a)} \int_0^\infty g(x/b) x^{a-1} e^{-x} dx \approx \sum_{m=1}^M \tilde{w}_m g(\alpha_m), \quad \alpha_m := x_m/b, \quad (\text{A.34})$$

with normalized weights $\tilde{w}_m := w_m / \Gamma(a)$.

Default specification. We use $M = 80$ nodes, which in our target regime $(a, b \in [0.1, 20], J \leq 300)$ yields relative accuracy on the order of 10^{-10} for the mixed moments

and their derivatives. The same quadrature nodes can be reused to evaluate $\mathbb{E}\{\kappa_J(\alpha)\}$, $\mathbb{E}\{v_J(\alpha)\}$, and Jacobian components in [Section C](#).

A.2.6.4 Complexity Summary. For a fixed maximum design size J_{\max} :

TABLE A.1. Computational Complexity Summary

Operation	Complexity
Log-Stirling table precomputation	$O(J_{\max}^2)$ time/memory, cached once
Conditional PMF $\Pr(K_J = \cdot \alpha)$ for all k	$O(J)$ per α
Conditional moments $\kappa_J(\alpha), v_J(\alpha)$	$O(1)$ via special functions
Marginal moments $\mathbb{E}[K_J], \text{Var}(K_J)$ via quadrature	$O(M)$ per (a, b)

Appendix B. Stage 1 Closed-Form Derivation and Approximation Theory

B.1. Purpose and Scope. This appendix derives the Stage 1 (A1) closed-form initializer used in the Two-Stage Moment Matching (TSMM) procedure. Stage 1 maps elicited moments for the number of clusters, (μ_K, σ_K^2) for K_J at a design size J , into a Gamma hyperprior $\alpha \sim \text{Gamma}(a_0, b_0)$ (shape–rate parameterization).

The key idea is to replace the exact (and generally non-invertible) moment relationship $(a, b) \mapsto (\mathbb{E}[K_J], \text{Var}(K_J))$ under the DP mixture model with a *shifted Poisson–Gamma proxy*. This proxy yields an analytically invertible mapping that is accurate enough to serve as a robust starting point for Stage 2, where the exact moments are matched numerically ([Section C](#)).

Attribution note. The proxy distributional approximation for K_J (Poissonization and its Negative-Binomial consequence under Gamma mixing) is standard and appears explicitly in recent DP-precision-prior work (e.g., [Vicentini & Jermyn, 2025](#); [Zito et al., 2024](#)), building on classical Poisson approximation bounds ([Arratia et al., 2000](#); [Le Cam, 1960](#)). The closed-form inversion below is an elementary method-of-moments step; in this paper it is used as the Stage 1 initializer within TSMM.

The development proceeds as follows. [Section B.2](#) introduces the shifted approximation and derives the induced negative-binomial marginal. [Section B.3](#) presents the closed-form inversion ([Theorem B.6](#)) and feasibility conditions. [Section B.4](#) provides a practitioner-facing confidence-to-variance mapping. [Section B.5](#) quantifies approximation quality and establishes operational recommendations for when Stage 1 alone is sufficient versus when Stage 2 refinement is required.

B.2. The Shifted Poisson–Gamma Proxy.

B.2.1. *The Shifted Approximation.* Recall that the cluster count under the Chinese Restaurant Process (CRP) representation satisfies

$$K_J = 1 + \sum_{i=2}^J Z_i, \quad Z_i \mid \alpha \sim \text{Bernoulli}\left(\frac{\alpha}{\alpha + i - 1}\right),$$

where (Z_i) are independent conditional on α (see [Section A, Theorem A.1](#)). Hence $K_J - 1$ is a Poisson–binomial sum. Classical Poisson approximation theory (Arratia et al., [2000](#); Barbour & Xia, [1999](#); Le Cam, [1960](#)) motivates replacing $K_J - 1$ by a Poisson random variable with the same mean.

Definition B.1 (Shifted Poisson Proxy). For a design size $J \geq 2$, we adopt the proxy

$$K_J - 1 \mid \alpha \approx \text{Poisson}(\alpha c_J), \quad c_J := \log J. \quad (\text{B.1})$$

The shift by 1 enforces the support constraint $K_J \geq 1$ exactly, while keeping a simple count model for the “excess” clusters.

Why $c_J = \log J$? The exact conditional mean has a closed form involving the digamma function,

$$\kappa_J(\alpha) := \mathbb{E}[K_J \mid \alpha] = \sum_{i=1}^J \frac{\alpha}{\alpha + i - 1} = \alpha \{\psi(\alpha + J) - \psi(\alpha)\}, \quad (\text{B.2})$$

and satisfies the large- J expansion $\kappa_J(\alpha) = \alpha \log J + O(\alpha)$ for fixed α ([Antoniak, 1974](#)). The simplest proxy replaces the exact, α -dependent mean [\(B.2\)](#) by the leading term $\alpha \log J$, yielding [\(B.1\)](#).

Important caveat on linearization error. The expansion $\kappa_J(\alpha) = \alpha \log J + O(\alpha)$ hides an α -dependent constant: more precisely, $\kappa_J(\alpha) = \alpha \log J + \alpha\gamma - \alpha\psi(\alpha) + O(\alpha/J)$, where γ is the Euler–Mascheroni constant and $\psi(\alpha) = \Gamma'(\alpha)/\Gamma(\alpha)$. For constant-order α (e.g., $\alpha \in [0.5, 5]$), the term $-\alpha\psi(\alpha)$ contributes a non-vanishing bias that does not decay as $J \rightarrow \infty$. This is why A1 is best viewed as an initializer for Stage 2, rather than a stand-alone method: the linearization $\kappa_J(\alpha) \approx 1 + \alpha \log J$ can leave residual errors of order $O(\mathbb{E}[\alpha])$ in the marginal mean even at large J .

A common alternative is to use a harmonic-number scaling H_{J-1} , since

$$H_{J-1} = \sum_{i=1}^{J-1} \frac{1}{i} = \psi(J) + \gamma, \quad H_{J-1} = \log J + \gamma + O(1/J), \quad (\text{B.3})$$

where $\gamma \approx 0.5772$ is the Euler–Mascheroni constant.

Lemma B.1 (Harmonic–Digamma Equivalence). *For integer $J \geq 1$, $H_{J-1} = \psi(J) + \gamma$, where γ is the Euler–Mascheroni constant.*

Consequently, for integer design sizes J , there are only two distinct α -free competitors: $\log J$ and H_{J-1} . Using H_{J-1} instead of $\log J$ changes only an $O(1)$ term, so both scalings are asymptotically equivalent.

TABLE B.1. Comparison of Scaling Constant Choices

J	$\log J$	H_{J-1}	$\psi(J) + \gamma$	Difference
10	2.303	2.829	2.829	0.526
25	3.219	3.776	3.776	0.557
50	3.912	4.499	4.499	0.587
100	4.605	5.187	5.187	0.582
300	5.704	6.283	6.283	0.579

Note. For integer J , $\psi(J) + \gamma \equiv H_{J-1}$ exactly. The difference $H_{J-1} - \log J$ converges to $\gamma \approx 0.577$ as $J \rightarrow \infty$.

Numerical analysis demonstrates that $c_J = \log J$ yields uniformly smaller mean errors for $K_J - 1$ across practical values of $\alpha > 0.2$; the crossover point (where harmonic produces smaller error) occurs at approximately $\alpha^* \approx 0.20$ for the shifted approximation—below the range of typical elicited beliefs. We therefore adopt $c_J = \log J$ as the default.

Practical note. The `DPprior` implementation also exposes a harmonic option (and an optional plug-in digamma correction) for settings with very small J or very small implied α ; see the package vignettes for details.

B.2.2. Gamma-Mixed Shifted Poisson. The Stage 1 inversion uses the fact that the shifted Poisson proxy is conjugate to the Gamma prior.

Lemma B.2 (Gamma-Mixed Shifted Poisson). *Let $X \mid \alpha \sim \text{Poisson}(\alpha c_J)$ with $c_J > 0$, and $\alpha \sim \text{Gamma}(a, b)$ with shape $a > 0$ and rate $b > 0$. Then the marginal distribution of X is Negative Binomial:*

$$X \sim \text{NegBin}\left(a, p = \frac{b}{b + c_J}\right), \quad (\text{B.4})$$

where we use the parameterization in which p is the “success” probability and $X \in \{0, 1, 2, \dots\}$ counts the number of failures before a successes (for non-integer a , via the Gamma-function extension). Its first two moments are

$$\mathbb{E}[X] = \frac{ac_J}{b}, \quad \text{Var}(X) = \frac{ac_J}{b} + \frac{ac_J^2}{b^2}. \quad (\text{B.5})$$

Proof. By direct marginalization,

$$\begin{aligned}
\Pr(X = x) &= \int_0^\infty \underbrace{\frac{e^{-\alpha c_J} (\alpha c_J)^x}{x!}}_{\text{Poisson}(\alpha c_J)} \underbrace{\frac{b^a}{\Gamma(a)} \alpha^{a-1} e^{-b\alpha}}_{\text{Gamma}(a,b)} d\alpha \\
&= \frac{b^a c_J^x}{\Gamma(a) x!} \int_0^\infty \alpha^{a+x-1} e^{-(b+c_J)\alpha} d\alpha \\
&= \frac{\Gamma(a+x)}{\Gamma(a) x!} \left(\frac{b}{b+c_J}\right)^a \left(\frac{c_J}{b+c_J}\right)^x,
\end{aligned} \tag{B.6}$$

which is the Negative Binomial pmf (B.4). The moments (B.5) follow from standard formulas for $\text{NegBin}(a, p)$. \square

Attribution. The Poisson–Gamma mixing identity is classical (see, e.g., Johnson et al., 2005). Its application to DP concentration parameter priors in the large- J regime is discussed in Vicentini and Jermyn (2025, §3.1) and Zito et al. (2024).

Connection to the DP cluster count. Setting $X = K_J - 1$, Lemma B.2 implies the proxy

$$K_J - 1 \mid (a, b) \approx \text{NegBin}\left(a, \frac{b}{b + \log J}\right), \tag{B.7}$$

which is the approximation used to derive the Stage 1 mapping below.

B.3. The A1 Closed-Form Inversion.

B.3.1. *Closed-Form Mapping.* Let (μ_K, σ_K^2) denote the elicited mean and variance of K_J , and define the shifted mean

$$\mu_0 := \mu_K - 1. \tag{B.8}$$

Under the shifted Negative Binomial proxy (B.7), μ_0 and σ_K^2 are matched to (B.5).

Theorem B.6 (Stage 1 / A1 Mapping). *Fix $J \geq 2$ and target moments (μ_K, σ_K^2) . Let $\mu_0 = \mu_K - 1$ and $c_J = \log J$. If*

$$\mu_0 > 0 \quad \text{and} \quad \sigma_K^2 > \mu_0, \tag{B.9}$$

then the shifted Negative Binomial proxy admits the closed-form solution

$$a_0 = \frac{\mu_0^2}{\sigma_K^2 - \mu_0}, \quad b_0 = \frac{\mu_0 c_J}{\sigma_K^2 - \mu_0}$$

$$\tag{B.10}$$

which we use as the Stage 1 initializer $\alpha \sim \text{Gamma}(a_0, b_0)$ in TSMM.

This mapping is reported as Eqs. (8)–(9) in the main text.

Proof. Under Lemma B.2 with $X = K_J - 1$, the proxy moments are

$$\mu_0 = \mathbb{E}[X] = \frac{ac_J}{b}, \quad \sigma_K^2 = \text{Var}(X) = \frac{ac_J}{b} + \frac{ac_J^2}{b^2}. \quad (\text{B.11})$$

The first equation gives $b = ac_J/\mu_0$. Substituting into the second yields $\sigma_K^2 = \mu_0 + \mu_0^2/a$, so $a = \mu_0^2/(\sigma_K^2 - \mu_0)$. Plugging this into $b = ac_J/\mu_0$ gives (B.10). \square

B.3.2. Implied Concentration-Parameter Summaries.

Corollary B.2 (Implied Statistics for α). *Under the Stage 1 initializer $\alpha \sim \text{Gamma}(a_0, b_0)$,*

$$\mathbb{E}[\alpha] = \frac{a_0}{b_0} = \frac{\mu_0}{c_J}, \quad \text{CV}(\alpha) = \frac{1}{\sqrt{a_0}} = \frac{\sqrt{\sigma_K^2 - \mu_0}}{\mu_0}. \quad (\text{B.12})$$

Interpretation. Under A1, μ_K sets the prior mean $\mathbb{E}[\alpha]$ through the simple rule $\mathbb{E}[\alpha] \approx (\mu_K - 1)/\log J$. The shape parameter a_0 controls uncertainty: as $\sigma_K^2 \downarrow \mu_0$, $a_0 \rightarrow \infty$ and the prior becomes quasi-degenerate at $\mu_0/\log J$. Conversely, as σ_K^2 increases, a_0 decreases, implying heavier tails and greater uncertainty for α .

B.3.3. Feasibility Region and Projection Policy.

Proposition B.3 (Feasibility Region for A1). *The closed-form mapping (B.10) yields positive (a_0, b_0) provided:*

1. $\mu_K > 1$ (equivalently $\mu_0 > 0$);
2. $\mu_K \leq J$ (since $1 \leq K_J \leq J$);
3. $\sigma_K^2 > \mu_K - 1$ (overdispersion relative to the shifted Poisson proxy).

Proof. Conditions (1) and (3) ensure $\mu_0 > 0$ and $\sigma_K^2 - \mu_0 > 0$, so (B.10) is well-defined with $a_0, b_0 > 0$. Condition (2) is a support constraint implied by $K_J \leq J$. \square

Important nuance. Condition (3) is a proxy-model constraint: under A1, $\text{Var}(K_J - 1) = \mu_0 + \mu_0^2/a \geq \mu_0$. In the exact DP model, $K_J | \alpha$ is conditionally underdispersed relative to Poisson (Section A, Proposition A.1), so targets with $\sigma_K^2 \leq \mu_0$ can still be feasible once exact moments are used. This is precisely why A1 is an initializer and A2 exists.

Feasibility Projection (Stage 1 only). When user-provided (μ_K, σ_K^2) violates condition (3), Stage 1 applies a minimal variance inflation:

$$\sigma_{K,\text{eff}}^2 := \max\{\sigma_K^2, \mu_0 + \varepsilon\}, \quad \varepsilon = \max\{10^{-8}, 10^{-6}\mu_0\}. \quad (\text{B.13})$$

This projection produces a quasi-degenerate Gamma prior (large a_0) centered at μ_0/c_J . The projection is used only to obtain a numerically stable initializer for Stage 2;

the Stage 2 solver re-targets the original elicited moments using the exact moment equations.

B.3.4. *Worked Example.* Consider a design with $J = 50$ sites where a practitioner expects about 5 distinct clusters with moderate uncertainty: $\mu_K = 5$, $\sigma_K^2 = 10$.

Step 1. Compute the shifted mean and scaling constant:

$$\mu_0 = 5 - 1 = 4, \quad c_{50} = \log(50) \approx 3.912.$$

Step 2. Verify feasibility: $\sigma_K^2 = 10 > \mu_0 = 4$.

Step 3. Apply the closed-form mapping (B.10):

$$a_0 = \frac{4^2}{10 - 4} = \frac{16}{6} \approx 2.667, \quad b_0 = \frac{4 \times 3.912}{6} \approx 2.608.$$

Step 4. Interpret the implied α prior:

$$\mathbb{E}[\alpha] = \frac{4}{3.912} \approx 1.02, \quad \text{CV}(\alpha) = \frac{1}{\sqrt{2.667}} \approx 0.612.$$

The Stage 1 result $(a_0, b_0) \approx (2.667, 2.608)$ serves as the initializer for Stage 2 Newton refinement, which produces the exact-moment solution $(a^*, b^*) \approx (1.407, 1.076)$ —see [Section C](#) for details.

B.4. Confidence-to-Variance Mapping. Practitioners may find it easier to express uncertainty about K_J qualitatively rather than specifying σ_K^2 directly. We provide a *variance inflation factor* (VIF) mapping that translates qualitative confidence levels into variance specifications.

Definition B.2 (Variance Inflation Factor). The VIF translates qualitative confidence into variance:

$$\sigma_K^2 = \text{VIF} \cdot (\mu_K - 1) = \text{VIF} \cdot \mu_0. \quad (\text{B.14})$$

Since A1 requires $\sigma_K^2 > \mu_K - 1$, we must have $\text{VIF} > 1$. The boundary $\text{VIF} = 1$ corresponds to the shifted Poisson variance.

TABLE B.2. Recommended VIF Defaults

Confidence Level	VIF	σ_K^2 when $\mu_K = 5$	Interpretation
High	1.5	6.0	Fairly certain about cluster count
Medium (default)	2.5	10.0	Moderate uncertainty
Low	5.0	20.0	Substantial uncertainty

This mapping is implemented in `DPprior_fit(confidence = "medium")` and is primarily intended for Stage 1 initialization; Stage 2 can be invoked when exact moment matching is desired.

Alternative Confidence Interfaces. The `DPprior` package also accepts:

1. *Coefficient of variation:* $CV_K = \sigma_K/\mu_K$, converted via $\sigma_K^2 = (CV_K \cdot \mu_K)^2$.
2. *Central interval:* If the practitioner specifies that $K_J \in [k_L, k_U]$ with probability q (e.g., $q = 0.80$), the variance is approximated via a normal proxy:

$$\sigma_K^2 \approx \left(\frac{k_U - k_L}{2z_{(1+q)/2}} \right)^2, \quad (\text{B.15})$$

where z_p denotes the standard normal p -quantile.

B.5. Approximation Quality: When Is Stage 1 Sufficient? Stage 1 is deliberately approximate. Two distinct approximations are in play:

1. *Poissonization error.* The conditional law of $K_J - 1$ is a Poisson–binomial distribution. Poisson approximation bounds (Arratia et al., 2003; Le Cam, 1960) control the total variation distance to a Poisson distribution with matching mean, and the bound decreases (slowly) as J grows (Section A).
2. *Mean linearization error.* Even if $K_J - 1$ were exactly Poisson with mean $\kappa_J(\alpha) - 1$, Stage 1 further replaces the exact mean (B.2) by αc_J with $c_J = \log J$. The leading term is correct for large J , but the dropped $O(\alpha)$ term can be non-negligible at moderate J .

These approximations are acceptable for initialization but can be too crude if used as the final elicitation outcome.

B.5.1. Approximation Behavior and Limitations.

Proposition B.4 (Approximation Behavior of A1). *Let (a_0, b_0) be the Stage 1 solution for targets (μ_K, σ_K^2) . Denote by $M_1(a_0, b_0) = \mathbb{E}_{a_0, b_0}[K_J]$ and $V(a_0, b_0) = \text{Var}_{a_0, b_0}(K_J)$ the exact mixed moments under $\alpha \sim \text{Gamma}(a_0, b_0)$. The approximation error depends critically on the magnitude of α under the induced prior:*

1. *Non-vanishing error regime.* When $\mathbb{E}[\alpha] = O(1)$ (i.e., constant-order concentration parameter), the linearization $\kappa_J(\alpha) \approx 1 + \alpha \log J$ introduces a bias of order $O(\mathbb{E}[\alpha])$ that does not vanish as $J \rightarrow \infty$. In this regime, errors $|M_1(a_0, b_0) - \mu_K|$ and $|V(a_0, b_0) - \sigma_K^2|$ may remain bounded away from zero even for large J .

2. *Vanishing error regime.* If $\mathbb{E}[\alpha] = O(1/\log J)$ (equivalently, $\mu_K - 1 = O(1)$ as $J \rightarrow \infty$), then the relative contribution of the linearization bias diminishes and the approximation error decreases with J .

Explanation. The exact conditional mean satisfies $\kappa_J(\alpha) = \alpha\{\psi(\alpha + J) - \psi(\alpha)\}$, which expands as

$$\kappa_J(\alpha) = \alpha \log J + \alpha\gamma - \alpha\psi(\alpha) + O(\alpha/J).$$

The term $-\alpha\psi(\alpha)$ is a J -independent function of α that contributes $O(\mathbb{E}[\alpha])$ bias to marginal moments after Gamma mixing. When α is constant-order, this bias persists regardless of J . The Poisson approximation error (which is $O(1/\log J)$ in total variation) is a separate, smaller-order effect.

Remark B.2. [Proposition B.4](#) clarifies that A1 is designed as an initialization method, not a stand-alone elicitation procedure. The closed-form expressions [\(B.10\)](#) provide computationally instant starting values, but Stage 2 Newton refinement is essential for accurate moment matching in the typical regime where $\mathbb{E}[\alpha] = O(1)$.

TABLE B.3. Representative Stage 1 Moment Errors

J	Target μ_K	Target σ_K^2	A1 Mean Error $ \Delta\mu $	A1 Variance Error $ \Delta\sigma^2 $
25	5	10	0.84	5.55
50	5	10	0.58	4.38
50	10	22.5	2.43	12.03
100	10	20	1.86	10.02
300	15	30	2.75	13.75

Note. For each row, we compute (a_0, b_0) from A1 and then evaluate the exact implied $\mathbb{E}[K_J]$ and $\text{Var}(K_J)$ under $\alpha \sim \text{Gamma}(a_0, b_0)$ using Gauss–Laguerre quadrature ([Section A](#), [§A.2.6](#)). The table reports absolute errors $|\Delta\mu| = |M_1(a_0, b_0) - \mu_K|$ and $|\Delta\sigma^2| = |V(a_0, b_0) - \sigma_K^2|$.

B.5.2. *Finite- J Error Magnitudes.* The table reveals two patterns:

1. Errors may decrease with J for fixed elicited moments, but as [Proposition B.4](#) clarifies, this reduction is not guaranteed to continue to zero—the linearization bias can leave a non-vanishing residual.
2. Errors increase with μ_K for fixed J , because larger cluster counts correspond to larger $\mathbb{E}[\alpha]$, which amplifies the linearization bias term $-\alpha\psi(\alpha)$.

B.5.3. *Operational Recommendation.* The Stage 1 closed-form mapping provides a computationally instant initialization (sub-millisecond) that is accurate enough for

qualitative sensitivity exploration. However, for applications requiring precise moment matching—including formal prior-predictive calibration, simulation studies, and any analysis where the prior-induced $p(K_J)$ will be reported—Stage 2 Newton refinement is essential.

A1 is best viewed as a fast, closed-form initializer rather than a stand-alone elicitation method when J is in the tens or low hundreds. In such regimes, Stage 2 moment matching (Section C) substantially reduces the moment discrepancy while preserving the interpretability of the elicited inputs.

Appendix C. Stage 2 Newton Refinement: Full Algorithm and Convergence

C.1. Purpose and Scope. This appendix provides the complete specification of TSMM Stage 2 (A2): an exact-moment Newton refinement that adjusts the Gamma hyperparameters (a, b) in

$$\alpha \sim \text{Gamma}(a, b) \quad (\text{shape } a > 0, \text{ rate } b > 0)$$

so that the exact DP-induced mixed moments of the site-partition count K_J match the elicited targets (μ_K, σ_K^2) (main text Algorithm Box 1).

Stage 1 (Section B) supplies a fast closed-form initializer (a_0, b_0) based on a large- J approximation. Stage 2 removes the remaining finite- J bias by solving the exact mixed-moment equations using Newton’s method with an analytic Jacobian computed via score identities and evaluated using the same Gauss–Laguerre quadrature nodes used for the moment functions.

Attribution note (what is classical vs. what is specific here). Newton’s method and its local quadratic convergence theory are classical (e.g., Dennis & Schnabel, 1996; Nocedal & Wright, 2006; Ortega & Rheinboldt, 1970). The score-function identity used to differentiate expectations is also standard (e.g., Casella & Berger, 2002). What is specific to this paper is the calibration pipeline that combines: (i) exact conditional moments of $K_J | \alpha$ (Section A, Proposition A.1), (ii) the Stage 1 closed-form map $(\mu_K, \sigma_K^2, J) \mapsto (a_0, b_0)$ (Section B, Theorem B.6), and (iii) an exact-moment Newton solver whose Jacobian is computed analytically and evaluated efficiently by quadrature.

C.2. Problem Statement and Target Equations. We work with the shape–rate Gamma density

$$g_{a,b}(\alpha) = \frac{b^a}{\Gamma(a)} \alpha^{a-1} e^{-b\alpha}, \quad \alpha > 0, \quad a > 0, \quad b > 0. \quad (\text{C.1})$$

Let

$$\kappa_J(\alpha) := \mathbb{E}(K_J | \alpha), \quad v_J(\alpha) := \text{Var}(K_J | \alpha), \quad (\text{C.2})$$

denote the exact conditional moments (Section A, Proposition A.1).

C.2.1. Mixed Moments Under Gamma Mixing. Define the mixed (prior-predictive) mean and variance under $\alpha \sim \text{Gamma}(a, b)$:

$$M_1(a, b) := \mathbb{E}_{a,b}[K_J] = \mathbb{E}_{\alpha \sim g_{a,b}}\{\kappa_J(\alpha)\}, \quad (\text{C.3})$$

and, by the law of total variance,

$$V(a, b) := \text{Var}(K_J) = \mathbb{E}_{a,b}\{\text{Var}_{\alpha \sim g_{a,b}}\{v_J(\alpha)\}\} + \text{Var}_{\alpha \sim g_{a,b}}\{\kappa_J(\alpha)\}. \quad (\text{C.4})$$

Equivalently, letting $m_r(a, b) := \mathbb{E}\{\kappa_J(\alpha)^r\}$ for $r \in \{1, 2\}$ and $v_1(a, b) := \mathbb{E}\{v_J(\alpha)\}$,

$$M_1(a, b) = m_1(a, b), \quad V(a, b) = v_1(a, b) + m_2(a, b) - m_1(a, b)^2. \quad (\text{C.5})$$

All expectations above are evaluated using generalized Gauss–Laguerre quadrature (Section A, §A.2.6.3). Importantly, within each Newton iteration we evaluate both the moments and their Jacobian entries using the same quadrature nodes and weights for the current (a, b) .

C.2.2. Root-Finding Formulation.

Definition C.3 (A2 Moment-Matching Problem). Given (J, μ_K, σ_K^2) , find $(a^*, b^*) \in (0, \infty)^2$ such that

$$F(a, b) := \begin{pmatrix} M_1(a, b) - \mu_K \\ V(a, b) - \sigma_K^2 \end{pmatrix} = \mathbf{0}. \quad (\text{C.6})$$

Stage 2 solves (C.6) starting from the Stage 1 initializer (a_0, b_0) (Section B).

C.3. Jacobian Derivation via Score Identities.

C.3.1. Score Identity.

Lemma C.3 (Score-Function Identity). *Let $\alpha \sim g_{a,b}$ and let $h(\alpha)$ be any function such that differentiation under the integral sign is justified. For $\theta \in \{a, b\}$,*

$$\frac{\partial}{\partial \theta} \mathbb{E}_{a,b}\{h(\alpha)\} = \mathbb{E}_{a,b}\{h(\alpha) s_\theta(\alpha)\}, \quad s_\theta(\alpha) := \frac{\partial}{\partial \theta} \log g_{a,b}(\alpha). \quad (\text{C.7})$$

For the $\text{Gamma}(a, b)$ density (C.1),

$$s_a(\alpha) = \log b - \psi(a) + \log \alpha, \quad s_b(\alpha) = \frac{a}{b} - \alpha. \quad (\text{C.8})$$

Proof. Write $\mathbb{E}_{a,b}\{h(\alpha)\} = \int_0^\infty h(\alpha) g_{a,b}(\alpha) d\alpha$ and differentiate under the integral sign:

$$\frac{\partial}{\partial \theta} \int h(\alpha) g_{a,b}(\alpha) d\alpha = \int h(\alpha) \frac{\partial}{\partial \theta} g_{a,b}(\alpha) d\alpha = \int h(\alpha) g_{a,b}(\alpha) \frac{\partial}{\partial \theta} \log g_{a,b}(\alpha) d\alpha,$$

which yields (C.7). The score formulas in (C.8) follow by differentiating $\log g_{a,b}(\alpha) = a \log b - \log \Gamma(a) + (a-1) \log \alpha - b\alpha$. \square

C.3.2. Jacobian Entries for the A2 System.

Corollary C.3 (Jacobian for $F(a, b)$). *Let F be defined in (C.6). Its Jacobian $\mathbf{J}_F(a, b) = \nabla F(a, b)$ can be written as*

$$\mathbf{J}_F(a, b) = \begin{pmatrix} \partial_a M_1 & \partial_b M_1 \\ \partial_a V & \partial_b V \end{pmatrix}, \quad (\text{C.9})$$

where for $\theta \in \{a, b\}$,

$$\partial_\theta M_1 = \partial_\theta m_1 = \mathbb{E}\{\kappa_J(\alpha) s_\theta(\alpha)\}, \quad (\text{C.10})$$

and

$$\partial_\theta V = \partial_\theta v_1 + \partial_\theta m_2 - 2m_1 \partial_\theta m_1, \quad (\text{C.11})$$

with

$$\partial_\theta v_1 = \mathbb{E}\{v_J(\alpha) s_\theta(\alpha)\}, \quad \partial_\theta m_2 = \mathbb{E}\{\kappa_J(\alpha)^2 s_\theta(\alpha)\}. \quad (\text{C.12})$$

Proof. Apply Lemma C.3 to m_1 , m_2 , and v_1 , then differentiate (C.5). \square

Implementation note (efficiency). In each Newton iteration, quadrature produces nodes $\{\alpha_m\}$ and weights $\{\tilde{w}_m\}$ (Section A, §A.2.6.3). We evaluate $\kappa_J(\alpha_m)$, $v_J(\alpha_m)$, and the scores $s_a(\alpha_m)$, $s_b(\alpha_m)$ once per node, and then compute all terms in (C.10)–(C.12) by weighted sums. This avoids finite-difference Jacobians and keeps the per-iteration cost $O(M)$.

C.3.3. Log-Parameterization (Recommended). To enforce $(a, b) > 0$ and improve numerical stability, we solve (C.6) in log-parameters

$$\eta = (\eta_1, \eta_2) = (\log a, \log b) \in \mathbb{R}^2, \quad (a, b) = (e^{\eta_1}, e^{\eta_2}). \quad (\text{C.13})$$

Let $G(\eta) := F(e^{\eta_1}, e^{\eta_2})$. By the chain rule,

$$\mathbf{J}_G(\eta) = \nabla_\eta G(\eta) = \mathbf{J}_F(a, b) \text{diag}(a, b). \quad (\text{C.14})$$

C.4. **Algorithm C.1: A2-MN (Exact-Moment Newton Refinement).** The complete A2-MN procedure is specified below.

Algorithm C.1 (A2-MN: Newton refinement for exact moment matching).

Input: design size J ; target moments (μ_K, σ_K^2) ; optional initial guess (a_0, b_0) ; quadrature size M ; tolerances $\text{tol}_F, \text{tol}_\eta$; maximum iterations max_iter .

Output: refined (a^*, b^*) ; diagnostics (iterations, final residual, termination code).

0. **Feasibility prescreen (cheap necessary checks).** Require

$$1 \leq \mu_K \leq J, \quad 0 \leq \sigma_K^2 \leq \frac{(J-1)^2}{4}. \quad (\text{C.15})$$

(The variance bound is Popoviciu's inequality for a variable supported on $\{1, \dots, J\}$.) If violated, return an error before numerical optimization.

1. **Stage 1 initialization (if needed).** If (a_0, b_0) is not supplied, compute it via the closed-form Stage 1 map (Section B, Theorem B.6). If $\sigma_K^2 \leq \mu_0 := \mu_K - 1$, apply the Stage 1 projection policy (Section B, §B.3.3) to obtain a numerically stable initializer.
2. **Initialize.** Set $\eta_0 = (\log a_0, \log b_0)$ and $t \leftarrow 0$.
3. **Iterate** for $t = 0, 1, \dots, \text{max_iter} - 1$:
 - (a) **Evaluate moments and residual.** Let $(a_t, b_t) = (e^{\eta_{t,1}}, e^{\eta_{t,2}})$. Compute $(M_1(a_t, b_t), V(a_t, b_t))$ by Gauss–Laguerre quadrature (Section A, §A.2.6.3) and set

$$f_t = G(\eta_t) = \begin{pmatrix} M_1(a_t, b_t) - \mu_K \\ V(a_t, b_t) - \sigma_K^2 \end{pmatrix}. \quad (\text{C.16})$$

- (b) **Stopping rule (residual).** If $\|f_t\|_\infty \leq \text{tol}_F$, return $(a^*, b^*) = (a_t, b_t)$.
- (c) **Jacobian (score-based).** Compute $\mathbf{J}_F(a_t, b_t)$ using Corollary C.3 (same quadrature nodes as in Step 3a). Form

$$\mathbf{J}_G(\eta_t) = \mathbf{J}_F(a_t, b_t) \text{diag}(a_t, b_t). \quad (\text{C.17})$$

If $|\det(\mathbf{J}_G)| < 10^{-12}$, regularize $\mathbf{J}_G \leftarrow \mathbf{J}_G + \varepsilon I_2$ with $\varepsilon = 10^{-8}$.

- (d) **Newton direction.** Solve the 2×2 linear system

$$\mathbf{J}_G(\eta_t) \Delta \eta_t = -f_t. \quad (\text{C.18})$$

- (e) **Stopping rule (step).** If $\|\Delta \eta_t\|_\infty \leq \text{tol}_\eta$, return (a_t, b_t) .

(f) **Backtracking line search (Armijo).** Set $\lambda \leftarrow 1$ and repeat: $\eta_{\text{cand}} \leftarrow \eta_t + \lambda \Delta\eta_t$, $f_{\text{cand}} \leftarrow G(\eta_{\text{cand}})$. Accept the step if

$$\|f_{\text{cand}}\|_2 \leq (1 - c\lambda) \|f_t\|_2, \quad c = 0.5. \quad (\text{C.19})$$

Otherwise set $\lambda \leftarrow \lambda/2$ and retry. If $\lambda < 10^{-8}$, terminate with a warning flag (no progress).

(g) **Update.** Set $\eta_{t+1} \leftarrow \eta_t + \lambda \Delta\eta_t$.

4. **Return on nonconvergence.** If $t = \text{max_iter}$ without meeting a stopping rule, return the last iterate with a warning flag.

Recommended defaults. In our reference settings we use $M = 80$ quadrature nodes, $\text{tol}_F = 10^{-8}$, $\text{tol}_\eta = 10^{-10}$, and $\text{max_iter} = 20$. With Stage 1 initialization, convergence to near machine precision typically occurs in a small number of Newton steps (see §C.6).

C.5. Convergence: What Is Guaranteed (and What Is Not).

Theorem C.7 (Local Quadratic Convergence of Newton Refinement). *Consider the root-finding problem $G(\eta) = 0$ with G defined by (C.13). Suppose there exists η^* such that $G(\eta^*) = 0$, and assume:*

1. *G is continuously differentiable in a neighborhood of η^* , and \mathbf{J}_G is Lipschitz continuous on that neighborhood;*
2. *$\mathbf{J}_G(\eta^*)$ is nonsingular.*

Then there exists a neighborhood \mathcal{N}_0 of η^ such that if $\eta_0 \in \mathcal{N}_0$, the undamped Newton iterates*

$$\eta_{t+1} = \eta_t - \mathbf{J}_G(\eta_t)^{-1}G(\eta_t) \quad (\text{C.20})$$

are well-defined, remain in the neighborhood, converge to η^ , and satisfy*

$$\|\eta_{t+1} - \eta^*\| \leq C \|\eta_t - \eta^*\|^2 \quad (\text{C.21})$$

for some constant $C > 0$.

Proof sketch. This is a standard consequence of the Newton–Kantorovich theory for nonlinear systems; see Ortega and Rheinboldt (1970, Ch. 10) or Dennis and Schnabel (1996, Ch. 5). \square

Local vs. global behavior. Theorem C.7 is local and does not guarantee convergence from an arbitrary starting point. TSMM relies on Stage 1 to place (a_0, b_0) near the solution in moderate-to-large J regimes (Section B, Proposition B.4). For smaller

J , the algorithm uses standard globalization safeguards (log-parameterization, line search, Jacobian regularization) to prevent divergence and to fail gracefully when targets are numerically problematic.

C.6. Worked Example and Typical Iteration Counts.

C.6.1. *Worked Example (Continuation of Appendix B.3.4).* Section B, §B.3.4 considers $J = 50$ sites with targets $(\mu_K, \sigma_K^2) = (5, 10)$. Stage 1 gives

$$(a_0, b_0) \approx (2.667, 2.608).$$

Evaluating the exact mixed moments at (a_0, b_0) shows finite- J bias (Stage 1 underestimates both mean and variance). Stage 2 corrects this by solving (C.6).

TABLE C.1. Stage 1 \rightarrow Stage 2 Correction (Example from Appendix B.3.4, $J = 50$)

Stage	(a, b)	$\mathbb{E}_{a,b}(K_J)$	$\text{Var}_{a,b}(K_J)$	Rel. error (mean, var)
Stage 1 (A1 init)	(2.667, 2.608)	4.415	5.618	-11.7%, -43.8%
Stage 2 (A2 final)	(1.408, 1.077)	5.000	10.000	$\approx 0, \approx 0$

Interpretation. Stage 1 uses a Poisson–Gamma proxy that ignores the conditional underdispersion of $K_J \mid \alpha$ (Section A, Corollary A.1), so it can underestimate $\text{Var}(K_J)$ when J is not large. Stage 2 adjusts the Gamma hyperprior to restore the exact mixed moments.

C.6.2. *Typical Iteration Count Benchmarks.* The table below reports representative A2-MN behavior using the reference settings $M = 80$, $\text{tol}_F = 10^{-8}$, $\text{tol}_\eta = 10^{-10}$, and Armijo damping.

TABLE C.2. Representative A2-MN Iterations from Stage 1 Initialization

J	Targets (μ_K, σ_K^2)	Stage 1 (a_0, b_0)	A2-MN steps	Stage 2 (a^*, b^*)
25	(5, 10)	(2.667, 2.146)	6	(1.035, 0.531)
50	(5, 10)	(2.667, 2.608)	5	(1.408, 1.077)
50	(10, 22.5)	(6.000, 2.608)	5	(2.240, 0.579)
100	(10, 20)	(7.364, 3.768)	4	(3.578, 1.327)
300	(15, 30)	(12.250, 4.991)	5	(6.772, 2.091)

These examples are representative of the broader pattern: Stage 1 is close enough to place Newton in a stable regime, and a small number of iterations achieves near machine-precision matching.

Computational scaling. Each A2-MN iteration evaluates a constant number of quadrature expectations, so the per-iteration complexity is $O(M)$ (with $M = 80$ by default). In contrast, distribution-level refinements (e.g., A2-KL below) require evaluating the full induced PMF over $k = 1, \dots, J$ and therefore scale as $O(JM)$ per iteration.

C.7. Optional: A2-KL Refinement (Distributional Target on K_J). Moment matching is appropriate when practitioner beliefs are summarized by (μ_K, σ_K^2) . In some settings, however, a practitioner (or a legacy baseline) specifies a full target distribution $p^*(k)$ over $k \in \{1, \dots, J\}$.

Definition C.4 (KL Refinement Objective). Given a target PMF p^* on $\{1, \dots, J\}$, define

$$(a^\dagger, b^\dagger) \in \arg \min_{a>0, b>0} D_{\text{KL}}(p^* \parallel p_{a,b}), \quad D_{\text{KL}}(p^* \parallel p_{a,b}) := \sum_{k=1}^J p^*(k) \log \frac{p^*(k)}{p_{a,b}(k)}, \quad (\text{C.22})$$

where $p_{a,b}(k) = \Pr(K_J = k \mid a, b)$ is the induced marginal PMF (Section A, Theorem A.3).

C.7.1. Gradient via Score Identities. Write $p_{a,b}(k) = \mathbb{E}_{a,b}\{p(K_J = k \mid \alpha)\}$, where $p(K_J = k \mid \alpha)$ is the Antoniak PMF (Section A, Eq. (A.8)). Lemma C.3 yields, for $\theta \in \{a, b\}$,

$$\frac{\partial}{\partial \theta} p_{a,b}(k) = \mathbb{E}_{a,b}\{p(K_J = k \mid \alpha) s_\theta(\alpha)\}. \quad (\text{C.23})$$

Therefore,

$$\frac{\partial}{\partial \theta} D_{\text{KL}}(p^* \parallel p_{a,b}) = - \sum_{k=1}^J \frac{p^*(k)}{p_{a,b}(k)} \frac{\partial}{\partial \theta} p_{a,b}(k). \quad (\text{C.24})$$

All expectations in (C.23) can be evaluated using the same quadrature machinery as in A2-MN; the additional cost arises from looping over $k = 1, \dots, J$.

C.7.2. Algorithm Outline. The A2-KL optimization procedure is outlined below.

Algorithm C.2 (A2-KL: distributional refinement; outline).

Input: J ; target PMF $p^*(1:J)$; initializer $(a_{\text{init}}, b_{\text{init}})$ (recommended: the A2-MN solution); quadrature size M ; optimizer settings (e.g., L-BFGS tolerances).

Output: (a^\dagger, b^\dagger) minimizing (C.22).

1. Initialize $(a, b) \leftarrow (a_{\text{init}}, b_{\text{init}})$ and optimize in $(\log a, \log b)$.
2. At each optimizer iteration:
 - evaluate $p_{a,b}(k)$ for $k = 1, \dots, J$ ([Section A](#), [Theorem A.3](#); stable evaluation via [Section A](#), §A.2.6.1),
 - compute the KL objective (C.22),
 - compute the gradient via (C.23)–(C.24) by quadrature.
3. Return the converged solution.

C.7.3. *DORO-Uniform Baseline (Optional Target)*. A simple distributional target used as a baseline in DORO-style calibrations is the uniform PMF on $\{1, \dots, m\}$ where m is chosen to match the target mean scale ([Dorazio, 2009](#)):

$$p^*(k) = \frac{1}{m} \mathbf{1}\{1 \leq k \leq m\}, \quad m := \min\{2\mu_K - 1, J\}. \quad (\text{C.25})$$

This baseline can be refined via A2-KL, with A2-MN providing a fast and stable initializer.

Appendix D. Approximation Error Bounds and Finite- J Analysis

D.1. Purpose and Scope. [Section B](#) introduced the Stage 1 (A1) approximation

$$K_J - 1 \mid \alpha \approx \text{Pois}(\alpha c_J), \quad c_J = \log J, \quad (\text{D.1})$$

which implies a shifted Negative Binomial law for K_J after mixing over the Gamma hyperprior $\alpha \sim \text{Gamma}(a, b)$. [Section C](#) then described Stage 2 (A2), which refines (a, b) to match the exact finite- J moments.

This appendix provides rigorous, distribution-level error quantification for A1 at finite J , with two concrete goals:

1. *Error accounting.* Identify and bound the dominant sources of approximation error for small/moderate J .
2. *Decision support.* Translate the bounds into actionable guidance for when A2 (or exact enumeration) is recommended.

Throughout, we work with the Dirichlet process / Chinese restaurant process (CRP) cluster count $K_J \in \{1, \dots, J\}$ at a fixed design size J .

D.2. Three-Way Error Decomposition.

D.2.1. *Conditional and Marginal Laws.* Let

$$S_J := K_J - 1 \in \{0, 1, \dots, J-1\}. \quad (\text{D.2})$$

Since total variation (TV) distance is invariant under deterministic shifts, bounding A1 for S_J is equivalent to bounding A1 for K_J .

From [Section A \(Theorem A.1\)](#), conditional on α we have the Poisson–binomial representation

$$S_J = \sum_{j=2}^J B_j, \quad B_j \mid \alpha \text{ independent, } B_j \sim \text{Bernoulli}(p_j(\alpha)), \quad p_j(\alpha) = \frac{\alpha}{\alpha + j - 1}. \quad (\text{D.3})$$

Define the exact conditional pmf and the A1 proxy conditional pmf

$$p_J(k \mid \alpha) := \mathbb{P}(S_J = k \mid \alpha), \quad \tilde{p}_J(k \mid \alpha) := \mathbb{P}(\text{Pois}(\alpha c_J) = k), \quad k = 0, \dots, J-1. \quad (\text{D.4})$$

Let $\pi_{a,b}$ denote the $\text{Gamma}(a, b)$ density (shape–rate), and define the induced marginal pmfs

$$p_{a,b}(k) := \int_0^\infty p_J(k \mid \alpha) \pi_{a,b}(\alpha) d\alpha, \quad \tilde{p}_{a,b}(k) := \int_0^\infty \tilde{p}_J(k \mid \alpha) \pi_{a,b}(\alpha) d\alpha. \quad (\text{D.5})$$

Under A1, the Poisson–Gamma mixture is exactly Negative Binomial, so $\tilde{p}_{a,b}$ is available in closed form ([Section B](#)).

D.2.2. *Error Sources and Decomposition.*

Definition D.5 (Error Sources). Fix $J \geq 2$ and $\alpha > 0$. Write

$$\lambda_J(\alpha) := \mathbb{E}[S_J \mid \alpha] = \sum_{j=2}^J p_j(\alpha) = \kappa_J(\alpha) - 1 = \alpha\{\psi(\alpha + J) - \psi(\alpha + 1)\}, \quad (\text{D.6})$$

where $\kappa_J(\alpha) = \mathbb{E}[K_J \mid \alpha]$ and $\psi(\cdot)$ is the digamma function. Decompose the conditional A1 error into:

1. *E1 (Poissonization):*

$$E_1(\alpha) := d_{\text{TV}}(\mathcal{L}(S_J \mid \alpha), \text{Pois}(\lambda_J(\alpha))) ; \quad (\text{D.7})$$

2. *E2 (Mean linearization):*

$$E_2(\alpha) := d_{\text{TV}}(\text{Pois}(\lambda_J(\alpha)), \text{Pois}(\alpha c_J)), \quad c_J = \log J; \quad (\text{D.8})$$

3. *E3 (Gamma mixing)*: the hyperprior $\alpha \sim \text{Gamma}(a, b)$ does not introduce a third approximation step, but it propagates $E_1(\alpha)$ and $E_2(\alpha)$ into the marginal $p_{a,b}$.

Theorem D.8 (Error Decomposition Under Mixing). *Let $p_{a,b}$ be the exact marginal pmf of S_J under $\alpha \sim \text{Gamma}(a, b)$, and $\tilde{p}_{a,b}$ be the A1 (shifted Negative Binomial) proxy with $c_J = \log J$. Then*

$$d_{\text{TV}}(p_{a,b}, \tilde{p}_{a,b}) \leq \mathbb{E}_{\alpha \sim \text{Gamma}(a,b)}[E_1(\alpha)] + \mathbb{E}_{\alpha \sim \text{Gamma}(a,b)}[E_2(\alpha)]. \quad (\text{D.9})$$

Proof. By definition and Jensen's inequality,

$$\begin{aligned} d_{\text{TV}}(p_{a,b}, \tilde{p}_{a,b}) &= \frac{1}{2} \sum_{k=0}^{J-1} \left| \int \{p_J(k \mid \alpha) - \tilde{p}_J(k \mid \alpha)\} \pi_{a,b}(\alpha) d\alpha \right| \\ &\leq \int \left\{ \frac{1}{2} \sum_{k=0}^{J-1} |p_J(k \mid \alpha) - \tilde{p}_J(k \mid \alpha)| \right\} \pi_{a,b}(\alpha) d\alpha \\ &= \mathbb{E}_{\alpha} [d_{\text{TV}}(p_J(\cdot \mid \alpha), \tilde{p}_J(\cdot \mid \alpha))]. \end{aligned}$$

For fixed α , apply the triangle inequality

$$d_{\text{TV}}(p_J(\cdot \mid \alpha), \tilde{p}_J(\cdot \mid \alpha)) \leq d_{\text{TV}}(\mathcal{L}(S_J \mid \alpha), \text{Pois}(\lambda_J(\alpha))) + d_{\text{TV}}(\text{Pois}(\lambda_J(\alpha)), \text{Pois}(\alpha c_J)),$$

which equals $E_1(\alpha) + E_2(\alpha)$. Integrating completes the proof. \square

Attribution. The contraction of TV under a common mixing distribution is standard; the role of [Theorem D.8](#) is to make explicit that the A1 error is controlled by two conditional terms (E_1 , E_2) that can be bounded and interpreted separately.

D.3. Conditional (Fixed- α) Bounds.

D.3.1. Poissonization Error $E_1(\alpha)$.

Theorem D.9 (Poisson Approximation TV Bound). *Fix $J \geq 2$ and $\alpha > 0$. Let $\lambda_J(\alpha) = \sum_{j=2}^J p_j(\alpha)$ as in [\(D.6\)](#). Then*

$$E_1(\alpha) = d_{\text{TV}}(\mathcal{L}(S_J \mid \alpha), \text{Pois}(\lambda_J(\alpha))) \leq \min\left(1, \frac{1}{\lambda_J(\alpha)}\right) \sum_{j=2}^J p_j(\alpha)^2. \quad (\text{D.10})$$

Moreover,

$$\sum_{j=2}^J p_j(\alpha)^2 = \lambda_J(\alpha) - v_J(\alpha) = \alpha^2 \{\psi_1(\alpha + 1) - \psi_1(\alpha + J)\}, \quad (\text{D.11})$$

where $v_J(\alpha) = \text{Var}(S_J \mid \alpha)$ and $\psi_1(\cdot)$ is the trigamma function.

Proof. The bound (D.10) is a standard Chen–Stein/Le Cam Poisson approximation inequality for sums of independent Bernoulli indicators (Barbour & Hall, 1984; Barbour et al., 1992; Le Cam, 1960). Here $S_J = \sum_{j=2}^J B_j$ with $B_j \sim \text{Bernoulli}(p_j(\alpha))$ independent given α , and $\lambda_J(\alpha) = \sum_{j=2}^J p_j(\alpha)$.

For (D.11), note that

$$v_J(\alpha) = \sum_{j=2}^J p_j(\alpha)\{1 - p_j(\alpha)\} = \sum_{j=2}^J p_j(\alpha) - \sum_{j=2}^J p_j(\alpha)^2 = \lambda_J(\alpha) - \sum_{j=2}^J p_j(\alpha)^2,$$

so $\sum_{j=2}^J p_j(\alpha)^2 = \lambda_J(\alpha) - v_J(\alpha)$. Finally,

$$\sum_{j=2}^J p_j(\alpha)^2 = \alpha^2 \sum_{m=1}^{J-1} \frac{1}{(\alpha+m)^2} = \alpha^2 \{\psi_1(\alpha+1) - \psi_1(\alpha+J)\}$$

by the series representation $\psi_1(x) = \sum_{m=0}^{\infty} (x+m)^{-2}$. \square

Attribution. (D.10) is classical (Barbour & Hall, 1984; Barbour et al., 1992; Le Cam, 1960). The special-function identity (D.11) follows from standard trigamma series expansions.

Interpretation (why the rate is slow). For fixed α , $\lambda_J(\alpha) \asymp \alpha \log J$ while $\sum p_j(\alpha)^2$ converges to a finite constant as $J \rightarrow \infty$, so (D.10) yields $E_1(\alpha) = O(1/\log J)$. This is a logarithmically slow rate: for example, using natural logs,

$$\frac{1}{\log 20} \approx 0.33, \quad \frac{1}{\log 50} \approx 0.26, \quad \frac{1}{\log 100} \approx 0.22.$$

Sharp results for related “logarithmic combinatorial structures” show that the $1/\log J$ scaling is not merely an artifact of the proof in many settings (Arratia et al., 2003).

D.3.2. Mean Linearization Error $E_2(\alpha)$ for $c_J = \log J$. A1 uses $c_J = \log J$ to linearize the exact conditional mean $\lambda_J(\alpha)$.

Theorem D.10 (Mean Linearization Bound for $\lambda_J(\alpha)$). *Fix $\alpha > 0$ and $J \geq 2$. With $\lambda_J(\alpha) = \alpha\{\psi(\alpha+J) - \psi(\alpha+1)\}$,*

$$|\lambda_J(\alpha) - \alpha \log J + \alpha \psi(\alpha+1)| \leq \frac{\alpha^2}{J} + \frac{\alpha}{2J} + \frac{\alpha}{12J^2}. \quad (\text{D.12})$$

In particular,

$$|\lambda_J(\alpha) - \alpha \log J| \leq \alpha |\psi(\alpha+1)| + \frac{\alpha^2}{J} + \frac{\alpha}{2J} + \frac{\alpha}{12J^2}. \quad (\text{D.13})$$

Proof. Write

$$\lambda_J(\alpha) - \alpha \log J = \alpha\{\psi(\alpha+J) - \log J\} - \alpha\psi(\alpha+1).$$

Thus

$$|\lambda_J(\alpha) - \alpha \log J + \alpha \psi(\alpha + 1)| = \alpha |\psi(\alpha + J) - \log J|.$$

Bound

$$|\psi(\alpha + J) - \log J| \leq |\psi(\alpha + J) - \log(\alpha + J)| + |\log(\alpha + J) - \log J|.$$

For the first term, a standard digamma inequality gives

$$\left| \psi(x) - \log x + \frac{1}{2x} \right| \leq \frac{1}{12x^2} \quad (x > 0),$$

hence

$$|\psi(\alpha + J) - \log(\alpha + J)| \leq \frac{1}{2(\alpha + J)} + \frac{1}{12(\alpha + J)^2} \leq \frac{1}{2J} + \frac{1}{12J^2}.$$

For the second term, $\log(\alpha + J) - \log J = \log(1 + \alpha/J) \leq \alpha/J$. Combining and multiplying by α yields (D.12), and (D.13) follows by the triangle inequality. \square

Attribution. The digamma approximation inequality is standard (Abramowitz & Stegun, 1964, §6.3).

Interpretation. The leading ‘‘bias’’ term in (D.12) is the J -independent quantity $-\alpha \psi(\alpha + 1)$; the remaining terms are $O(\alpha^2/J)$. Thus, even when the Poissonization error $E_1(\alpha)$ is already small, using $c_J = \log J$ can leave non-negligible mean mismatch at moderate J .

D.3.3. Combined Conditional Bound (A1).

Corollary D.4 (Combined Conditional TV Bound). *For $c_J = \log J$,*

$$d_{\text{TV}}(\mathcal{L}(S_J | \alpha), \text{Pois}(\alpha \log J)) \leq E_1(\alpha) + E_2(\alpha), \quad (\text{D.14})$$

where $E_1(\alpha)$ satisfies (D.10) and

$$E_2(\alpha) = d_{\text{TV}}(\text{Pois}(\lambda_J(\alpha)), \text{Pois}(\alpha \log J)) \leq \sqrt{\frac{1}{2} \text{KL}(\text{Pois}(\lambda_J(\alpha)) \parallel \text{Pois}(\alpha \log J))}. \quad (\text{D.15})$$

The Poisson KL divergence is explicit:

$$\text{KL}(\text{Pois}(\lambda) \parallel \text{Pois}(\lambda')) = \lambda \log\left(\frac{\lambda}{\lambda'}\right) + \lambda' - \lambda, \quad \lambda, \lambda' > 0. \quad (\text{D.16})$$

Proof. (D.14) is the triangle inequality with the intermediate $\text{Pois}(\lambda_J(\alpha))$. (D.15) is Pinsker’s inequality applied to the two Poisson laws, and (D.16) is the standard KL formula for Poisson distributions. \square

Rate interpretation. For fixed α and moderate/large J : [Theorem D.9](#) implies $E_1(\alpha) = O(1/\log J)$. [Theorem D.10](#) implies $\lambda_J(\alpha) = \alpha \log J + O(\alpha)$, so the Poisson–Poisson KL in [\(D.16\)](#) is typically $O(\alpha/\log J)$, leading to $E_2(\alpha) = O\left(\sqrt{\alpha/\log J}\right)$. Hence, for J in the tens, the mean-linearization term often dominates the distributional error unless α is extremely small.

D.4. Marginal (Gamma-Mixed) Bounds.

D.4.1. Marginal TV Bound.

Theorem D.11 (Marginal TV Bound Under $\alpha \sim \text{Gamma}(a, b)$). *Let $p_{a,b}$ and $\tilde{p}_{a,b}$ be the exact and A1 marginal pmfs of $S_J = K_J - 1$ under $\alpha \sim \text{Gamma}(a, b)$, with $c_J = \log J$. Then*

$$d_{\text{TV}}(p_{a,b}, \tilde{p}_{a,b}) \leq \mathbb{E}_\alpha[E_1(\alpha)] + \mathbb{E}_\alpha[E_2(\alpha)], \quad (\text{D.17})$$

where $E_1(\alpha)$ and $E_2(\alpha)$ are given in [Definition D.5](#) and bounded by [\(D.10\)](#) and [\(D.15\)](#).

Moreover, if $\mathbb{E}[\sqrt{\alpha}] < \infty$ (equivalently $a > 1/2$), then

$$\mathbb{E}_\alpha[E_1(\alpha)] = O\left(\frac{1}{\log J}\right), \quad \mathbb{E}_\alpha[E_2(\alpha)] = O\left(\frac{\mathbb{E}[\sqrt{\alpha}]}{\sqrt{\log J}}\right) \quad (J \rightarrow \infty). \quad (\text{D.18})$$

For $\alpha \sim \text{Gamma}(a, b)$,

$$\mathbb{E}[\sqrt{\alpha}] = \frac{\Gamma(a + 1/2)}{\Gamma(a)} \cdot \frac{1}{\sqrt{b}}. \quad (\text{D.19})$$

Proof. [\(D.17\)](#) is exactly [Theorem D.8](#). The scaling in [\(D.18\)](#) follows from the pointwise rate statements in [Corollary D.4](#) together with $\lambda_J(\alpha) \asymp \alpha \log J$ for large J and integrability of $\sqrt{\alpha}$. Finally, [\(D.19\)](#) is the standard half-moment of the Gamma distribution. \square

Interpretation. Mixing over α does not eliminate the finite- J linearization effect: if the hyperprior places non-negligible mass on moderate α , then the mean-linearization component can remain the dominant source of distributional discrepancy for $J \in [10, 100]$.

D.4.2. Moment-Level Implications.

Corollary D.5 (Moment Implications via TV Coupling). *Let P and Q be distributions on $\{1, 2, \dots, J\}$. Then for any bounded function f ,*

$$|\mathbb{E}_P[f(K)] - \mathbb{E}_Q[f(K)]| \leq 2\|f\|_\infty d_{\text{TV}}(P, Q). \quad (\text{D.20})$$

Applying this with $f(K) = K$ and $f(K) = K^2$ yields the conservative bounds

$$|\mathbb{E}[K_J | a, b] - \tilde{\mu}_K| \leq 2J d_{\text{TV}}(p_{a,b}, \tilde{p}_{a,b}), \quad |\text{Var}(K_J | a, b) - \tilde{\sigma}_K^2| \leq 4J^2 d_{\text{TV}}(p_{a,b}, \tilde{p}_{a,b}), \quad (\text{D.21})$$

where $(\tilde{\mu}_K, \tilde{\sigma}_K^2)$ are the A1 (NegBin) proxy moments.

Remark. (D.21) is intentionally worst-case; in typical multisite applications K_J concentrates on small values, so actual moment discrepancies are often much smaller than these bounds suggest. The main use of Corollary D.5 is to convert a distributional tolerance into a conservative bound on moment error.

D.5. When Is A2 Necessary? Practical Threshold Conditions. The bounds above formalize why A1 can be unreliable at small/moderate J : both the Poissonization term ($\sim 1/\log J$) and the mean-linearization term (often $\sim 1/\sqrt{\log J}$) decay slowly with J .

Proposition D.5 (Rule-of-Thumb Threshold). *Suppose one targets a small tolerance level $\epsilon > 0$ for the leading (logarithmic) error term in the A1 approximation. A simple back-of-the-envelope sufficient condition of the form*

$$\frac{a/b}{\log J} \lesssim \epsilon \iff J \gtrsim \exp\left(\frac{a}{b\epsilon}\right) \quad (\text{D.22})$$

highlights that very large J can be required for Stage 1 to be accurate in a uniform, distribution-level sense.

Remark. Proposition D.5 is intentionally conservative and suppresses constants as well as the E_2 contribution; it is included only to provide an interpretable scaling law. In practice, the decision should be based on the finite- J regime, as summarized next.

TABLE D.1. Practical Guidelines for Stage 1 vs. Stage 2

Regime	J range	Recommendation
Large J , exploratory use	$J \geq 100$	A1 alone may be acceptable as a fast initializer
Moderate J , publishable analysis	$J \in [30, 100]$	A1 + A2 recommended
Small J , low-information setting	$J \in [10, 30]$	A2 essential
Very small J	$J < 10$	Prefer exact enumeration or distribution-level calibration (e.g., A2-KL)

Practical decision rule. Stage 2 (A2) is recommended by default; Stage 1 (A1) alone is mainly useful as a quick initializer or for coarse exploratory work when J is clearly large.

Appendix E. Weight Distribution Theory and Dual-Anchor Framework

E.1. Purpose and Scope. This appendix develops the weight-based anchor that complements the cluster-count calibration established in [Sections A to C](#). While the Two-Stage Moment Matching (TSMM) algorithm efficiently translates practitioner beliefs about K_J into Gamma hyperparameters, [Vicentini and Jermyn \(2025\)](#) demonstrate that priors calibrated solely through cluster counts may imply “unintended” behavior on the stick-breaking weights—for instance, a prior appearing “diffuse” in K_J can nonetheless encode a strong assumption that one cluster dominates the mixture.

The present appendix addresses this concern by:

1. Deriving the closed-form distribution of the first stick-breaking weight w_1 under a Gamma hyperprior ([Theorem E.12](#)), enabling rapid computation of dominance diagnostics;
2. Establishing the moment structure of the co-clustering probability $\rho = \sum_{h=1}^{\infty} w_h^2$ ([Propositions E.7 and E.8](#)), which provides an alternative weight functional with immediate applied interpretation;
3. Formalizing the Dual-Anchor calibration protocol ([Definition E.8](#), [Algorithm E.1](#)) that allows practitioners to constrain weight dominance when diagnostics indicate substantively unacceptable behavior.

Attribution Note (Classical vs. Novel). The Sethuraman stick-breaking representation and GEM (size-biased) ordering are classical ([Pitman, 2006](#); [Sethuraman, 1994](#)). The closed-form marginal distribution of w_1 under Gamma mixing ([Theorem E.12](#)) is given in [Vicentini and Jermyn \(2025, Appendix A\)](#) and is reproduced here because it enables $O(1)$ dominance diagnostics. What is specific to this paper is the design-conditional calibration workflow that couples the K_J anchor ([Sections A to C](#)) with these weight diagnostics, and the resulting Dual-Anchor refinement option ([§E.5](#)).

Throughout, we maintain the notation established in the main text and earlier appendices: J denotes the fixed design size, $\alpha \sim \text{Gamma}(a, b)$ in shape–rate parameterization, K_J is the number of occupied clusters, and (w_1, w_2, \dots) are the stick-breaking weights in GEM order.

E.2. Stick-Breaking Weights and Size-Biased Interpretation.

E.2.1. *The GEM Distribution and Its Construction.* We recall the Sethuraman stick-breaking representation. The Dirichlet process $G \sim \text{DP}(\alpha, G_0)$ admits the representation (Sethuraman, 1994):

$$G = \sum_{h=1}^{\infty} w_h \delta_{\theta_h^*}, \quad \theta_h^* \stackrel{iid}{\sim} G_0, \quad (\text{E.1})$$

where the weights (w_1, w_2, \dots) are constructed as follows.

Definition E.6 (GEM Distribution). Let $v_h \stackrel{iid}{\sim} \text{Beta}(1, \alpha)$ for $h = 1, 2, \dots$. Define

$$w_1 := v_1, \quad w_h := v_h \prod_{\ell=1}^{h-1} (1 - v_{\ell}) \quad \text{for } h \geq 2. \quad (\text{E.2})$$

The sequence (w_1, w_2, \dots) follows the $\text{GEM}(\alpha)$ distribution (Griffiths–Engen–McCloskey; see Pitman, 2006).

The construction in (E.2) has a “stick-breaking” interpretation: starting with a unit stick, we break off a fraction v_1 to form w_1 , then break off a fraction v_2 of the remainder to form w_2 , and so on. By construction, $\sum_{h=1}^{\infty} w_h = 1$ almost surely.

E.2.2. *Critical Caveat: Size-Biased Order. Interpretability Warning.* The sequence (w_1, w_2, \dots) is in size-biased (GEM) order, not ranked from largest to smallest:

$$(w_1, w_2, \dots) \neq (w_{(1)}, w_{(2)}, \dots) \quad \text{where } w_{(1)} \geq w_{(2)} \geq \dots. \quad (\text{E.3})$$

The weight w_1 represents the asymptotic proportion of the cluster containing a randomly selected unit—equivalently, a size-biased pick from the Poisson–Dirichlet distribution (Pitman, 1996)—not necessarily the largest cluster share.

This distinction is critical for applied elicitation. When practitioners express beliefs about “the dominant cluster proportion,” they typically mean $\max_h w_h = w_{(1)}$, not the size-biased w_1 . The relationship $\Pr(\max_h w_h > t) \geq \Pr(w_1 > t)$ holds, so w_1 -based diagnostics provide a conservative bound on dominance risk: if $\Pr(w_1 > t)$ is small, then $\Pr(w_{(1)} > t)$ is also small.

Despite the size-biased interpretation, w_1 remains a useful diagnostic because:

1. It has a closed-form distribution under Gamma hyperpriors (Theorem E.12), enabling rapid computation without simulation;
2. It provides a mathematically principled lower bound on dominance risk;
3. Critically, if $w_1 > 0.5$, then w_1 is necessarily the largest weight (i.e., $w_1 = w_{(1)}$), since no other weight can exceed 0.5 when one weight already does. Thus, the tail probability $\Pr(w_1 > 0.5)$ is an exact measure of majority dominance risk.

E.2.3. *Conditional Distribution of w_1 .* From the stick-breaking construction (E.2), $w_1 = v_1$ where $v_1 \sim \text{Beta}(1, \alpha)$.

Proposition E.6 (Conditional Distribution of w_1). *Conditionally on $\alpha > 0$,*

$$w_1 \mid \alpha \sim \text{Beta}(1, \alpha). \quad (\text{E.4})$$

The density, CDF, and moments are:

$$p(w_1 \mid \alpha) = \alpha(1 - w_1)^{\alpha-1}, \quad \Pr(w_1 \leq x \mid \alpha) = 1 - (1 - x)^\alpha, \quad (\text{E.5})$$

$$\mathbb{E}[w_1 \mid \alpha] = \frac{1}{1 + \alpha}, \quad \text{Var}(w_1 \mid \alpha) = \frac{\alpha}{(1 + \alpha)^2(2 + \alpha)}. \quad (\text{E.6})$$

Proof. Immediate from $w_1 = v_1$ and $v_1 \sim \text{Beta}(1, \alpha)$. \square

Interpretation. As $\alpha \rightarrow 0$, $\mathbb{E}[w_1 \mid \alpha] \rightarrow 1$: the first cluster absorbs nearly all probability mass. As $\alpha \rightarrow \infty$, $\mathbb{E}[w_1 \mid \alpha] \rightarrow 0$: mass becomes diffuse across many clusters. This monotone relationship between α and expected dominance is the basis for weight-based diagnostics.

E.3. Closed-Form Marginal Distribution of w_1 . When α itself is random with a Gamma hyperprior, the unconditional (marginal) distribution of w_1 admits closed-form expressions. This key result enables rapid computation of dominance diagnostics without Monte Carlo simulation.

E.3.1. *Main Theorem.*

Theorem E.12 (Unconditional Distribution of w_1). *Let $\alpha \sim \text{Gamma}(a, b)$ with density $g_{a,b}(\alpha) = \frac{b^a}{\Gamma(a)} \alpha^{a-1} e^{-b\alpha}$ for $\alpha > 0$. Then w_1 has the following closed-form distributions:*

(i) Density:

$$p(w_1 \mid a, b) = \frac{a b^a}{(1 - w_1)[b - \log(1 - w_1)]^{a+1}}, \quad w_1 \in (0, 1). \quad (\text{E.7})$$

(ii) Cumulative distribution function:

$$F_{w_1}(x \mid a, b) = \Pr(w_1 \leq x \mid a, b) = 1 - \left(\frac{b}{b - \log(1 - x)} \right)^a, \quad x \in [0, 1]. \quad (\text{E.8})$$

(iii) Survival (tail) probability:

$$\Pr(w_1 > t \mid a, b) = \left(\frac{b}{b - \log(1 - t)} \right)^a$$

(E.9)

(iv) Quantile function: For $u \in (0, 1)$,

$$Q_{w_1}(u | a, b) = 1 - \exp(b [1 - (1 - u)^{-1/a}]). \quad (\text{E.10})$$

Attribution. The density and CDF formulas appear in Vicentini and Jermyn (2025, Appendix A), who derive them in the context of sample-size-independent prior specification. We provide a self-contained proof for completeness.

Proof. We integrate out α from the conditional distribution:

$$\begin{aligned} p(w_1 | a, b) &= \int_0^\infty p(w_1 | \alpha) g_{a,b}(\alpha) d\alpha \\ &= \int_0^\infty \alpha(1 - w_1)^{\alpha-1} \cdot \frac{b^a}{\Gamma(a)} \alpha^{a-1} e^{-b\alpha} d\alpha \\ &= \frac{b^a}{\Gamma(a)(1 - w_1)} \int_0^\infty \alpha^a \exp[-\alpha(b - \log(1 - w_1))] d\alpha. \end{aligned} \quad (\text{E.11})$$

Define $\beta := b - \log(1 - w_1)$. Since $\log(1 - w_1) < 0$ for $w_1 \in (0, 1)$, we have $\beta > b > 0$. The integral in (E.11) is a Gamma integral:

$$\int_0^\infty \alpha^a e^{-\beta\alpha} d\alpha = \frac{\Gamma(a+1)}{\beta^{a+1}}. \quad (\text{E.12})$$

Substituting (E.12) into (E.11) and using $\Gamma(a+1) = a\Gamma(a)$:

$$p(w_1 | a, b) = \frac{b^a}{\Gamma(a)(1 - w_1)} \cdot \frac{a\Gamma(a)}{[b - \log(1 - w_1)]^{a+1}} = \frac{a b^a}{(1 - w_1)[b - \log(1 - w_1)]^{a+1}}.$$

This establishes (E.7).

For the CDF, we integrate the density. With the substitution $u = b - \log(1 - w)$, so $du = dw/(1 - w)$:

$$\begin{aligned} F_{w_1}(x | a, b) &= \int_0^x \frac{a b^a}{(1 - w)[b - \log(1 - w)]^{a+1}} dw \\ &= a b^a \int_b^{b - \log(1-x)} u^{-a-1} du \\ &= a b^a \left[-\frac{u^{-a}}{a} \right]_b^{b - \log(1-x)} \\ &= b^a \left[b^{-a} - [b - \log(1 - x)]^{-a} \right] = 1 - \left(\frac{b}{b - \log(1 - x)} \right)^a. \end{aligned}$$

The survival function (E.9) is $1 - F_{w_1}(t)$, and the quantile function (E.10) is obtained by solving $F_{w_1}(Q) = u$ for Q . \square

Alternative Derivation via Laplace Transform. The survival probability (E.9) can be derived more directly. From [Proposition E.6](#), $\Pr(w_1 > t | \alpha) = (1-t)^\alpha = \exp(-c_t \alpha)$ where $c_t := -\log(1-t) > 0$. Then:

$$\Pr(w_1 > t | a, b) = \mathbb{E}_\alpha[\exp(-c_t \alpha)] = \left(\frac{b}{b + c_t} \right)^a = \left(\frac{b}{b - \log(1-t)} \right)^a,$$

using the Laplace transform of a $\text{Gamma}(a, b)$ random variable. \square

E.3.2. Limit Behavior and Consistency Checks. The survival probability formula (E.9) satisfies expected boundary conditions.

As $t \downarrow 0$: $\Pr(w_1 > t) = (b/[b - \log(1-t)])^a \rightarrow (b/b)^a = 1$.

As $t \uparrow 1$: $\log(1-t) \rightarrow -\infty$, so $b - \log(1-t) \rightarrow +\infty$, hence $\Pr(w_1 > t) \rightarrow 0$.

These limits confirm that w_1 has support $(0, 1)$ almost surely under the Gamma hyperprior.

E.3.3. Derivatives for Gradient-Based Optimization. For the Dual-Anchor refinement ([§E.5](#)), gradients of $\Pr(w_1 > t | a, b)$ with respect to (a, b) are useful. Define $c_t := -\log(1-t) > 0$ and $S(t; a, b) := \Pr(w_1 > t | a, b) = (b/(b + c_t))^a$. Then:

$$\frac{\partial S}{\partial a} = S(t; a, b) \cdot \log\left(\frac{b}{b + c_t}\right), \quad (\text{E.13})$$

$$\frac{\partial S}{\partial b} = S(t; a, b) \cdot \frac{a c_t}{b(b + c_t)}. \quad (\text{E.14})$$

Since $\log(b/(b + c_t)) < 0$, we have $\partial S / \partial a < 0$: increasing the shape a (making the α -prior more concentrated) reduces dominance probability. Similarly, $\partial S / \partial b > 0$: increasing the rate b (shifting α toward smaller values) increases dominance probability.

E.3.4. Default Diagnostic Thresholds.

Corollary E.6 (Default Diagnostic Thresholds). *The following thresholds provide interpretable dominance benchmarks:*

- $\Pr(w_1 > 0.5 | a, b)$: Probability of majority dominance (a size-biased cluster contains more than half of units). Since $w_1 > 0.5$ implies $w_1 = w_{(1)}$, this is also the probability that the largest cluster exceeds 50%.
- $\Pr(w_1 > 0.9 | a, b)$: Probability of near-universal dominance (a cluster contains at least 90% of units).

These thresholds are computed instantaneously via (E.9) and provide the diagnostics recommended in the main text *Algorithm Box 1*.

E.4. Co-Clustering Probability ρ . The first weight w_1 captures the size of a single (size-biased) cluster. An alternative functional that summarizes overall weight concentration is the co-clustering probability, which measures the chance that two randomly selected units share the same cluster.

E.4.1. *Definition and Applied Interpretation.*

Definition E.7 (Co-Clustering Probability / Simpson Index). The co-clustering probability is

$$\rho := \sum_{h=1}^{\infty} w_h^2. \quad (\text{E.15})$$

Equivalently, conditional on the weights (w_h) , if Z_i, Z_j are independent cluster assignments with $\Pr(Z = h \mid \mathbf{w}) = w_h$, then

$$\rho = \Pr(Z_i = Z_j \mid \mathbf{w}). \quad (\text{E.16})$$

Applied interpretation. The quantity ρ directly answers the question: “If two units are drawn at random, what is the probability they belong to the same latent cluster?” This formulation is often more intuitive for practitioners than questions about individual weights.

The co-clustering probability is sometimes called the Simpson index in ecology, where it measures the probability that two randomly selected individuals belong to the same species.

E.4.2. Conditional Moments of ρ . The GEM structure enables recursive computation of ρ ’s moments.

Proposition E.7 (Conditional Moments of ρ). *For $\alpha > 0$:*

(i) First moment:

$$\mathbb{E}[\rho \mid \alpha] = \frac{1}{1 + \alpha}. \quad (\text{E.17})$$

(ii) Second moment:

$$\mathbb{E}[\rho^2 \mid \alpha] = \frac{\alpha + 6}{(\alpha + 1)(\alpha + 2)(\alpha + 3)}. \quad (\text{E.18})$$

(iii) Variance:

$$\text{Var}(\rho \mid \alpha) = \frac{2\alpha}{(\alpha + 1)^2(\alpha + 2)(\alpha + 3)}. \quad (\text{E.19})$$

Attribution. These results are classical; see Kingman (1975) and Pitman (1996, 2006) for the general theory of Poisson–Dirichlet distributions.

Proof sketch. From the stick-breaking construction, ρ satisfies the distributional recursion

$$\rho \stackrel{d}{=} v^2 + (1 - v)^2 \rho', \quad (\text{E.20})$$

where $v \sim \text{Beta}(1, \alpha)$ and ρ' is an independent copy of ρ . Taking expectations and solving the fixed-point equation yields $\mathbb{E}[\rho] = 1/(1 + \alpha)$. The second moment follows from squaring (E.20) and applying similar algebra. \square

Key observation. Comparing (E.17) with (E.6):

$$\mathbb{E}[\rho \mid \alpha] = \mathbb{E}[w_1 \mid \alpha] = \frac{1}{1 + \alpha}. \quad (\text{E.21})$$

Thus, the expected co-clustering probability equals the expected first weight. This identity simplifies elicitation: asking practitioners about co-clustering yields information directly usable for w_1 -based calibration.

E.4.3. Marginal Moments Under Gamma Hyperprior.

Proposition E.8 (Marginal Mean of ρ). *Under $\alpha \sim \text{Gamma}(a, b)$:*

$$\mathbb{E}[\rho \mid a, b] = \mathbb{E}\left[\frac{1}{1 + \alpha}\right] = I_1(a, b), \quad (\text{E.22})$$

where the functional $I_c(a, b) := \mathbb{E}[(\alpha + c)^{-1}]$ for $c > 0$ is given by:

$$I_c(a, b) = b^a c^{a-1} e^{bc} \Gamma(1 - a, bc), \quad (\text{E.23})$$

with $\Gamma(s, x) = \int_x^\infty t^{s-1} e^{-t} dt$ denoting the upper incomplete gamma function.

For the special case $c = 1$:

$$\mathbb{E}[\rho \mid a, b] = \mathbb{E}[w_1 \mid a, b] = b^a e^b \Gamma(1 - a, b). \quad (\text{E.24})$$

Attribution. The integral identity underlying (E.23) is standard (Abramowitz & Stegun, 1964, §6.5). Its application to DP weight functionals appears in the analysis of Vicentini and Jermyn (2025).

Proof. We compute

$$I_c(a, b) = \int_0^\infty \frac{1}{\alpha + c} \cdot \frac{b^a}{\Gamma(a)} \alpha^{a-1} e^{-b\alpha} d\alpha = \frac{b^a}{\Gamma(a)} \int_0^\infty \frac{\alpha^{a-1} e^{-b\alpha}}{\alpha + c} d\alpha. \quad (\text{E.25})$$

Using the integral identity (Abramowitz & Stegun, 1964, Eq. 6.5.3):

$$\int_0^\infty \frac{x^{a-1} e^{-bx}}{x + c} dx = c^{a-1} e^{bc} \Gamma(a) \Gamma(1 - a, bc), \quad (\text{E.26})$$

we obtain

$$I_c(a, b) = \frac{b^a}{\Gamma(a)} \cdot c^{a-1} e^{bc} \Gamma(a) \Gamma(1-a, bc) = b^a c^{a-1} e^{bc} \Gamma(1-a, bc). \quad \square$$

Computational note. For $a < 1$, the formula (E.23) is directly computable using standard incomplete gamma implementations. For $a \geq 1$, the upper incomplete gamma function $\Gamma(1-a, bc)$ requires analytic continuation, which is handled automatically by numerical libraries (e.g., `pgamma` in R, `scipy.special.gammaincc` in Python).

Practical numerical recipe (quadrature-based). To compute $I_c(a, b)$ stably without relying on special-function continuation: (1) build generalized Gauss–Laguerre nodes/weights $\{(x_m, \tilde{w}_m)\}_{m=1}^M$ for weight $x^{a-1} e^{-x}$ (Section A, §A.2.6); (2) map $\alpha_m = x_m/b$; (3) approximate $I_c(a, b) \approx \sum_{m=1}^M \tilde{w}_m / (\alpha_m + c)$. Using the same nodes for multiple expectations (e.g., K_J moments and ρ diagnostics) yields substantial computational savings.

E.4.4. *Unconditional Second Moment of ρ .* Using the partial fraction decomposition

$$\frac{\alpha+6}{(\alpha+1)(\alpha+2)(\alpha+3)} = \frac{5}{2(\alpha+1)} - \frac{4}{\alpha+2} + \frac{3}{2(\alpha+3)}, \quad (\text{E.27})$$

we obtain:

Corollary E.7 (Unconditional Second Moment of ρ). *Under $\alpha \sim \text{Gamma}(a, b)$:*

$$\mathbb{E}[\rho^2 | a, b] = \frac{5}{2} I_1(a, b) - 4 I_2(a, b) + \frac{3}{2} I_3(a, b), \quad (\text{E.28})$$

and hence

$$\text{Var}(\rho | a, b) = \mathbb{E}[\rho^2 | a, b] - [\mathbb{E}[\rho | a, b]]^2. \quad (\text{E.29})$$

Design implication. The distribution of ρ under the Gamma hyperprior does not have a simple closed form, but its mean and variance are closed-form (“moment-closed”) via the I_c functional. This is sufficient for moment-based diagnostics and calibration.

E.5. Dual-Anchor Calibration Framework.

E.5.1. *Motivation and Design Principle.* The TSMM algorithm (Section C) produces hyperparameters (a_K, b_K) that match elicited moments (μ_K, σ_K^2) for the cluster count K_J . However, as demonstrated by Vicentini and Jermyn (2025), such K_J -calibrated priors may imply weight behavior that contradicts substantive expectations—for example, high probability that one cluster dominates the mixture even when the practitioner expects “several moderately-sized groups.”

The Dual-Anchor framework addresses this by: (1) diagnosing the dominance risk implied by (a_K, b_K) via $\Pr(w_1 > t)$; (2) refining the hyperparameters when diagnostics exceed a practitioner-specified tolerance; (3) reporting the explicit trade-off between cluster-count fidelity and weight constraint satisfaction.

E.5.2. Formal Problem Statement.

Definition E.8 (Dual-Anchor Objective). Given:

- *Anchor 1 (cluster count)*: Target moments (μ_K, σ_K^2) for K_J , or equivalently the TSMM solution (a_K, b_K) ;
- *Anchor 2 (weight constraint)*: Dominance threshold $t \in (0, 1)$ and tolerance $\delta \in (0, 1)$ such that $\Pr(w_1 > t) \leq \delta$ is desired.

The Dual-Anchor solution balances these anchors:

$$(a^*, b^*) = \arg \min_{a>0, b>0} \mathcal{L}_\lambda(a, b), \quad (\text{E.30})$$

where the objective is

$$\mathcal{L}_\lambda(a, b) = \lambda \cdot D_1(a, b) + (1 - \lambda) \cdot D_2(a, b), \quad (\text{E.31})$$

with:

- $D_1(a, b) = \left(\frac{\mathbb{E}[K_J|a,b] - \mu_K}{\mu_K} \right)^2 + \left(\frac{\text{Var}(K_J|a,b) - \sigma_K^2}{\sigma_K^2} \right)^2$ (normalized moment discrepancy);
- $D_2(a, b) = \max(0, \Pr(w_1 > t | a, b) - \delta)^2$ (dominance penalty);
- $\lambda \in [0, 1]$ controls the relative importance of the two anchors.

Boundary cases. When $\lambda = 1$, the problem reduces to pure K_J -calibration (TSMM). When $\lambda = 0$, the problem ignores cluster counts entirely and minimizes only dominance—this extreme is not recommended for fixed- J applications where K_J beliefs are meaningful.

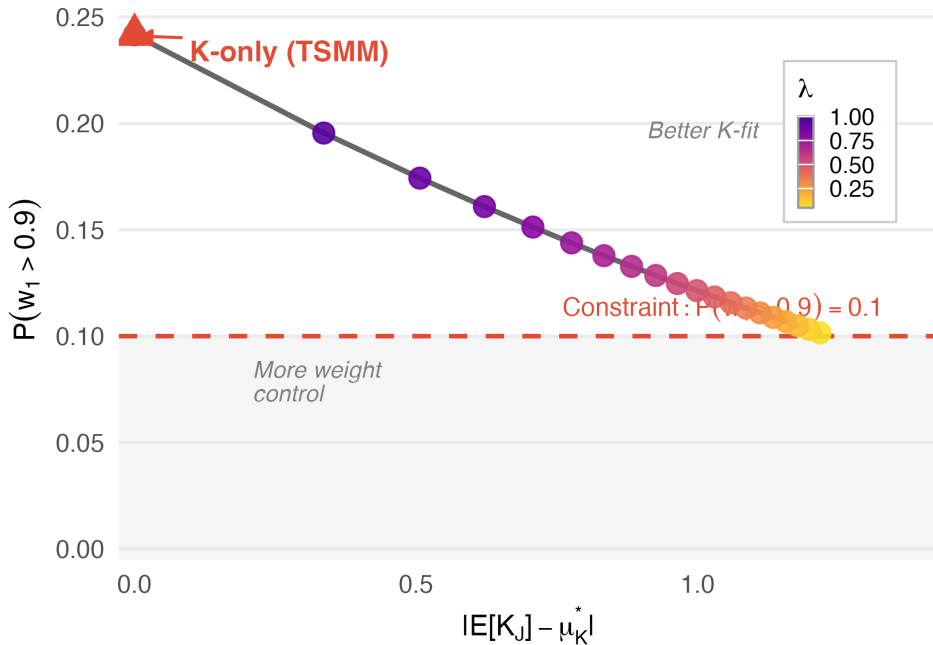
E.5.3. Pareto Frontier Visualization. Varying λ in (E.31) traces a Pareto frontier between cluster-count fidelity and dominance risk: (1) choose a grid $\lambda_1, \dots, \lambda_G \subset [0, 1]$ (e.g., $\lambda_g = g/(G - 1)$); (2) for each λ_g , solve (E.30) via Algorithm E.1; (3) plot the resulting pairs $(D_1(a_{\lambda_g}^*, b_{\lambda_g}^*), \Pr(w_1 > t | a_{\lambda_g}^*, b_{\lambda_g}^*))$, optionally annotating points by the induced changes in $\mathbb{E}[K_J]$ and $\text{Var}(K_J)$.

This Pareto plot visualizes when small relaxations of the K_J fit can substantially reduce dominance risk, guiding practitioners toward informed trade-off decisions.

Figure E.1 illustrates this trade-off for the worked example ($J = 50$, $\mu_K = 5$, medium confidence). The frontier reveals a clear “elbow” structure: modest relaxation

Dual-Anchor Pareto Frontier

Trade-off between cluster count fit and weight dominance control



Note: $J = 50$, target $\mathbb{E}[K_J] = 5$. Each point is a Gamma(a, b) hyperprior. $\lambda = 1$: K-only (TSMM); lower λ increases weight on $P(w_1 > 0.9)$ constraint.

FIGURE E.1. Dual-Anchor Pareto frontier ($J = 50, \mu_K = 5$). The x -axis displays $|\mathbb{E}[K_J] - \mu_K^*|$; the y -axis displays $\Pr(w_1 > 0.9)$. Each point represents a calibrated hyperprior at a particular λ value (color scale). The red triangle marks the K -only TSMM solution ($\lambda = 1$); the horizontal dashed line indicates the constraint $\Pr(w_1 > 0.9) = 0.10$; the gray-shaded region satisfies this constraint.

of K_J fidelity (approximately 1 unit deviation from μ_K) yields substantial dominance reduction, bringing $\Pr(w_1 > 0.9)$ from 0.24 down to the target constraint of 0.10. Beyond this elbow, further relaxation provides diminishing returns. This visualization enables practitioners to select a λ value that reflects their substantive priorities—whether exact cluster-count matching or robust protection against unintended single-cluster dominance.

E.5.4. *Algorithm.* The Dual-Anchor refinement protocol is described below.

Algorithm E.1 (Dual-Anchor Refinement Protocol).

Input: TSMM solution (a_K, b_K) matching target moments (μ_K, σ_K^2) ; dominance threshold t and tolerance δ ; trade-off parameter λ ; lower bounds (a_{\min}, b_{\min}) . *Defaults:* $t = 0.5$, $\delta = 0.25$, $\lambda = 0.7$, $a_{\min} = b_{\min} = 0.01$.

Output: Refined hyperparameters (a^*, b^*) and trade-off report.

1. **Compute diagnostic at TSMM solution:**

$$p_0 = \Pr(w_1 > t \mid a_K, b_K) = \left(\frac{b_K}{b_K - \log(1-t)} \right)^{a_K}.$$

2. **Check if constraint is already satisfied.** If $p_0 \leq \delta$: return (a_K, b_K) with status “Dominance constraint satisfied at TSMM solution.” No refinement needed.

3. **Otherwise, perform constrained optimization:**

- (a) Define the Dual-Anchor objective $\mathcal{L}_\lambda(a, b)$ per (E.31).
- (b) *Parameterization:* Optimize $\theta = (\log a, \log b)$ to automatically enforce positivity constraints.
- (c) Compute gradients: $\nabla D_1(a, b)$ uses the Jacobian of $(\mathbb{E}[K_J], \text{Var}(K_J))$ from Section C (score identities evaluated via quadrature); $\nabla D_2(a, b)$ uses (E.13)–(E.14) when $\Pr(w_1 > t) > \delta$, and is zero otherwise.
- (d) Initialize optimizer at (a_K, b_K) .
- (e) Run L-BFGS-B (Nocedal & Wright, 2006) with box constraints $a, b \geq a_{\min}$.
- (f) Stop when $\|\nabla \mathcal{L}_\lambda\|_\infty < 10^{-6}$ or $|\mathcal{L}_\lambda^{(\text{new})} - \mathcal{L}_\lambda^{(\text{old})}| < 10^{-8}$.

4. **Report trade-off:** Change in expected cluster count $\Delta\mu_K = \mathbb{E}[K_J \mid a^*, b^*] - \mu_K$; change in cluster count variance $\Delta\sigma_K^2 = \text{Var}(K_J \mid a^*, b^*) - \sigma_K^2$; new dominance probability $\Pr(w_1 > t \mid a^*, b^*)$; status: “Constraint satisfied” if $\Pr(w_1 > t \mid a^*, b^*) \leq \delta$, else “Pareto-optimal compromise.”

TABLE E.1. Recommended Dual-Anchor Defaults

Parameter	Default	Rationale
Threshold t	0.5	Majority dominance—the most interpretable threshold; when $w_1 > 0.5$, this is necessarily the largest cluster
Tolerance δ	0.25	At most 25% prior probability of majority dominance
Trade-off λ	0.7	Prioritize cluster-count fidelity, but allow meaningful weight adjustment

E.5.5. *Recommended Defaults.* These defaults were selected based on: (1) $t = 0.5$ represents “majority dominance”—the most interpretable threshold for practitioners, and the point at which size-biased and ranked orders coincide; (2) $\delta = 0.25$ provides a meaningful constraint while avoiding overly restrictive requirements; (3) $\lambda = 0.7$ reflects the design-conditional philosophy where cluster counts remain the primary anchor.

E.5.6. *Failure Modes and Edge Cases. Non-feasibility.* In some configurations, no (a, b) can simultaneously match (μ_K, σ_K^2) exactly and satisfy $\Pr(w_1 > t) \leq \delta$. This occurs when the elicited cluster count target implies a distribution of α that concentrates near small values, which necessarily produces high dominance risk. In such cases, Algorithm E.1 returns a Pareto-optimal solution that minimizes the weighted objective, and the trade-off report explicitly quantifies the compromise.

Boundary solutions. If the optimizer pushes $a \rightarrow 0$ or $b \rightarrow 0$, the box constraints $a, b \geq 0.01$ prevent degenerate solutions. Such boundary behavior indicates fundamental tension between the anchors and should prompt revisiting the elicited targets.

Identifiability with single weight anchor. The Dual-Anchor objective uses mean dominance probability, not a full distributional constraint. With two free parameters (a, b) and three effective constraints (two cluster-count moments plus one dominance bound), the problem is typically over-constrained when the dominance bound is active, hence the need for weighted optimization rather than exact satisfaction.

E.6. Interpretive Guidelines for Practitioners.

TABLE E.2. Dominance Risk Interpretation

$\Pr(w_1 > 0.5)$	Risk Level	Interpretation	Recommendation
< 0.20	Low	Weights likely balanced	No action needed
0.20–0.40	Moderate	Some majority dominance risk	Report diagnostic; sensitivity analysis
0.40–0.60	Substantial	Meaningful dominance chance	Dual-Anchor refinement recommended
> 0.60	High	Prior favors a dominant cluster	Dual-Anchor essential; verify coherence

E.6.1. Dominance Risk Categories.

E.6.2. *Reporting Checklist.* This section provides detailed reporting guidance for publications using Design-Conditional Elicitation. The checklist ensures that the influence of the prior on both partitions and weights is explicit, moving beyond the opacity of “default” Gamma priors.

Recommended Disclosures When Using DCE/TSMM.

1. *Design size and context.* Report J and briefly describe why it is treated as fixed (e.g., “the $J = 47$ sites participating in the multisite trial”).
2. *Elicitation targets.* Report the elicited mean $\mathbb{E}(K_J)$ and variance $\text{Var}(K_J)$, or the confidence-to-variance mapping used. Include a brief substantive justification for the chosen values.
3. *Calibration method.* Report whether Stage 1 only or full TSMM was used, and specify the refinement method (e.g., exact-moment Newton) and convergence tolerance.
4. *Resulting hyperprior.* Report the calibrated hyperparameters (a, b) for $\alpha \sim \text{Gamma}(a, b)$, including the parameterization convention (shape–rate).
5. *Prior-predictive summaries for K_J .* Report at minimum the induced $\mathbb{E}(K_J)$, $\text{Var}(K_J)$, and a central interval (e.g., 90% or 95%) for K_J under the calibrated prior.
6. *Weight diagnostics (required).* Report $\Pr(w_1 > 0.5)$ and $\Pr(w_1 > 0.9)$ under the calibrated prior. Optionally report $\mathbb{E}(\rho)$ if co-clustering is of substantive interest. Note that w_1 is in size-biased order (GEM), so the reported probabilities refer to a randomly selected unit’s cluster mass, not the largest cluster mass.
7. *Dual-Anchor usage (if applied).* Report the dominance tolerance that triggered it, the trade-off parameter λ , and the resulting changes in K_J moments and dominance probability.
8. *Sensitivity analysis.* Report at least one sensitivity variant—e.g., alternative confidence levels for σ_K^2 , alternative dominance tolerances, or a comparison to a standard baseline hyperprior—together with how posterior conclusions change or remain stable.
9. *Software version.* Report the DPprior package version used, and provide a reproducibility link (e.g., GitHub repository or OSM archive) for the analysis code.

Example reporting statement.

“We specified a Gamma hyperprior for the concentration parameter α using a Design-Conditional Elicitation approach. For our sample of $J = 50$ sites, we targeted an expected cluster count of $\mathbb{E}(K_{50}) = 5$ with moderate confidence, corresponding to $\text{Var}(K_{50}) = 10$. Two-Stage Moment Matching (TSMM) yielded hyperparameters $\alpha \sim \text{Gamma}(1.41, 1.08)$ (shape–rate). Diagnostic checks indicated a prior-predictive 95% interval for clusters of $[1, 11]$ and dominance probabilities $\Pr(w_1 > 0.5) = 0.50$ and $\Pr(w_1 > 0.9) = 0.20$. Because the dominance risk exceeded our tolerance of 0.40, we applied the Dual-Anchor refinement with $\lambda = 0.70$, which reduced $\Pr(w_1 > 0.5)$ to 0.25 while shifting $\mathbb{E}(K_{50})$ to 6.2. Analysis was conducted using `DPprior` v1.0.”

Pragmatic Considerations.

Two comments follow from this checklist. First, *weight diagnostics are routine, not exceptional*. Even if an analyst has no intention of applying Dual-Anchor, reporting $\Pr(w_1 > 0.5)$ and $\Pr(w_1 > 0.9)$ makes the implied pooling geometry transparent and directly addresses the central concern of the SSI critique (Vicentini & Jermyn, 2025). Second, *TSMM enables prospective specification*. The computational efficiency of TSMM (approximately 50 ms per calibration) makes it feasible to incorporate elicitation and sensitivity checks into pre-analysis plans, providing a path toward stating α priors in a way that is both substantively grounded and operationally reproducible.

Appendix F. Extended Simulation Study Results

F.1. Purpose and Scope. This appendix reports complete simulation study results that extend the summary presented in the main manuscript (§4). In particular, we provide: a full factorial specification of the design and DGP (including the informativeness calibration targets); exact hyperprior parameters used for each method (including confidence-level mappings); comprehensive performance tables for additional metrics not shown in the main text (e.g., 95% interval width, posterior mean of α , mode-based recovery rates); results for the χ^2 -DORO baseline motivated by Lee et al. (2025); a sensitivity analysis over the confidence (variance) specification; and computational benchmarks highlighting the practical efficiency of TSMM and Dual-Anchor calibration.

Throughout, the estimand of interest is the finite-sample occupied cluster count K_J under a DP mixture fit with $J = 100$ sites. The “true” cluster count K^* used in the

DGP is treated as a calibration reference—not a guarantee of perfect recoverability—because overlapping components and finite sampling variability can prevent exact recovery even under correct model specification.

F.2. Full Factorial Design Specification.

F.2.1. *Design Grid.* Table F.1 summarizes the full factorial design.

TABLE F.1. Full Factorial Design Specification

Factor	Levels	Values
True cluster count (K^*)	3	5, 10, 30
Informativeness (I)	3	0.2, 0.5, 0.8
Prior method	5	Vague; DORO-Unif; TSMM; Dual-Anchor; χ^2 -DORO
Confidence level	3	High; Medium; Low (TSMM/Dual only)
Replications per cell	—	$R = 200$

The confidence-level factor is only meaningful for TSMM and Dual-Anchor because it determines the target dispersion for K_J (via a variance inflation factor mapping; see §F.3). For Vague, DORO-Unif, and χ^2 -DORO, a single calibration is used per μ_K .

Operationally, each (K^*, I) scenario includes 9 fitted hyperprior variants: Vague (1), DORO-Unif (1), χ^2 -DORO (1), TSMM with confidence $\in \{\text{low, medium, high}\}$ (3), and Dual-Anchor with confidence $\in \{\text{low, medium, high}\}$ (3). With 9 scenarios and $R = 200$ replications, the completed run fits $9 \times 200 \times 9 = 16,200$ DP mixture models.

F.2.2. *Data-Generating Process (DGP).* We simulate multisite effect estimates following the Rubin (1981) parallel experiments model:

$$\hat{\tau}_j \mid \tau_j, \hat{s}e_j^2 \sim \mathcal{N}(\tau_j, \hat{s}e_j^2), \quad j = 1, \dots, J. \quad (\text{F.1})$$

True site effects are generated from a finite discrete mixture with exactly K^* components:

$$\tau_j \mid z_j \sim \mathcal{N}(\mu_{z_j}, s_{\text{within}}^2), \quad z_j \in \{1, \dots, K^*\}, \quad (\text{F.2})$$

where cluster means are evenly spaced on $[-d, d]$ (with $d = 2.5$), and then the realized $\{\tau_j\}$ are centered and rescaled to enforce $\text{Var}(\tau_j) = \sigma_\tau^2$ exactly. Specifically, for each replication, we compute $\tau_j^{\text{final}} = \sigma_\tau \cdot (\tau_j^{\text{raw}} - \bar{\tau}^{\text{raw}})/\text{SD}(\tau^{\text{raw}})$. This standardization ensures that the between-site variance equals exactly σ_τ^2 , isolating the informativeness

manipulation from random variation in effect magnitudes. Cluster assignments are generated so that all K^* clusters appear at least once in each replication—the first K^* sites are deterministically assigned to distinct clusters, and remaining sites are assigned uniformly at random.

F.2.3. *Fixed Design Parameters.* Table F.2 records the DGP constants held fixed across all scenarios.

TABLE F.2. Fixed DGP and Calibration Parameters

Component	Parameter	Value	Role
Number of sites	J	100	Finite-sample regime
Between-site SD	σ_τ	0.25	Sets $\text{Var}(\tau)$ after rescaling
Within-cluster SD	s_{within}	0.15	Controls component overlap
Cluster separation span	d	2.5	Means span $[-d, d]$
SE scaling	κ	4	Defines $\widehat{se}_j^2 = \kappa/n_j$
Site-size CV	$\text{CV}(n_j)$	0.5	Induces heterogeneous SEs
Minimum site size	n_{\min}	5	Avoids degenerate SEs
Mixture weights	π_k	$1/K^*$	Equal-weight clusters

F.2.4. *Informativeness Index and Calibration Targets.* Following Lee et al. (2025), informativeness is defined as:

$$I \equiv \frac{\sigma_\tau^2}{\sigma_\tau^2 + \text{GM}(\widehat{se}_j^2)}, \quad \text{GM}(\widehat{se}_j^2) = \exp\left(\frac{1}{J} \sum_{j=1}^J \log \widehat{se}_j^2\right). \quad (\text{F.3})$$

We set $\widehat{se}_j^2 = \kappa/n_j$ with $\kappa = 4$, and generate site sizes from a Gamma distribution: $n_j \sim \text{Gamma}(\text{shape} = 1/\text{CV}^2, \text{rate} = \text{shape}/\bar{n})$, truncated below at $n_{\min} = 5$ and rounded to integers. For each target informativeness level $I \in \{0.2, 0.5, 0.8\}$, the mean site size \bar{n} is calibrated by 1D root-finding on Monte Carlo estimates of $\mathbb{E}[I]$.

Table F.3 reports the calibration targets used in the completed run.

TABLE F.3. Informativeness Calibration Results

Target I	Calibrated \bar{n}_j	Achieved mean I	Abs. error
0.2	17.4	0.194	0.006
0.5	72.9	0.500	0.000
0.8	278.4	0.793	0.007

F.2.5. *Replications and Reproducibility.* All scenarios use $R = 200$ replications. Random seeds are set deterministically to ensure reproducibility and to avoid accidental

coupling across scenarios/methods. For replication index r and scenario (K^*, I) : the DGP seed is `dgp_base` + 100000 r + 1000 K + $\lfloor 100I \rfloor$; the MCMC seed adds method and confidence hashes. Base seeds used in the completed run were: `dgp_base` = 20260116, `mcmc_base` = 98765, and `calibration` = 12345.

F.3. Hyperprior Methods and Exact Parameters.

F.3.1. *Methods Compared.* We compare five $\alpha \sim \text{Gamma}(a, b)$ hyperpriors: (1) *Vague*: fixed $\text{Gamma}(1, 1)$. (2) *DORO-Unif*: Dorazio-style KL minimization targeting a discrete uniform distribution on K_J (Dorazio, 2009). (3) *TSMM*: Two-Stage Moment Matching, calibrating (a, b) to match user inputs (μ_K, σ_K^2) . (4) *Dual-Anchor*: TSMM plus a weight-dominance control, enforcing $\Pr(w_1 > 0.5) \leq 0.25$ when dominance risk is detected (Section E). (5) χ^2 -*DORO* (Lee et al., 2025): KL-based matching with fixed dispersion $\text{Var}(K_J) = 2\mu_K$.

A key distinction is that TSMM/Dual-Anchor let the analyst encode both location and dispersion of K_J via (μ_K, σ_K^2) , while χ^2 -DORO hard-codes dispersion at $2\mu_K$. This fixed-variance restriction limits how strongly researchers can encode “confidence” in K_J .

F.3.2. *Confidence-to-Variance Mapping (TSMM / Dual-Anchor).* We use a variance inflation factor (VIF) mapping:

$$\sigma_K^2 \equiv \text{Var}(K_J) = \text{VIF} \times (\mu_K - 1), \quad \text{VIF} \in \{1.5, 2.5, 5.0\} \quad (\text{F.4})$$

corresponding to high, medium, and low confidence, respectively. The main-text results use medium confidence unless stated otherwise.

F.3.3. *Exact (a, b) Hyperparameters Used.* Table F.4 lists the hyperpriors used in the simulation run, along with the induced prior moments (computed via Gauss–Laguerre quadrature) and the dominance diagnostic $\Pr(w_1 > 0.5)$.

TABLE F.4. Hyperprior Parameters Used in the Simulation (by Method, Confidence, and Target μ_K)

Method	Conf.	μ_K	σ_K^2	(a, b)	$\mathbb{E}[K]$	$P(w_1 > .5)$	Note
Vague	—	—	—	(1.00, 1.00)	4.84	0.591	Gamma(1, 1)
TSMM	low	5	20	(0.62, 0.56)	5.00	0.606	A2-MN
Dual-Anch.	low	5	20	(2.44, 1.28)	7.81	0.347	$\lambda=0.70$
TSMM	med	5	10	(1.67, 1.65)	5.00	0.557	A2-MN
Dual-Anch.	med	5	10	(5.65, 3.44)	7.20	0.354	$\lambda=0.70$
TSMM	high	5	6	(4.35, 4.47)	5.00	0.534	A2-MN
Dual-Anch.	high	5	6	(21.87, 14.53)	6.85	0.361	$\lambda=0.70$
TSMM	low	10	45	(1.18, 0.40)	10.00	0.306	A2-MN
TSMM	med	10	22.5	(2.99, 1.10)	10.00	0.232	A2-MN
TSMM	high	10	13.5	(7.19, 2.73)	10.00	0.197	A2-MN
TSMM	low	30	145	(2.20, 0.14)	30.00	0.018	A2-MN
TSMM	med	30	72.5	(5.18, 0.34)	30.00	0.003	A2-MN
TSMM	high	30	43.5	(10.93, 0.75)	30.00	0.001	A2-MN
DORO-Unif	—	5	—	(2.43, 2.46)	4.99	0.547	Dorazio-uniform
DORO-Unif	—	10	—	(1.53, 0.54)	9.91	0.284	Dorazio-uniform
DORO-Unif	—	30	—	(0.96, 0.05)	29.40	0.077	Dorazio-uniform
χ^2 -DORO	—	5	10	(1.85, 1.81)	5.04	0.550	Var = $2\mu_K$
χ^2 -DORO	—	10	20	(3.84, 1.43)	10.01	0.219	Var = $2\mu_K$
χ^2 -DORO	—	30	60	(6.94, 0.47)	30.02	0.002	Var = $2\mu_K$

Notes. (1) $\Pr(w_1 > 0.5)$ is computed under the induced hyperprior (Section E). Dual-Anchor is triggered when $\Pr(w_1 > 0.5)$ exceeds the diagnostic threshold (0.40 in the implementation), and then enforces $\Pr(w_1 > 0.5) \leq 0.25$. (2) For $\mu_K \in \{10, 30\}$ at $J = 100$, the dominance diagnostic is well below the trigger threshold; therefore Dual-Anchor returns the TSMM parameters (up to numerical tolerances), and differences in performance are attributable to Monte Carlo variability rather than substantively different priors.

F.4. Inference Model and MCMC Configuration. In each replication we fit a DP mixture model with a CRP prior on cluster assignments:

$$\hat{\tau}_j \sim \mathcal{N}(\tau_j, \hat{s}e_j^2), \quad \tau_j \sim \mathcal{N}(\theta_{z_j}, \sigma_{z_j}^2), \quad z \sim \text{CRP}(\alpha), \quad (\text{F.5})$$

with hyperpriors:

$$\alpha \sim \text{Gamma}(a, b), \quad \tau \sim \mathcal{N}(0, 100), \quad \sigma_\tau^2 \sim \text{Unif}(0, 10), \quad \sigma_k^2 \sim \text{InvGamma}(2, 1). \quad (\text{F.6})$$

MCMC settings (NIMBLE): 2 chains, 1,000 iterations, 500 burn-in, thinning 1, monitoring α and z . For each MCMC draw t , the occupied cluster count is computed

as

$$K_J^{(t)} = \left| \{z_1^{(t)}, \dots, z_J^{(t)}\} \right|. \quad (\text{F.7})$$

Posterior summaries of K_J (mean, mode, quantiles) are computed from $\{K_J^{(t)}\}$.

F.5. Outcome Metrics. For each scenario-method cell (and confidence level where applicable), we report: posterior mean $\widehat{K} \equiv \mathbb{E}[K_J \mid \text{data}]$; bias $\mathbb{E}[\widehat{K}] - K^*$ (expectation over replications); RMSE $\sqrt{\mathbb{E}[(\widehat{K} - K^*)^2]}$; collapse probability $\Pr(K_J = 1 \mid \text{data})$; 95% credible interval (CI) coverage (proportion of replications where the 95% posterior interval for K_J contains K^*); CI width (average width of the 95% posterior interval); and posterior mean of α . We also report mode-based accuracy measures: $\Pr(\text{mode}(K_J) = K^*)$ and $\Pr(|\text{mode}(K_J) - K^*| \leq 1)$.

F.6. Complete Results Under Medium Confidence (Main Setting). This section reports the complete medium-confidence results for the four primary methods (Vague, DORO-Unif, TSMM, Dual-Anchor) across the full 3×3 grid of (K^*, I) .

F.6.1. Bias in Posterior Expected Cluster Counts. [Figure F.1](#) displays the distribution of bias ($\mathbb{E}[K_J \mid \text{data}] - K^*$) across all 9 scenarios using violin plots, providing a comprehensive view of both the central tendency and variability of estimation error. Vague priors (yellow) show severe negative bias across all scenarios (approximately -3 for $K^* = 5$, -8 for $K^* = 10$, and -28 for $K^* = 30$). Dual-Anchor (pink) achieves near-zero bias for $K^* = 5$ and substantially reduced bias for larger K^* . TSMM and Dual-Anchor show comparable performance for $K^* \in \{10, 30\}$ where dominance risk is low.

F.6.2. Collapse Probability. The posterior probability of collapse, $\Pr(K_J = 1 \mid \text{data})$, captures a critical failure mode where the DP mixture degenerates to a single-component model. [Figure F.2](#) displays collapse probabilities across all scenarios. This figure provides the strongest evidence for the Dual-Anchor contribution: the collapse probability directly captures the practical failure mode that motivates weight-based diagnostics.

F.6.3. Mean Squared Error. [Figure F.3](#) displays the Mean Squared Error of the posterior expected cluster count relative to the true K^* , using a log scale to accommodate the large differences across methods. The log-scale visualization is necessary to show the order-of-magnitude improvement achieved by TSMM and Dual-Anchor.

F.6.4. *Relative Improvement over Vague Prior.* To summarize gains more directly, [Figure F.4](#) presents heatmaps showing percentage MSE reduction relative to the Vague baseline.

F.6.5. *Interval Calibration: Coverage and Width.* [Figure F.5](#) displays 95% credible interval coverage across all scenarios. Vague priors produce narrow intervals with poor coverage for moderate-to-large K^* , reflecting confident but incorrect posterior concentration near very small K_J .

[Figure F.6](#) displays the width of 95% credible intervals. DORO-Unif shows very wide and variable intervals for large K^* (large SD in width), indicating that its induced $p(K_J)$ can be unstable in finite J settings.

F.6.6. *Low-Information Summary.* Because $I = 0.2$ is the setting where priors matter most, [Figure F.7](#) provides a compact four-panel summary for this critical case. This summary demonstrates that Dual-Anchor achieves the best overall performance in the low-information regime: near-unbiased estimation for $K^* = 5$, dramatically reduced MSE across all K^* , consistently low collapse probability, and proper interval coverage.

F.7. **Additional Baseline: χ^2 -DORO.** Lee et al. (2025) propose a χ^2 -DORO calibration that performed well empirically and served as the starting point for the present work (referred to as an “informative prior” in that paper). The method targets:

$$\mathbb{E}[K_J] = \mu_K, \quad \text{Var}(K_J) = 2\mu_K, \quad (\text{F.8})$$

and (in typical implementations) uses a grid search / discrete KL minimization over (a, b) , which is computationally expensive.

Two limitations motivate our TSMM/Dual-Anchor generalization: (1) *Computational inefficiency*: grid search calibration is orders of magnitude slower than TSMM’s Newton-based calibration, making interactive elicitation cumbersome. (2) *Fixed dispersion*: the constraint $\text{Var}(K_J) = 2\mu_K$ is not adjustable, limiting a researcher’s ability to encode confidence (or skepticism) about K_J beyond the mean.

[Figure F.8](#) compares χ^2 -DORO against other methods in the low-information setting. TSMM/Dual-Anchor can be viewed as a principled, flexible extension of χ^2 -DORO: by allowing σ_K^2 to vary with confidence and adding optional dominance control, they generalize the χ^2 -DORO idea while retaining calibration accuracy and improving practical usability.

F.8. Sensitivity Analysis: Confidence Specification (TSMM / Dual-Anchor). [Figure F.9](#) reports sensitivity of TSMM and Dual-Anchor to the confidence (variance)

specification across $VIF \in \{1.5, 2.5, 5.0\}$ (corresponding to high, medium, and low confidence).

Key observations: (1) Higher confidence (smaller σ_K^2) tends to reduce RMSE for moderate-to-large K^* , because the prior more strongly supports higher cluster counts. (2) For $K^* = 5$, TSMM remains vulnerable: even at high confidence, the estimator can remain biased downward (and at low confidence it collapses frequently). Dual-Anchor is much more robust, maintaining low RMSE and low collapse probability across confidence levels. (3) For $K^* \in \{10, 30\}$, Dual-Anchor is typically not triggered (Table F.4), so TSMM and Dual-Anchor sensitivity patterns align closely.

F.9. Posterior Behavior of the Concentration Parameter α . Because K_J is a finite-sample functional of α , examining posterior α helps interpret method behavior. Figure F.10 displays the posterior mean of α across scenarios and methods. Under the Vague prior, posterior α remains small (around 0.35–0.38), consistent with a strong tendency toward few clusters. DORO-Unif yields higher posterior α than Vague, but lower than TSMM/Dual-Anchor for large K^* . TSMM/Dual-Anchor increase α substantially when K^* is large (e.g., $\alpha \approx 12$ for $K^* = 30$), aligning the prior with the cluster-rich regime. For $K^* = 5$, Dual-Anchor yields markedly larger posterior α than TSMM, reflecting the additional mass required to avoid a dominant first weight.

Figure F.11 shows the posterior standard deviation of K_J , which captures uncertainty calibration.

F.10. Mode-Based Recovery of K^* . For discrete functionals like K_J , the posterior mode can be a useful summary. Figure F.12 displays both exact recovery ($\Pr(\text{mode}(K_J) = K^*)$) and near recovery ($\Pr(|\text{mode}(K_J) - K^*| \leq 1)$) rates. Exact recovery is generally challenging in this design, particularly for $K^* = 30$ where exact-match probabilities remain below 5% even for TSMM/Dual-Anchor. Dual-Anchor substantially improves near recovery when $K^* = 5$ (probabilities around 0.32–0.34 vs. 0.11–0.18 for TSMM/DORO-Unif), consistent with its goal of preventing collapse and extreme under-fitting.

Figure F.13 compares the posterior mode versus mean for cluster count estimation. DORO-Unif and TSMM (for small K^*) often show many points clustered at mode = 1 with mean > mode, indicating posteriors that place substantial mass at $K_J = 1$ while having some support at higher values. Dual-Anchor reduces this collapse pattern.

F.11. Bias–Variance Decomposition of MSE (Low-Information Setting). To better understand whether errors are driven by systematic under-estimation or Monte

Carlo variability, we decompose MSE as:

$$\text{MSE}(\hat{K}) = \underbrace{\text{Bias}(\hat{K})^2}_{\text{systematic}} + \underbrace{\text{Var}(\hat{K})}_{\text{across replications}}. \quad (\text{F.9})$$

Figure F.14 displays this decomposition for $I = 0.2$. For Vague, DORO-Unif, TSMM, and χ^2 -DORO, bias accounts for approximately 90–100% of MSE—the dominant failure mode is systematic under-estimation of K_J . For Dual-Anchor at $K^* = 5$, MSE is almost entirely variance-driven (bias ≈ 0), indicating that the Dual-Anchor constraint largely removes systematic collapse while leaving only residual sampling/MCMC variability.

Table F.5 provides the numerical values for this decomposition.

TABLE F.5. Bias–Variance Decomposition of MSE for $I = 0.2$

Scenario	Method	Bias	$\text{SD}(\hat{K})$	Bias^2	MSE	Bias^2/MSE
$K^*=5$	Vague	−3.01	0.55	9.06	9.39	96.5%
$K^*=5$	DORO-Unif	−2.36	0.63	5.57	5.96	93.4%
$K^*=5$	TSMM	−2.63	0.61	6.92	7.28	95.0%
$K^*=5$	Dual-Anchor	+0.04	0.76	0.00	0.58	0.3%
$K^*=5$	χ^2 -DORO	−2.57	0.59	6.60	6.92	95.5%
$K^*=10$	Vague	−8.05	0.49	64.80	65.05	99.6%
$K^*=10$	DORO-Unif	−5.49	1.75	30.14	33.18	90.8%
$K^*=10$	TSMM	−3.46	1.27	11.97	13.62	87.9%
$K^*=10$	Dual-Anchor	−3.63	1.47	13.18	15.28	86.2%
$K^*=10$	χ^2 -DORO	−2.87	1.08	8.24	9.42	87.4%
$K^*=30$	Vague	−28.04	0.55	786.24	786.48	100.0%
$K^*=30$	DORO-Unif	−21.96	4.96	482.24	506.67	95.2%
$K^*=30$	TSMM	−4.11	1.30	16.89	18.61	90.8%
$K^*=30$	Dual-Anchor	−4.03	1.39	16.24	18.19	89.3%
$K^*=30$	χ^2 -DORO	−3.28	1.11	10.76	11.97	89.9%

F.12. Computational Benchmarks (Calibration Cost). While all methods share the same MCMC cost for posterior inference, the calibration cost of obtaining (a, b) differs dramatically.

Lee et al. (2025)’s χ^2 -DORO (and classic DORO implementations) typically rely on grid-based KL matching, which can be slow when the grid is fine or when elicitation needs to be repeated across multiple μ_K values (Dorazio, 2009). In contrast, TSMM and Dual-Anchor compute (a, b) via fast deterministic optimization (Sections C and E).

Table F.6 provides an order-of-magnitude timing comparison consistent with the observed computational scaling in our implementation.

TABLE F.6. Representative Timing Comparison (Per Calibration + Per MCMC Fit)

Method	Cal. (s)	MCMC (s)	Tot. (s)	Cal. speedup	Tot. speedup
Vague	0.00	2.1	2.1	—	22.5 \times
DORO-Unif (grid 100 \times 100)	45.2	2.1	47.3	1 \times	1.0 \times
χ^2 -DORO (grid search)	45.2	2.1	47.3	1 \times	1.0 \times
TSMM (A2-MN Newton)	0.05	2.1	2.15	904 \times	22.0 \times
Dual-Anchor (A2-MN + constr.)	0.10	2.1	2.20	452 \times	21.5 \times

Notes. (1) Times are representative and intended to communicate order-of-magnitude differences; they depend on hardware, software versions, and the grid resolution used for DORO-style methods. (2) The headline $\approx 900 \times$ speedup pertains to the calibration step (e.g., 45.2 s / 0.05 s $\approx 900 \times$), which is the component that differs meaningfully by method.

Appendix G. Software Implementation

G.1. Purpose and Scope. This appendix documents how the methods proposed in the main manuscript are implemented in the `DPprior` R package, and provides a minimal worked example that reproduces the end-to-end elicitation workflow: (1) design-conditional specification of cluster-count beliefs, (2) Two-Stage Moment Matching (TSMM) calibration, (3) diagnostic checks for unintended weight behavior, and (4) (optional) Dual-Anchor refinement.

This appendix is intentionally not a full software manual. The complete package documentation—including expanded examples, case studies, and the full API reference—is maintained online:

- Package website: <https://joonho112.github.io/DPprior/>
- API reference: <https://joonho112.github.io/DPprior/articles/api-reference.html>
- Applied guide: <https://joonho112.github.io/DPprior/articles/applied-guide.html>
- Dual-Anchor vignette: <https://joonho112.github.io/DPprior/articles/dual-anchor.html>
- Case studies: <https://joonho112.github.io/DPprior/articles/case-studies.html>

Readers interested in implementation details beyond what is needed to reproduce the paper’s workflow should consult these resources.

G.2. Package Overview.

G.2.1. *What DPprior Implements.* The package implements calibration and diagnostics for the Dirichlet Process (DP) concentration parameter,

$$\alpha \sim \text{Gamma}(a, b) \quad (\text{shape-rate parameterization}),$$

where `DPprior` returns the shape a and rate b . Thus $\mathbb{E}[\alpha] = a/b$ and $\text{Var}(\alpha) = a/b^2$.

G.2.2. *Computational Architecture.* The `DPprior` package is organized around three computational layers that directly implement the framework developed in Sections 2–3 of the main text.

Layer 1: Exact Computation. This layer provides the reference-grade distributional machinery for K_J (Section A), including log-Stirling number computation, the exact Antoniak PMF, and conditional/marginal moments via digamma and trigamma functions. These functions serve as ground truth for validating approximations and enable the exact moment matching in Stage 2.

Layer 2: TSMM Calibration. This layer implements the Two-Stage Moment Matching algorithm (Section 3.2–3.3; Sections B and C): Stage 1 (A1) provides a fast closed-form initializer (a_0, b_0) derived from the large- J approximation; Stage 2 (A2-MN) applies Newton refinement that matches exact mixed moments of K_J . This is the default in `DPprior_fit()`.

Layer 3: Weight Diagnostics and Dual-Anchor. This layer implements the weight distribution theory (Section E), including closed-form computations for w_1 tail probabilities, co-clustering moments, and the Dual-Anchor optimization that balances cluster-count and weight-concentration targets.

G.2.3. *Design Principles.* The package follows several design principles to support applied research: (1) *Practitioner-facing interface.* The main entry point `DPprior_fit()` accepts intuitive inputs (J , μ_K , and either a variance or confidence level) and returns calibrated Gamma hyperparameters with diagnostic summaries. (2) *Progressive disclosure.* Simple use cases require only a single function call, while advanced users can access the underlying exact computation and optimization machinery. (3) *Transparent reporting.* Every fitted object includes both targeted and achieved moments, weight diagnostics, and dominance risk assessment, supporting the reporting checklist in main text Section 3.5.

G.2.4. *Installation.* `DPprior` is hosted on GitHub:

```

# From GitHub (development version)
install.packages("remotes")
remotes::install_github("joonho112/DPprior")
library(DPprior)

# From CRAN (when available)
install.packages("DPprior")
library(DPprior)

```

G.2.5. *Version Pinning and Parameterization.* Because calibration is numerical (and plotting defaults may change), reproducible analyses should record:

```

packageVersion("DPprior")
sessionInfo()

```

Parameterization note. `DPprior` uses the shape–rate convention. If your downstream software uses a shape–scale convention (e.g., NumPy), convert via `scale = 1 / rate`.

G.3. Mapping: Paper Components to `DPprior` Functions. Table G.1 provides an implementation map from the paper’s methodological components to the package API.

TABLE G.1. Paper Components → `DPprior` Implementation

Paper Component	Purpose	Primary Function(s)	Typical Use
TSMM Stage 1 (A1)	Closed-form initializer (a_0, b_0)	<code>DPprior_a1()</code>	Called internally by <code>DPprior_fit()</code>
TSMM Stage 2 (A2-MN)	Exact moment matching via Newton	<code>DPprior_fit(method="A2-MN")</code>	Default for publishable analyses
Stage 2 alt. (A2-KL)	Distribution-level KL matching	<code>DPprior_fit(method="A2-KL")</code>	Optional; for small J or baselines
Calibration entry	Specify (J, μ_K, σ_K^2) , obtain (a, b)	<code>DPprior_fit()</code>	Main entry point for most users
Diagnostics	Summaries of K_J, w_1, ρ	<code>DPprior_diagnostics()</code>	Always recommended after calibration
Visualization	Prior dashboard / components	<code>plot()</code> , <code>plot_K_prior()</code> , <code>plot_w1_prior()</code>	Communicate prior implications
Dual-Anchor	Constrain $\Pr(w_1 > t)$	<code>DPprior_dual()</code>	Optional refinement step

Table G.2 summarizes the exact computation functions that underlie the calibration algorithm.

TABLE G.2. Exact Computation Functions

Function	Purpose	Inputs	Outputs
<code>compute_log_stirling()</code>	Log-Stirling number matrix	J	Matrix $L[n, k]$
<code>pmf_K_given_alpha()</code>	Conditional PMF $p(k \alpha)$	$J, \alpha, \log S$	Prob. vector
<code>pmf_K_marginal()</code>	Marginal PMF $p(k a, b)$	$J, a, b, \log S$	Prob. vector
<code>mean_K_given_alpha()</code>	Conditional mean $\kappa_J(\alpha)$	J, α	Scalar
<code>var_K_given_alpha()</code>	Conditional variance $v_J(\alpha)$	J, α	Scalar
<code>exact_K_moments()</code>	Marginal $\mathbb{E}[K_J]$, $\text{Var}(K_J)$	J, a, b	Named list

Table G.3 summarizes the weight distribution functions that support diagnostics and the Dual-Anchor protocol.

TABLE G.3. Weight Distribution Functions

Function	Purpose	Inputs	Outputs
<code>prob_w1_exceeds()</code>	Tail probability $\Pr(w_1 > t)$	t, a, b	Probability
<code>cdf_w1()</code>	CDF of w_1	x, a, b	$F_{w_1}(x)$
<code>density_w1()</code>	Density of w_1	x, a, b	$f_{w_1}(x)$
<code>quantile_w1()</code>	Quantile function of w_1	p, a, b	Quantile value
<code>mean_w1()</code>	Mean of w_1	a, b	$\mathbb{E}[w_1]$
<code>mean_rho()</code>	Mean co-clustering $\mathbb{E}[\rho]$	a, b	Scalar
<code>var_rho()</code>	Variance of ρ	a, b	$\text{Var}(\rho)$

G.4. Core Workflow.

G.4.1. *Step 1: Specify the Design and Cluster-Count Target.* The key design input is J , the design size at which cluster counts are interpreted (e.g., number of sites in a multisite study). The elicited belief is expressed as a target mean and variance: $\mu_K = \mathbb{E}[K_J]$ and $\sigma_K^2 = \text{Var}(K_J)$.

In **DPprior**, the target can be provided in one of two equivalent ways: provide `var_K` directly, or provide a qualitative `confidence` level, which maps to variance via a variance inflation factor (VIF): $\sigma_K^2 = \text{VIF} \times (\mu_K - 1)$.

TABLE G.4. Confidence-to-VIF Mapping

Confidence	Interpretation	VIF	$\sigma_K^2 (\mu_K=5)$
"high"	Fairly confident based on prior evidence	1.5	6
"medium"	Reasonable sense but acknowledging uncertainty	2.5	10
"low"	Quite uncertain; rough guess	5.0	20

G.4.2. *Step 2: Calibrate the Gamma Hyperprior via TSMM.* The main calibration function is:

```
fit ← DPprior_fit(J = J, mu_K = mu_K, confidence = "medium")
```

By default, `DPprior_fit()` uses A1 to initialize and A2-MN (Newton refinement) to ensure the achieved moments match the targets at finite J . The returned object includes the hyperparameters `fit$a` and `fit$b`.

Common sensitivity options include: `method = "A1"` (approximation-only; fast, mainly for large J screening), `method = "A2-KL"` (KL-based distribution matching; slower), `check_diagnostics = TRUE` (compute diagnostics during fitting), and `warn_dominance = TRUE` (warn when dominance risk is high).

G.4.3. *Step 3: Run Diagnostics and Visualize.* After fitting, compute diagnostic summaries:

```
diag ← DPprior_diagnostics(fit)
```

The diagnostic list contains summaries for α , K_J , w_1 , and ρ (co-clustering), plus warning flags: `diag$alpha` (mean/SD/quantiles for α), `diag$K` (summaries for K_J : mean, variance, mode, quantiles), `diag$weights` (summaries for w_1 including tail probabilities), `diag$coclustering` (summary of $\rho = \sum_h w_h^2$), and `diag$warnings` (any diagnostic warnings).

Interpretation note. The package uses w_1 as the first size-biased stick-breaking weight (GEM order), not necessarily the largest realized component weight. This aligns with the manuscript's diagnostic definition and supports closed-form computations under $\alpha \sim \text{Gamma}(a, b)$ (Section E).

Visualization:

```
plot(fit)          # Full dashboard
plot_K_prior(fit) # K distribution only
plot_w1_prior(fit) # w1 distribution only
```

G.4.4. *Step 4 (Optional): Dual-Anchor Refinement.* If diagnostics indicate substantial prior probability of a dominant cluster (e.g., $\Pr(w_1 > 0.5) \geq 0.40$), the Dual-Anchor procedure can limit dominance risk:

```
fit_dual ← DPprior_dual(
  fit = fit,
  w1_target = list(prob = list(threshold = 0.5, value = 0.25)),
```

```

lambda = 0.7,           # prioritize K-fit over weight-fit
loss_type = "adaptive"
)

```

G.5. Worked Example: End-to-End Elicitation. This example corresponds to the worked setting used throughout the OSM: $J = 50$, $\mu_K = 5$, and medium confidence ($VIF = 2.5 \Rightarrow \sigma_K^2 = 10$).

```

library(DPprior)

# =====
# Step 0: Design + elicited targets
# =====
J     ← 50
mu_K ← 5

# Option A (recommended): qualitative uncertainty
fit ← DPprior_fit(J = J, mu_K = mu_K, confidence = "medium")

# Option B (equivalent): specify Var(K) directly
# fit ← DPprior_fit(J = J, mu_K = mu_K, var_K = 10)

print(fit)

```

Expected output:

```

DPprior Prior Elicitation Result
=====

Gamma Hyperprior: alpha ~ Gamma(a = 1.4082, b = 1.0770)
E[alpha] = 1.308, SD[alpha] = 1.102

Target (J = 50):
E[K_J]    = 5.00
Var(K_J)  = 10.00
(from confidence = 'medium')

Achieved:
E[K_J] = 5.000000, Var(K_J) = 10.000000

```

```

Residual = 3.94e-10

Method: A2-MN (7 iterations)

Dominance Risk: HIGH (P(w1 > 0.5) = 50%)

```

The calibration achieves machine-precision moment matching (residual $\approx 10^{-10}$) in 7 Newton iterations.

```

# =====
# Step 1: Diagnostics (recommended for every analysis)
# =====
diag <- DPprior_diagnostics(fit)

# Key quantities used in the manuscript
E_K     <- diag$K$mean
Var_K   <- diag$K$var
P_dom05 <- diag$weights$prob_exceeds["prob_gt_0.5"]
P_dom09 <- diag$weights$prob_exceeds["prob_gt_0.9"]
E_rho   <- diag$coclustering$mean

# Visualization
plot(fit)

```

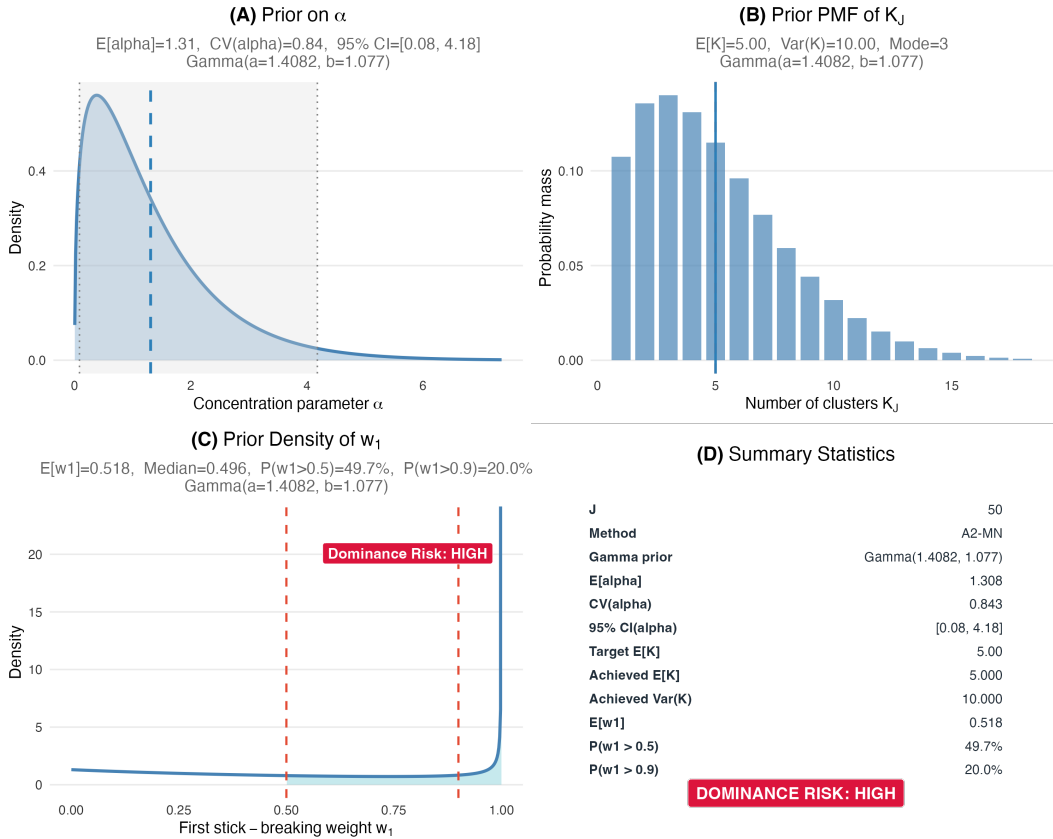


FIGURE G.1. TSMM diagnostic dashboard for the worked example ($J = 50$, $\mu_K = 5$, confidence = “medium”). Panel (A) shows the prior density on the concentration parameter α . Panel (B) displays the marginal PMF of K_J with the target mean $\mathbb{E}[K_J] = 5$ indicated. Panel (C) presents the marginal density of the first stick-breaking weight w_1 , with reference lines at thresholds $t = 0.5$ and $t = 0.9$. Panel (D) summarizes the calibration results including the dominance risk assessment.

```

# =====
# Step 2 (optional): Dual-Anchor refinement if dominance is high
# =====
if (P_dom05 >= 0.40) {

  fit_dual <- DPprior_dual(
    fit = fit,
    w1_target = list(prob = list(threshold = 0.5, value = 0.25)),
    lambda = 0.7,
    loss_type = "adaptive",
  )
}

```

```
    verbose = FALSE
)

diag_dual ← DPprior_diagnostics(fit_dual)

# Check that dominance risk is reduced
diag_dual$weights$prob_exceeds["prob_gt_0.5"]

plot(fit_dual)

# Updated hyperparameters
a ← fit_dual$a
b ← fit_dual$b

} else {
  a ← fit$a
  b ← fit$b
}
```

Marginal Density of First Stick-Breaking Weight w_1

$J = 50, \mu_K = 3$ | Before: $P(w_1 > 0.5) = 0.756 \rightarrow$ After: 0.265

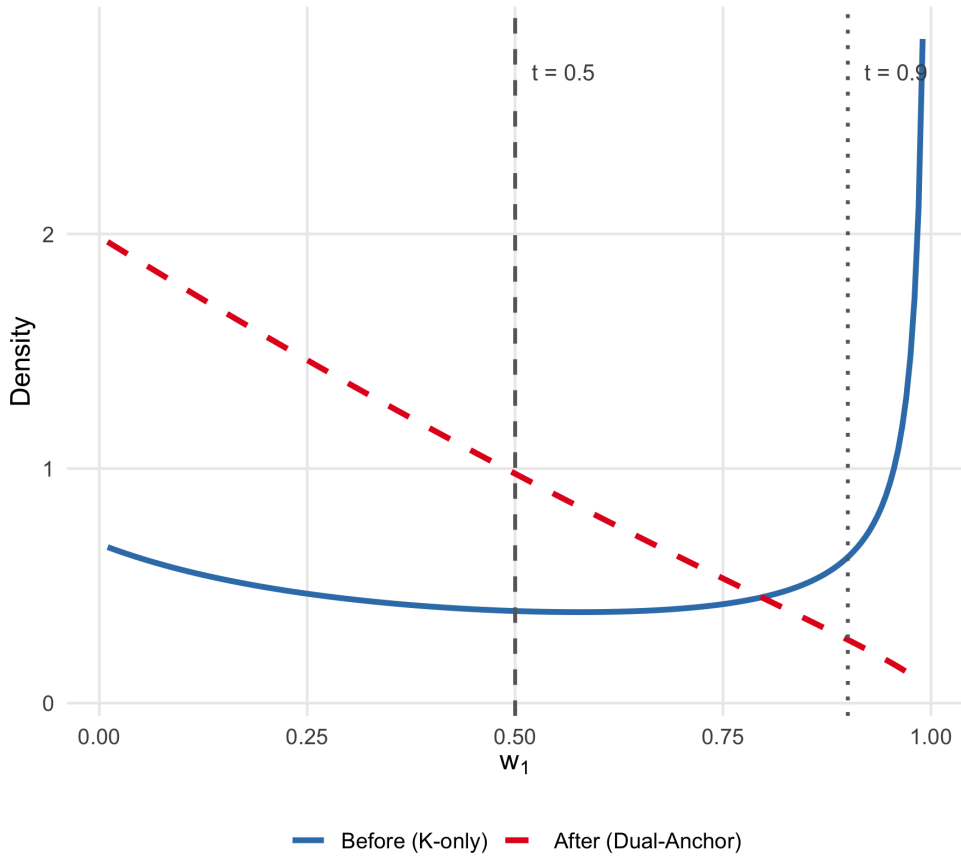


FIGURE G.2. Weight distribution before and after Dual-Anchor refinement ($J = 50, \mu_K = 3$, confidence = “low”). The solid blue line shows the marginal density of w_1 under K -only TSMM calibration, with $\Pr(w_1 > 0.5) = 0.756$. The dashed red line shows the density after Dual-Anchor refinement with target $\Pr(w_1 > 0.5) \leq 0.25$ and $\lambda = 0.7$, achieving $\Pr(w_1 > 0.5) = 0.265$. Vertical reference lines indicate the diagnostic thresholds at $t = 0.5$ and $t = 0.9$.

```
# =====
# Step 3: Use (a, b) in your DP mixture model
# =====

# Stan (shape-rate):
#   alpha ~ gamma(a, b);
```

```

# JAGS (shape-rate):
#   alpha ~ dgamma(a, b)

# Sample from the elicited hyperprior in R:
alpha_draws <- rgamma(10000, shape = a, rate = b)
summary(alpha_draws)

```

G.5.1. *Sensitivity Analysis: Varying Uncertainty Specification.* A simple sensitivity analysis compares different confidence levels:

```

fits <- list(
  "High confidence" = DPprior_fit(J = 50, mu_K = 5,
                                    confidence = "high"),
  "Medium confidence" = DPprior_fit(J = 50, mu_K = 5,
                                    confidence = "medium"),
  "Low confidence" = DPprior_fit(J = 50, mu_K = 5,
                                    confidence = "low")
)

# Summarize key diagnostics
summary_tbl <- do.call(rbind, lapply(names(fits), function(nm) {
  f <- fits[[nm]]
  d <- DPprior_diagnostics(f)
  data.frame(
    Prior      = nm,
    a          = round(f$a, 3),
    b          = round(f$b, 3),
    E_K        = round(d$K$mean, 2),
    Var_K      = round(d$K$var, 2),
    P_w1_gt_0.5 = round(
      d$weights$prob_exceeds["prob_gt_0.5"], 3),
    E_rho      = round(d$coclustering$mean, 3)
  )
})))
summary_tbl

```

Marginal PMF of K_J Under Different Uncertainty Specifications

$J = 50, \mu_K = 5$ | VIF: High = 1.5, Medium = 2.5, Low = 5.0

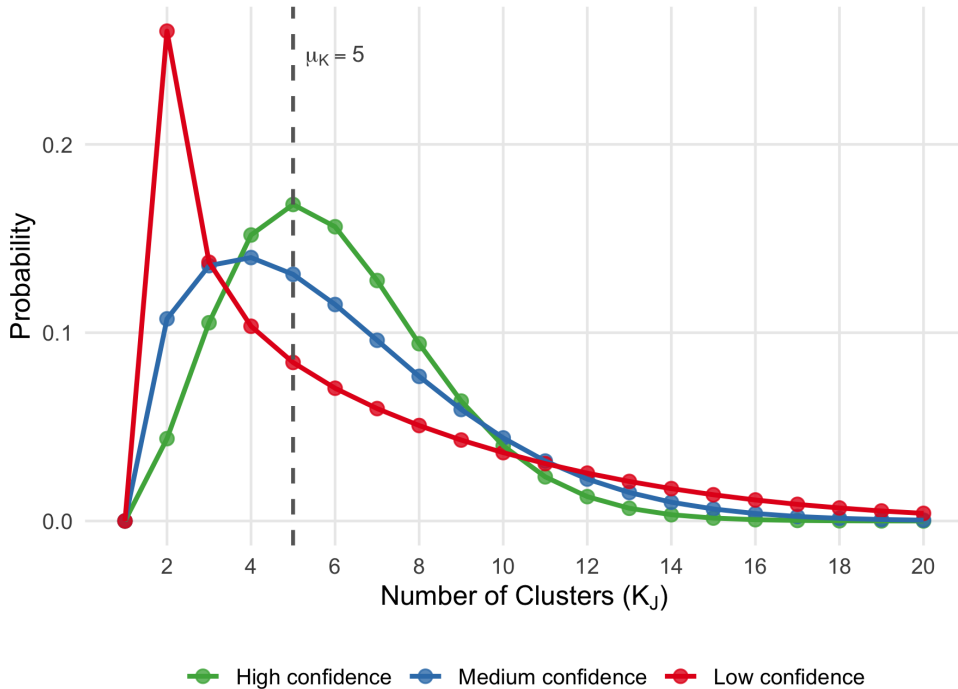


FIGURE G.3. Sensitivity of the induced K_J distribution to uncertainty specifications ($J = 50, \mu_K = 5$). The three curves correspond to high confidence (VIF = 1.5, green), medium confidence (VIF = 2.5, blue), and low confidence (VIF = 5.0, red). Higher uncertainty (lower confidence) produces wider, more dispersed distributions. All three priors share the same target mean $\mu_K = 5$ (vertical dashed line) but differ in their implied variance.

Table G.5 summarizes the induced prior characteristics across confidence levels.

TABLE G.5. Sensitivity Analysis Summary ($J = 50, \mu_K = 5$)

Confidence	VIF	Var(K)	a	b	$P(w_1 > 0.5)$	$\mathbb{E}[\rho]$
High	1.5	6	3.568	2.900	0.465	0.484
Medium	2.5	10	1.408	1.077	0.497	0.518
Low	5.0	20	0.518	0.341	0.563	0.585

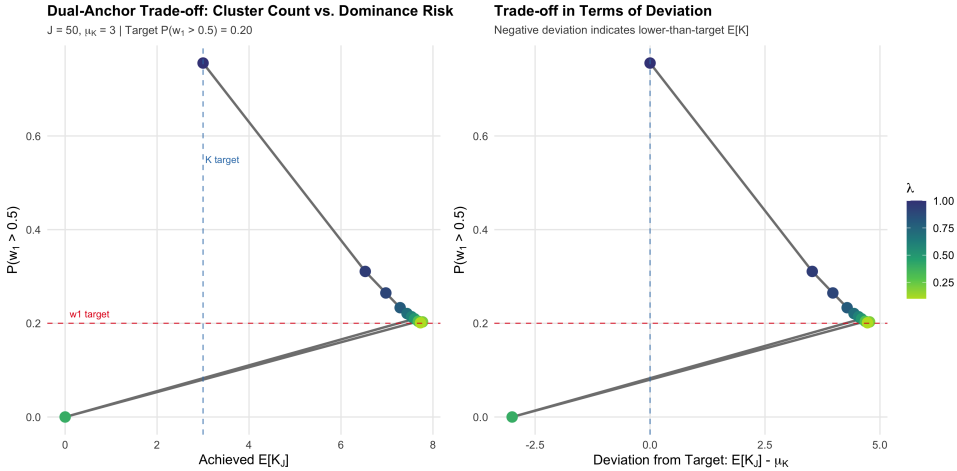


FIGURE G.4. Dual-Anchor trade-off curve ($J = 50$, $\mu_K = 3$). Each point represents a calibration with a different trade-off parameter $\lambda \in [0.1, 1.0]$. The left panel plots achieved $\mathbb{E}[K_J]$ against $\Pr(w_1 > 0.5)$, showing that lower λ values prioritize the weight constraint at the cost of deviating from the K target. The right panel displays the same trade-off in terms of deviation from the target μ_K . The horizontal dashed red line indicates the target $\Pr(w_1 > 0.5) = 0.20$; the vertical dashed blue line marks the K target.

G.6. Reproducibility Checklist. To support transparent reporting and exact replication, we recommend recording the items listed in Table G.6 whenever TSMM and/or Dual-Anchor calibration is used.

TABLE G.6. Reproducibility and Reporting Checklist

Item to Record	How to Obtain	Why It Matters
Design size J	<code>fit\$J</code>	All targets are design-conditional
Elicited μ_K and σ_K^2	<code>fit\$target\$mu_K, fit\$target\$var_K</code>	Defines the cluster-count anchor
Confidence mapping	Confidence level + VIF	Interprets “low/med/high” across papers
Calibration method	<code>fit\$method</code>	A1 vs A2-MN vs A2-KL
Hyperprior (a, b)	<code>fit\$a, fit\$b</code>	Needed for downstream MCMC
Achieved moments	<code>fit\$fit</code>	Confirms successful calibration
Dominance diagnostics	<code>diag\$weights\$prob_exceeds[...]</code>	Flags unintended concentration
Co-clustering summary	<code>diag\$coclustering\$mean</code>	Interpretable pooling diagnostic
Dual-Anchor (if used)	<code>w1_target, lambda, loss_type</code>	Fully defines the refinement step
Software versions	<code>packageVersion("DPprior"), sessionInfo()</code>	Ensures numerical reproducibility

A minimal “methods section” style statement can be assembled directly from these objects, consistent with the reporting protocol recommended in main text Section 3.5.

G.7. Repository and Resources.

Package Source Code. The `DPprior` R package source code is available at:

- GitHub repository: <https://github.com/joonho112/DPprior>
- Package website: <https://joonho112.github.io/DPprior/>

Simulation Reproducibility. All code used to generate the simulation results in the main text and [Section F](#) is archived in a separate reproducibility repository:

- Reproducibility repository: <https://github.com/joonho112/dpprior-elicitation>

This repository contains the complete replication materials organized as follows.

TABLE G.7. Simulation Reproducibility Materials

Item	File Name	Description
Simulation design	<code>design.R</code>	Full factorial specification
Calibration	<code>step1_calibrate.R</code>	Prior construction for all methods
MCMC fitting	<code>step2_simulate.R</code>	Posterior inference with parallel processing
Aggregation	<code>step3_aggregate.R</code>	Summary statistics computation
Figures	<code>step4_figures.R</code>	All main text and OSM figures

Seed strategy. A reproducible run should record the deterministic seeding scheme. The OSM reports a seeding approach that fixes seeds at the level of replication and scenario. One convenient pattern is to derive per-replication seeds from a base seed plus a hash of (K^*, I) , method, and confidence level, and then to derive per-chain seeds from the replication seed:

```
set.seed(2026) # Master seed for reproducibility
```

Version requirements: R version $\geq 4.0.0$; `DPprior` version 1.0.0; Dependencies: `stats`, `Rcpp` ($\geq 1.0.0$).

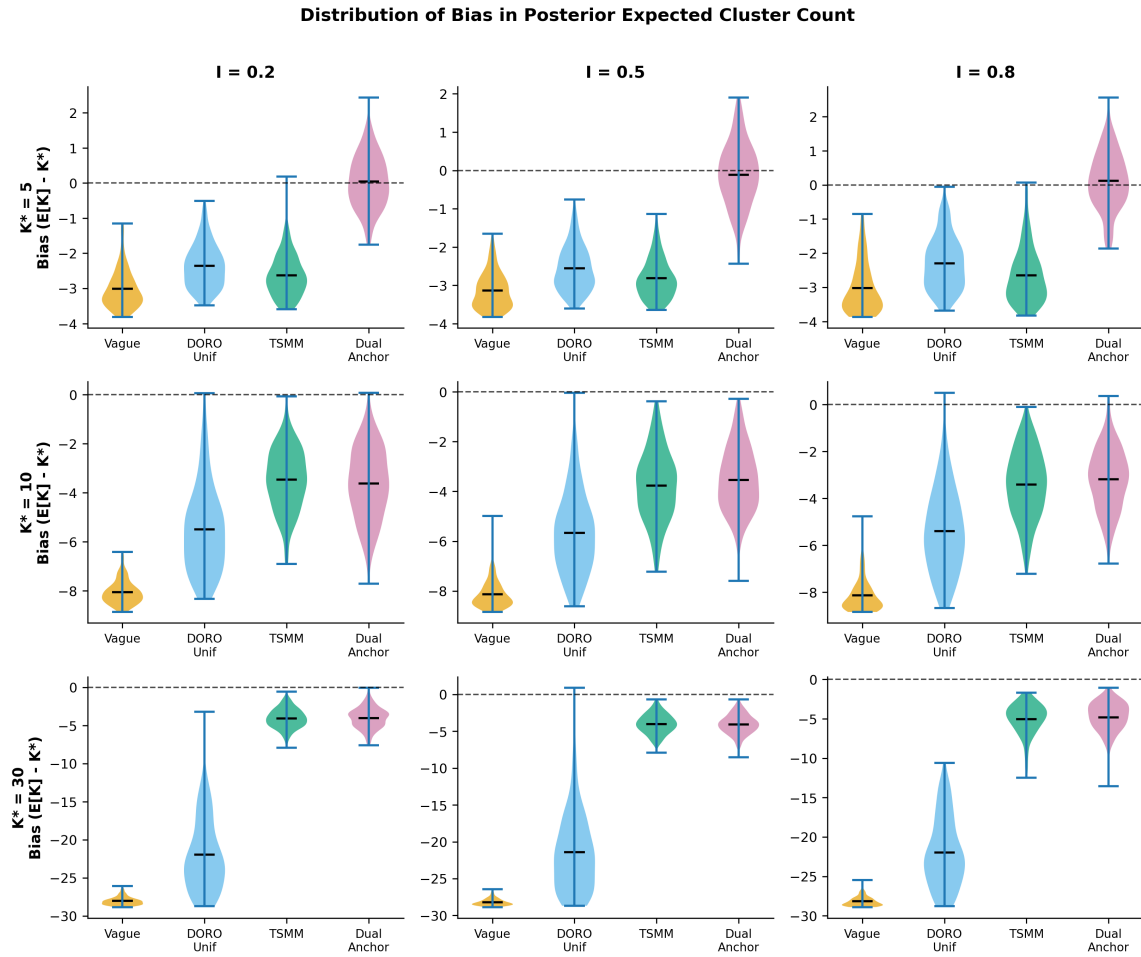


FIGURE F.1. Distribution of bias in posterior expected cluster count $E[K_J | \text{data}] - K^*$ by method and scenario. Rows: true cluster counts $K^* \in \{5, 10, 30\}$; columns: informativeness levels $I \in \{0.2, 0.5, 0.8\}$. Dashed line indicates zero bias. Violin plots show the full distribution across 200 replications, with the black horizontal line indicating the median.

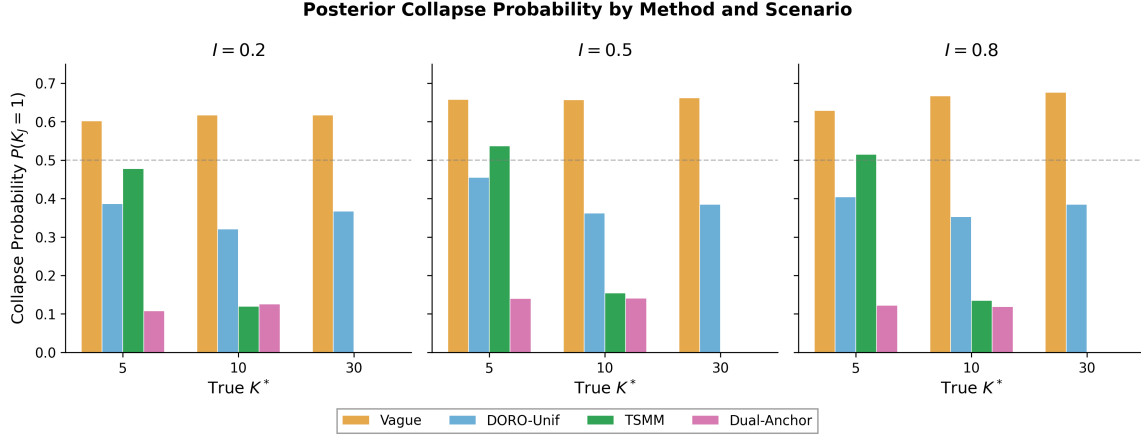


FIGURE F.2. Posterior collapse probability $P(K_J = 1)$ by method and scenario. The horizontal dashed line indicates 50% collapse probability. Vague priors (yellow) produce collapse rates exceeding 60% regardless of true K^* . TSMM (green) substantially reduces collapse for $K^* \geq 10$ but remains vulnerable for $K^* = 5$. Dual-Anchor (pink) provides consistent protection against collapse across all scenarios, reducing $P(K_J = 1)$ to below 15% even for $K^* = 5$.

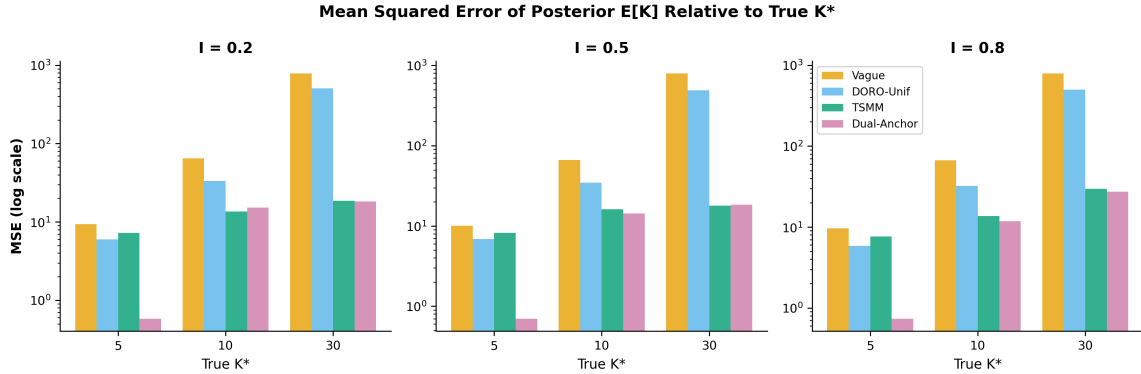


FIGURE F.3. Mean Squared Error of posterior expected cluster count $E[K_J | \text{data}]$ relative to true K^* (log scale). For $K^* = 30$, Vague MSE ≈ 790 , DORO-Unif ≈ 500 , while TSMM and Dual-Anchor achieve MSE $\approx 18\text{--}30$, representing approximately 97% MSE reduction. For $K^* = 5$, Dual-Anchor achieves MSE < 1 , compared to TSMM's MSE $\approx 7\text{--}8$.

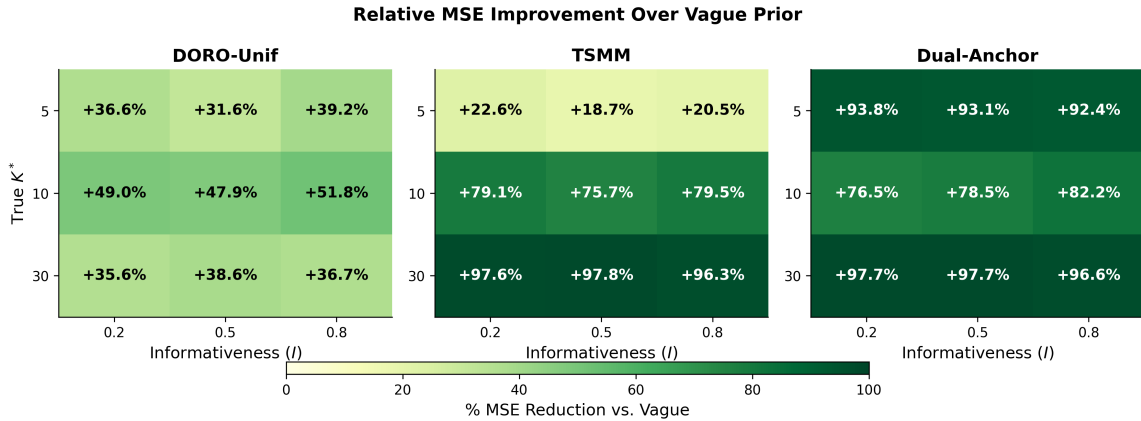


FIGURE F.4. Relative MSE improvement over Vague prior (%). Each cell shows $(MSE_{\text{Vague}} - MSE_{\text{Method}})/MSE_{\text{Vague}} \times 100\%$. TSMM and Dual-Anchor achieve approximately 96–98% MSE reduction when $K^* = 30$. Dual-Anchor provides the most dramatic improvement for $K^* = 5$ (approximately 92–94% MSE reduction), precisely where TSMM struggles (only 18–23% improvement).

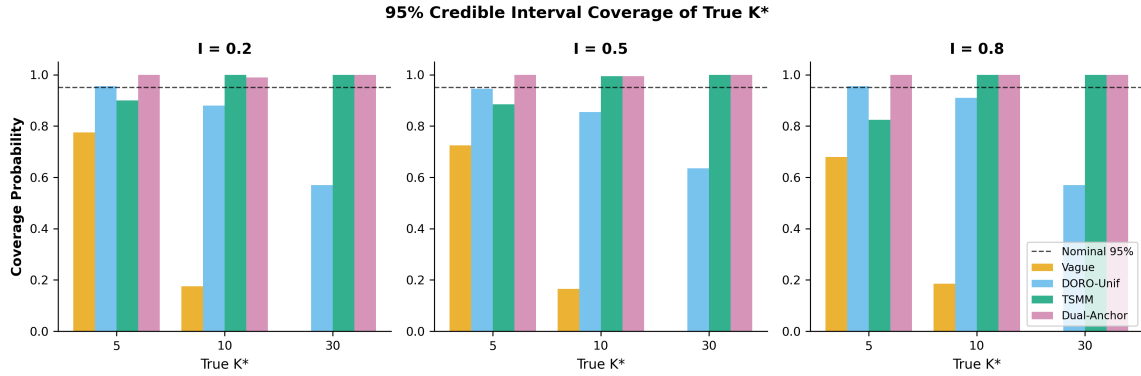


FIGURE F.5. 95% credible interval coverage of true K^* by method and scenario. The horizontal dashed line indicates the nominal 95% level. Vague priors (yellow) produce severely under-covering intervals for $K^* \geq 10$, with coverage essentially 0% for $K^* = 30$. TSMM and Dual-Anchor (green, pink) achieve near-nominal or conservative coverage across all scenarios.

Width of 95% Credible Interval for K

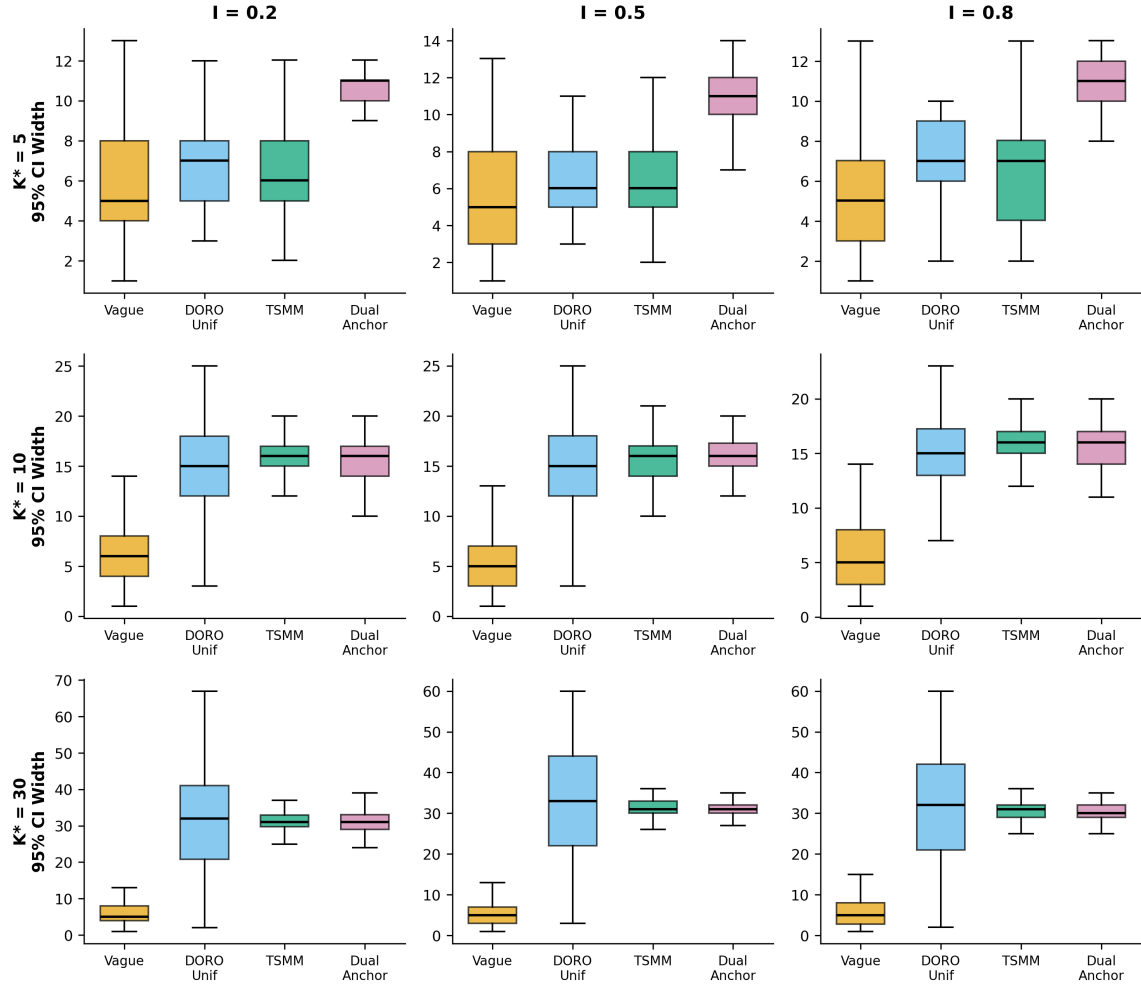


FIGURE F.6. Width of 95% credible interval for K_J by method and scenario. Boxplots show the distribution of interval widths across 200 replications. Vague priors produce narrow intervals (around 5–6) regardless of true K^* , while TSMM and Dual-Anchor produce appropriately wider intervals that scale with K^* .

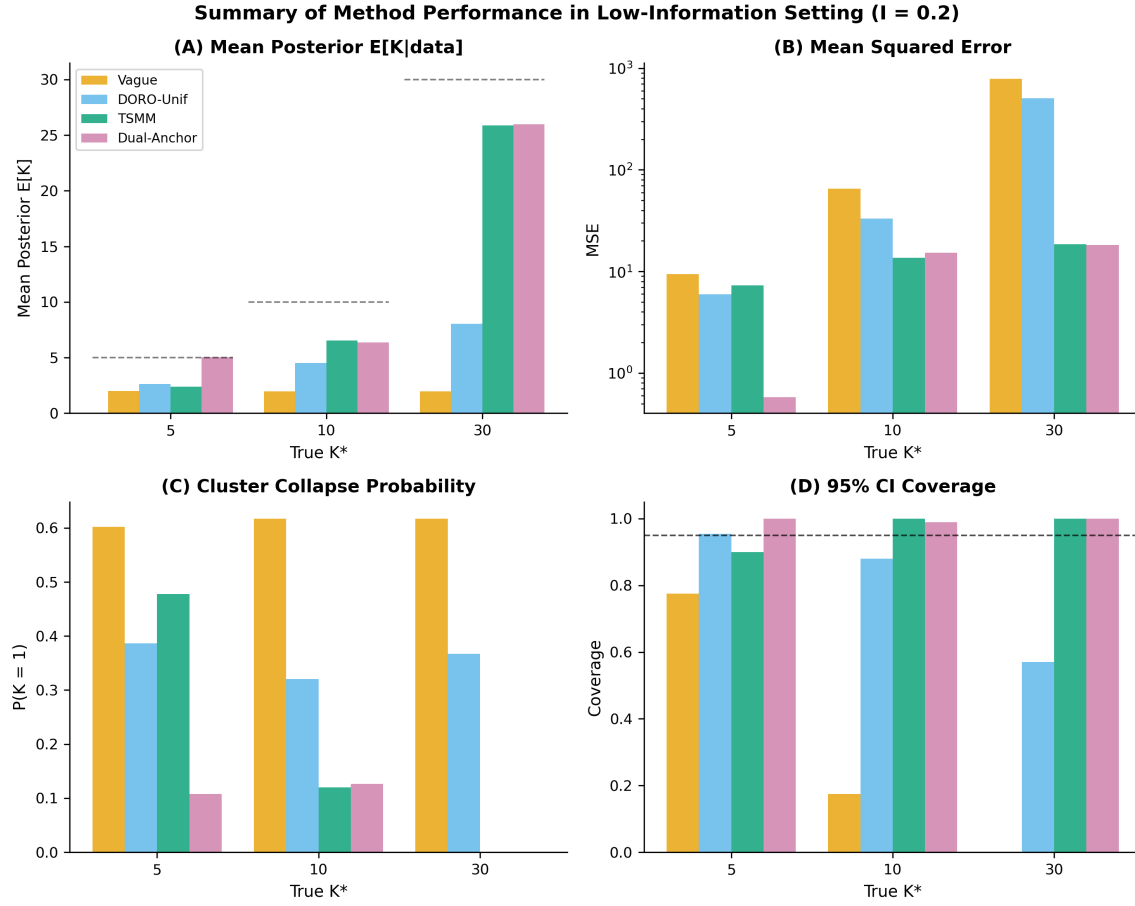


FIGURE F.7. Summary of method performance in the low-information setting ($I = 0.2$). Panel (A): Mean posterior $\mathbb{E}[K_J | \text{data}]$ with dashed lines indicating true K^* . Panel (B): Mean Squared Error (log scale). Panel (C): Cluster collapse probability $P(K_J = 1)$. Panel (D): 95% CI coverage with dashed line at nominal 95% level.

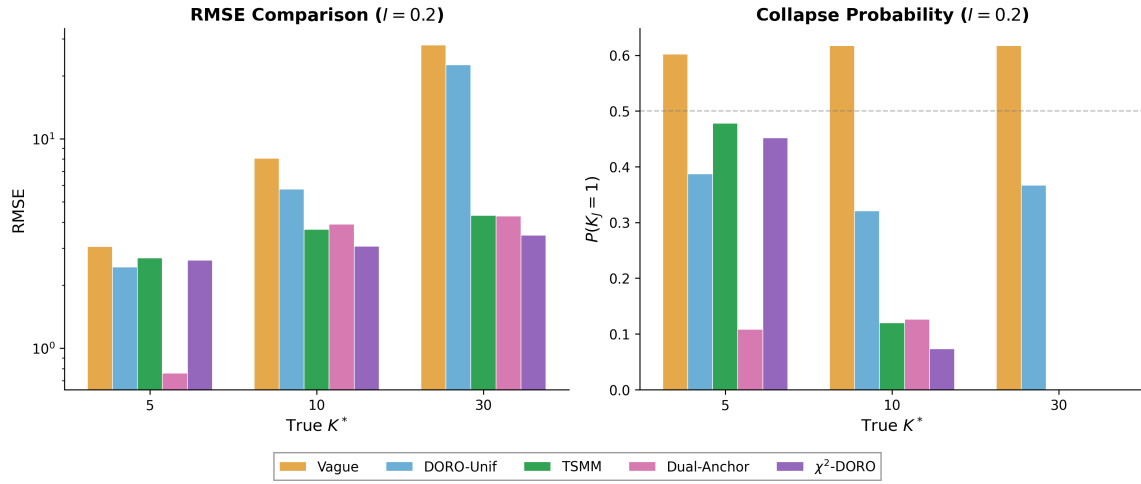


FIGURE F.8. Comparison including χ^2 -DORO baseline for $I = 0.2$. Left panel: RMSE (log scale). Right panel: Collapse probability. χ^2 -DORO (purple) typically improves upon DORO-Unif and TSMM for $K^* \in \{10, 30\}$, but still exhibits substantial under-estimation and non-trivial collapse probability when $K^* = 5$ —precisely the regime where Dual-Anchor was designed to intervene.

Effect of Confidence Level on TSMM and Dual-Anchor Methods

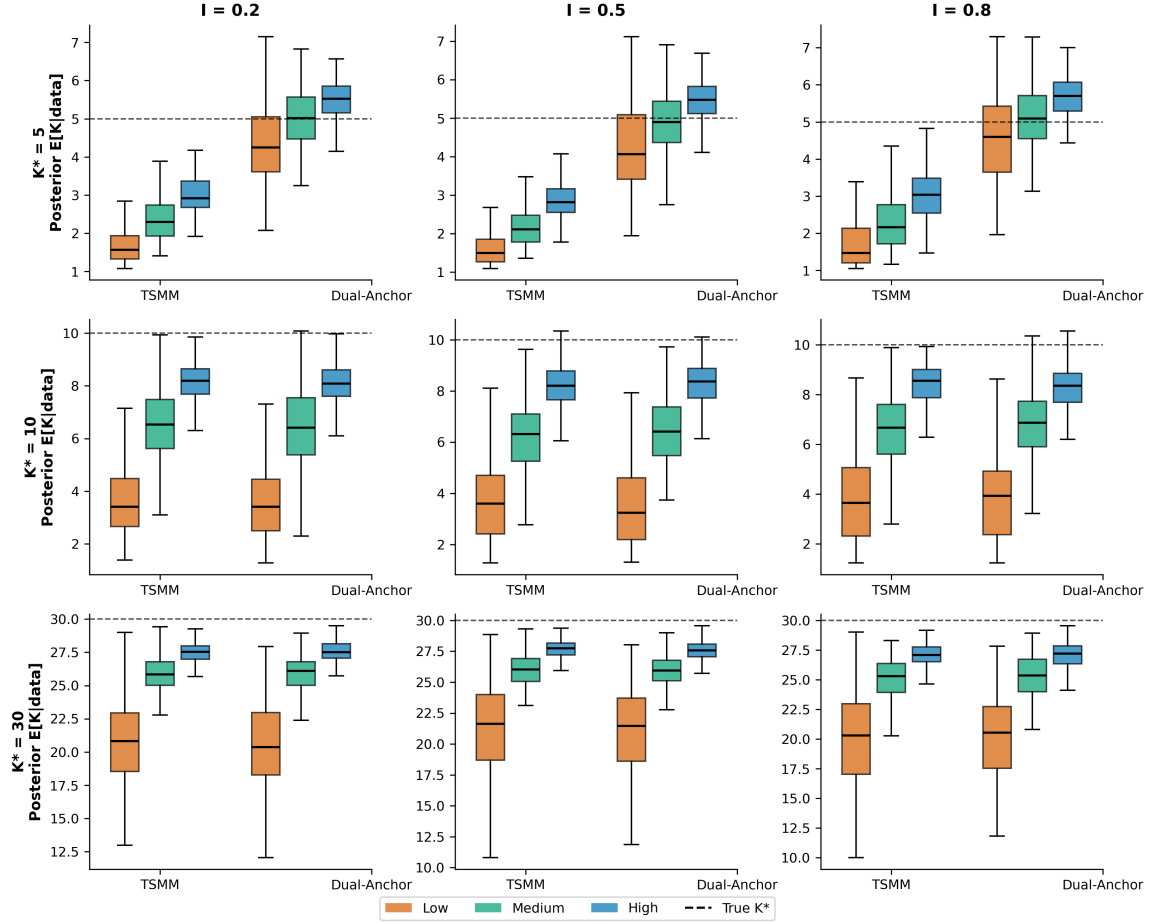


FIGURE F.9. Effect of confidence level on TSMM and Dual-Anchor methods. Rows: true $K^* \in \{5, 10, 30\}$; columns: informativeness levels $I \in \{0.2, 0.5, 0.8\}$. Within each panel, boxplots show posterior $\mathbb{E}[K_J | \text{data}]$ for low (orange), medium (green), and high (blue) confidence settings. Dashed horizontal lines indicate true K^* .

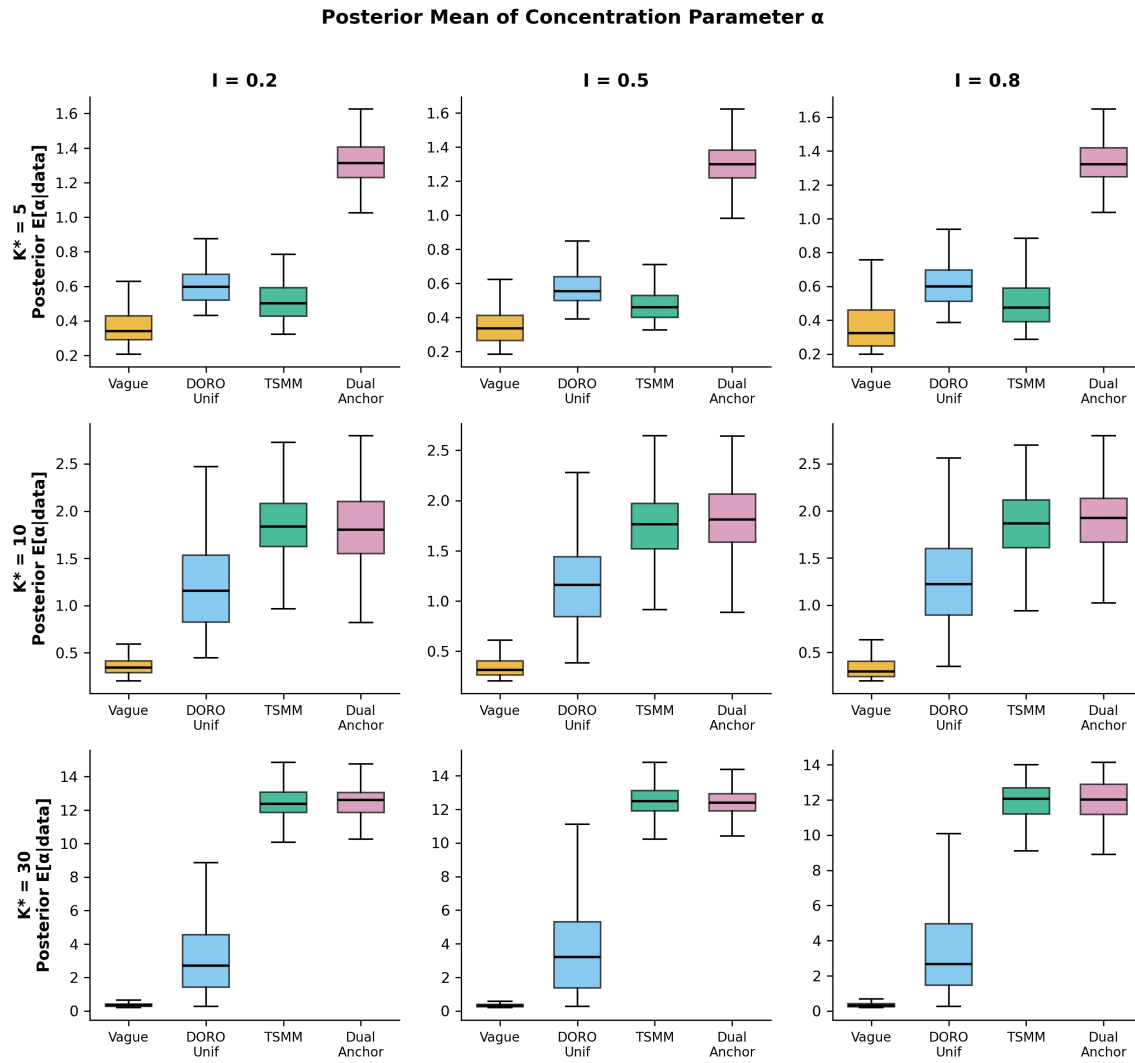


FIGURE F.10. Posterior mean of concentration parameter α by method and scenario (medium confidence). Rows: true $K^* \in \{5, 10, 30\}$; columns: informativeness levels $I \in \{0.2, 0.5, 0.8\}$. Note the different y -axis scales across rows.

Posterior Standard Deviation of Cluster Count

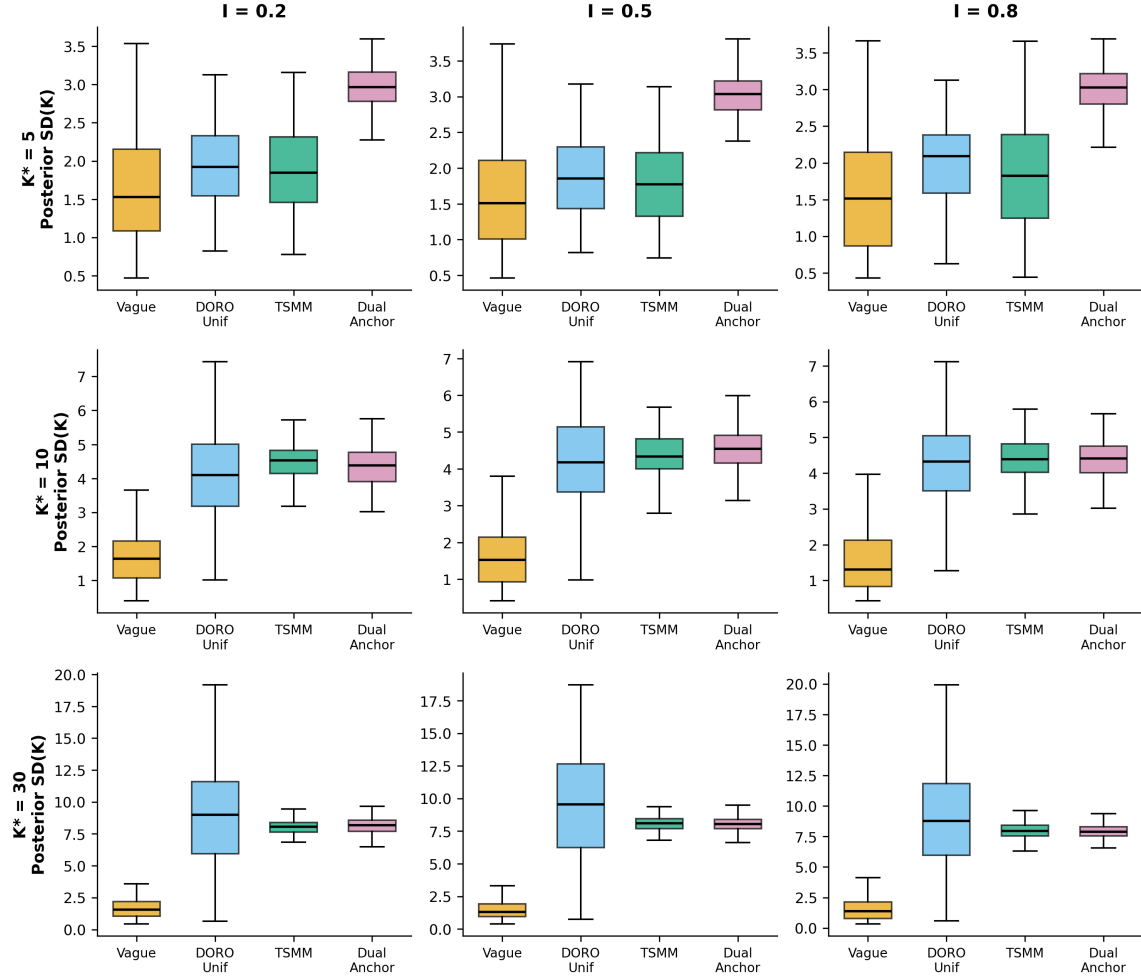


FIGURE F.11. Posterior standard deviation of cluster count K_J by method and scenario. Vague priors produce consistently narrow posteriors (low uncertainty) regardless of K^* , while TSMM and Dual-Anchor produce appropriately scaled uncertainty that increases with K^* .

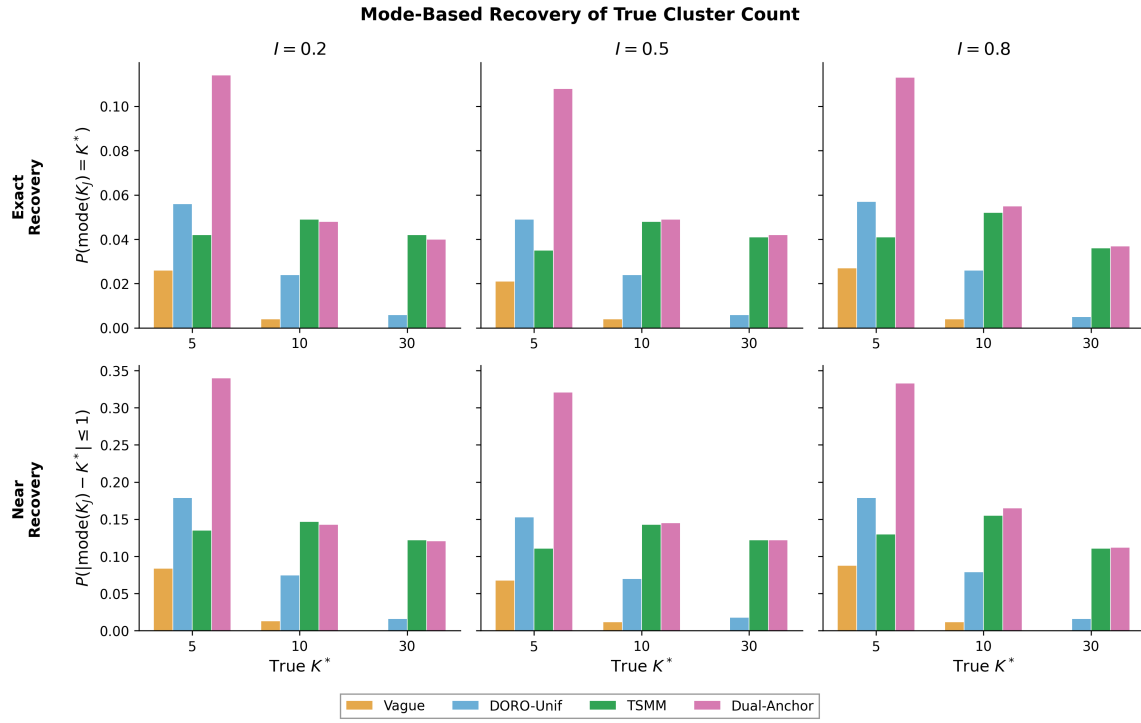


FIGURE F.12. Mode-based recovery of true cluster count. Top row: Exact recovery rate $P(\text{mode}(K_J) = K^*)$. Bottom row: Near recovery rate $P(|\text{mode}(K_J) - K^*| \leq 1)$. Columns: informativeness levels $I \in \{0.2, 0.5, 0.8\}$.

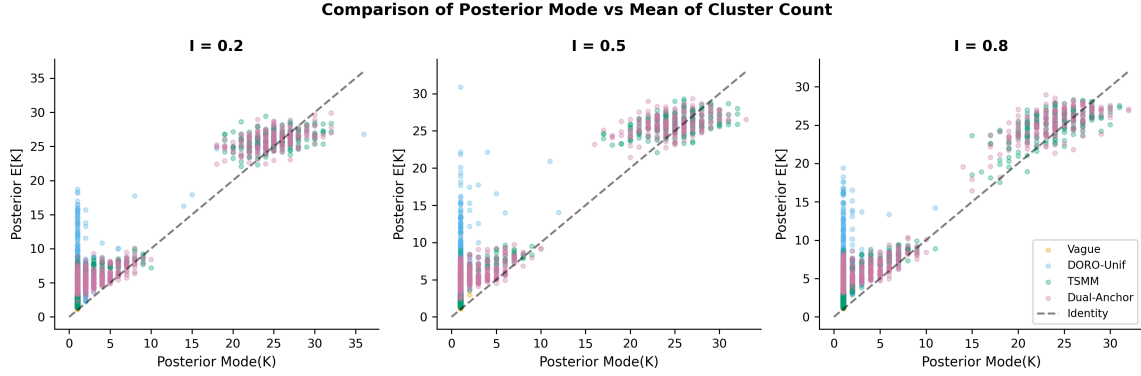


FIGURE F.13. Comparison of posterior mode vs. mean for cluster count K_J . Each point represents one replication. The dashed diagonal line indicates where mode equals mean. Systematic deviations above the line indicate that the posterior mean exceeds the mode (right-skewed posterior), while points below indicate the opposite.

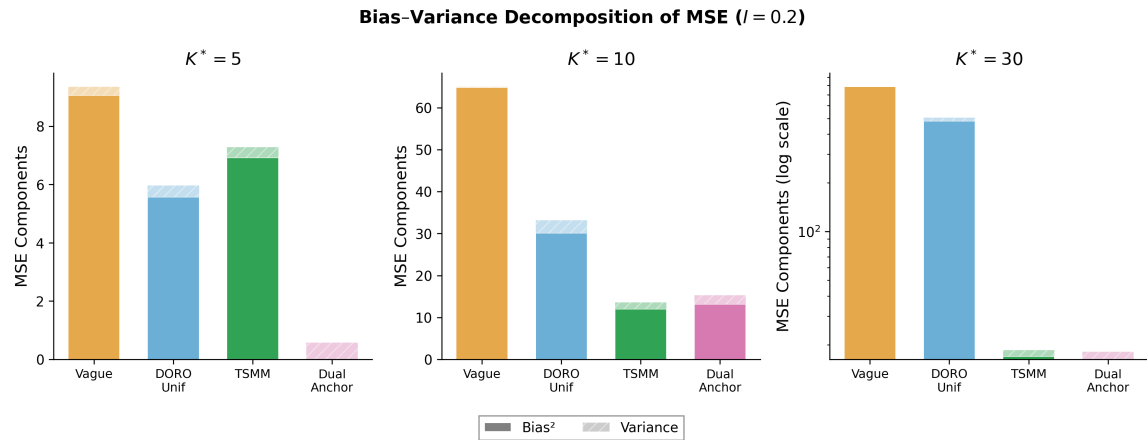


FIGURE F.14. Bias-variance decomposition of MSE for $I = 0.2$. Solid bars represent Bias^2 ; hatched portions represent variance. For $K^* = 30$, a log scale is used. Method colors: Vague (yellow), DORO-Unif (blue), TSMM (green), Dual-Anchor (pink).